The Rho GEF Trio is transported by microtubule plus-ends and involved in focal adhesion formation in migrating neural crest cells

Dissertation

zur Erlangung des Grades
Doktor der Naturwissenschaften
(Dr. rer. nat.)

dem Fachbereich Biologie der Philipps-Universität Marburg

vorgelegt von
Stefanie Gossen
geboren in Fulda

Marburg, November 2023

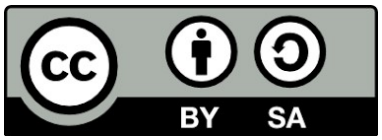

Die vorliegende Dissertation wurde von Oktober 2019 bis November 2023 unter der Betreuung von Prof. Dr. Annette Borchers am Fachbereich der Biologie sowie im Rahmen des Graduiertenkollegs GRK2213 „Membrane Plasticity in Tissue Development and Remodeling“ an der Philipps-Universität Marburg durchgeführt.

Vom Fachbereich Biologie der Philipps-Universität Marburg (Hochschulkennziffer 1180) als Dissertation angenommen am _____

Erstgutachterin:	Prof. Dr. Annette Borchers
Zweitgutachter:	Prof. Dr. Christian Helker
Tag der Disputation:	19.12.2023

Publications:

Gossen, S., Gerstner, S., Borchers, A. The Rho GEF Trio is transported by microtubules and affects microtubule stability in migrating neural crest cells (2023) (under Review)

Herchenröther, A., **Gossen, S.**, Friedrich, T. *et al.* The H2A.Z and NuRD associated protein HMG20A controls early head and heart developmental transcription programs. *Nat Commun* **14**, 472 (2023). https://doi.org/10.1038/s41467-023-36114-x

Publication resulted from a collaboration project with Prof. Dr. Sandra Hake. I contributed to conceptualization, methodology, validation, formal analysis, investigation, writing and visualization of the *Xenopus* data and supervised Leah Schwarz and Sarah Gerstner in performing and analyzing *Xenopus* experiments.

Abstract

Directed cell migration depends on cytoskeletal rearrangements, protrusion formation, cell contraction and focal adhesion turnover. These processes are regulated by spatiotemporal fine-tuning of Rho GTPase activity. The Rho guanine nucleotide exchange factor (GEF) Trio is well suited to control Rho GTPase activity by merging two catalytic GEF domains, allowing control over Rac1 and RhoA within a single protein. However, strict spatiotemporal control of the activity of the Trio GEF domains at the cellular level is necessary. We recently demonstrated that Trio is required for *Xenopus* neural crest (NC) cell protrusion formation and migration. Here, we examine the dynamic localization of Trio and its impact on Trio's role in NC cell migration. Live-cell imaging revealed that the Trio GEF2 domain co-localizes with EB3 at microtubule plus-ends. Microtubule trafficking of Trio appears to be important for its function, as a mutant GEF2 construct lacking the SxIP amino acid motif responsible for microtubule plus-end binding, was unable to rescue the Trio loss-of-function induced NC migration defects *in vivo* and *in vitro*. In addition, our analysis of microtubule dynamics in migrating neural crest cells revealed that Trio knockdown results in the stabilization of microtubules at cell-cell contacts, while destabilizing them at the leading edge compared to the control. Furthermore, our findings indicate that Trio is involved in focal adhesion dynamics, as analyzed by live-cell imaging of focal adhesion assembly and disassembly. Our data suggest that Trio is transported by microtubules to specific subcellular locations, where it has distinct functions in controlling microtubule stability, protrusion formation and adhesive functions during directed NC cell migration. Furthermore, *TRIO* gene mutations have been shown to cause neurodevelopmental disorders and facial dysmorphisms in patients, possibly by inhibiting the migration of neural crest cells. Similar clinical features were observed in individuals with mutations in the *MAPRE2* and *TUBB* genes. We successfully induced Mapre2 and Tubb loss-of-function in *Xenopus* embryos by injecting specific translation-blocking morpholinos and demonstrate, comparable to patient data, that this knockdown results in NC migration defects and craniofacial malformations. These experiments will serve as a starting point to analyze whether Trio, Mapre2 and Tubb operate within the same signaling pathways to regulate microtubule dynamics, focal adhesion turnover and, thereby, cell motility.

Zusammenfassung

Die gerichtete Zellmigration hängt von einem dynamischen Zytoskelett, der Bildung von Zellfortsätzen, der Zellkontraktion und dynamischen fokalen Adhäsionen ab. Diese Prozesse werden durch ein räumliches und zeitliches Feintuning der Aktivität von Rho-GTPasen reguliert. Der Rho-Guanin-Nukleotid-Austauschfaktor (GEF) Trio ist ein ausgezeichneter Kandidat, um die Aktivität von Rho-GTPasen zu kontrollieren, da er zwei katalytische GEF-Domänen vereint und so die Kontrolle über Rac1 und RhoA in einem einzigen Protein ermöglicht. Allerdings ist eine strikte räumliche und zeitliche Regulation der Aktivität der Trio-GEF-Domänen auf zellulärer Ebene erforderlich. Wir konnten bereits zeigen, dass Trio für die Bildung von Zellfortsätzen sowie für die gerichtete Zellmigration in *Xenopus*-Neuralleistenzellen notwendig ist. In dieser Studie untersuchen wir die dynamische Lokalisation von Trio und deren Einfluss auf seine Funktion bei der Neuralleistenzellmigration. Die Lebendzellanalyse zeigte, dass die Trio-GEF2-Domäne mit EB3 an Miktotubuli-Plus-Enden kolokalisiert. Der Transport von Trio durch Mikrotubuli scheint für seine Funktion wichtig zu sein, denn ein mutiertes GEF2-Konstrukt, dem das Aminosäuremotiv SxIP fehlte, welches für die Bindung an Mikrotubuli-Plus-Enden verantwortlich ist, konnte den Trio-Verlust in Neuralleistenzellen *in vivo* und *in vitro* nicht ausgleichen, während das Wildtyp-GEF2-Konstrukt dazu in der Lage war. Darüber hinaus zeigte unsere Analyse der Mikrotubuli-Dynamik in migrierenden Neuralleistenzellen, dass der Trio-Knockdown zu einer Stabilisierung der Mikrotubuli an Zell-Zell-Kontakten führt, während sie an der Zellfront im Vergleich zur Kontrolle destabilisiert werden. Gleichzeitig deuten unsere Ergebnisse darauf hin, dass Trio an der Dynamik der fokalen Adhäsionen beteiligt ist. Zusammenfassend zeigen wir hier, dass Trio über Mikrotubuli an spezifische subzelluläre Orte transportiert werden kann, wo es verschiedene Funktionen bei der Kontrolle der Mikrotubuli-Stabilität, der Ausbildung von Zellfortsätzen und der Zelladhäsion während der gerichteten Migration von Neuralleistenzellen ausübt. Weiterhin wurde bereits gezeigt, dass *TRIO*-Genmutationen zu neurologischen Entwicklungsstörungen und Gesichtsdysmorphien bei Patienten führen, möglicherweise durch eine beeinträchtigte Neuralleistenzellmigration. Ähnliche klinische Merkmale wurden bei Personen mit Mutationen in den Genen *MAPRE2* und *TUBB* beobachtet. Wir konnten den Funktionsverlust von Mapre2 und Tubb in *Xenopus* Embryonen durch Injektion spezifischer translationsblockierender Morpholino Oligonukleotide nachahmen und zeigen, dass dieser in *Xenopus*, ähnlich wie in Patienten, zu Defekten in der Neuralleistenzellmigration und zu kraniofazialen Fehlbildungen führt. Diese Experimente dienen als Ausgangspunkt, um zu analysieren, ob Trio, Mapre2 und Tubb innerhalb der gleichen Signalkaskaden agieren, um die Mikrotubuli-Dynamik, die fokale Adhäsion und damit die Zellmotilität zu regulieren.

Table of contents

Abbreviations

+TIP	Microtubule plus-end tracking protein
Abl	Abelson tyrosine kinase
ADS	Autism spectrum disorder
Arp2/3	Actin related protein 2/3 complex
C. elegans	*Caenorhabditis elegans*
CARMIL	Capping protein, Arp2/3, myosin I linker
CIL	Contact inhibition of locomotion
CLIP-170	Cytoplasmic linker protein 170
CRAL-Trio	Retinaldehyde-binding protein (CRALBP) and Trio guanine exchange factor
CSC-KT	Circumferential skin creases Kunze type
D. melanogaster	*Drosophila melanogaster*
Dbl	Diffuse B-cell lymphoma
DH	Dbl-Homology
DVL	Dishevelled
EB	End-binding protein
ECM	Extracellular matrix
EMT	Epithelial-mesenchymal transition
EMTB	Microtubule binding domain of ensconsin
FAK	Focal adhesion kinase
FHOD3	Formin Homology 2 domain containing 3 protein
Fig.	Figure
FnIII	Fibronectin type III domain
GAP	GTPase activating protein
GDI	Guanine dissociation inhibitor
GDP	Guanosine diphosphate
GEF	Guanine nucleotide exchange factor
GSK3	Glycogen synthase kinase 3
GTP	Guanosine triphosphate
GTPase	Guanosine triphosphate hydrolases
$G\alpha_q$	Guanine nucleotide-binding protein G(q) subunit alpha
Hsc70	Molecular chaperone heat shock cognate protein 70
Ig	Immunoglobulin domain
iPSC	Induced pluripotent stem cells
kDA	Kilo Dalton
RT	Room temperature
LAR	Leukocyte common antigen-related protein
MAPRE	Microtubule associated protein member
mCFP	Membrane cyan fluorescent protein
MDCK	Madin-Darby Canine Kidney

mDia	Mammalian Diaphanous-related (formin family of Rho-effector protein)
mGFP	Membrane green fluorescent protein
MO	Morpholino oligonucleotide
mRFP	Membrane red fluorescent protein
Myh9	Myosin heavy chain 9
NAV-1	Neuron Navigator 1
NC	Neural crest
NDD	Neurodevelopmental disorder
Pak1	P21 (RAC1) activated kinase 1
Par1b	Polarity-regulating kinase partitioning-defective 1b
Par3	Protein partitioning defective 3
PCP	Planar cell polarity
PH	Pleckstrin Homology
Rac1	Ras-related C3 botulinum toxin substrate 1
RhoA	Ras homolog family member A
RhoG	Ras homolog family member G
ROCK	Rho-associated protein kinase
SCFS	Single-cell force spectroscopy
SH3	Src homology 3
STEF	Sif and Tiam1-like exchange factor
STK	Serine/threonine kinase
SxIP	Serine-x- Isoleucine -Proline
Tab.	Table
Tara	Trio-associated repeat on actin
Tiam1	T-cell lymphoma invasion and metastasis 1
Trio	Triple functional domain protein
TUBB	Tubulin beta class I
WAVE	WASP-family verprolin-homologous protein
WRC	WAVE Regulatory Complex
X. laevis	*Xenopus laevis*

Chapter 1

The Rho GEF Trio as regulator of cell migration and embryonic development

1. Introduction

The study of cell migration is essential for understanding biological processes like morphogenesis, wound healing and cancer invasion. Neural crest (NC) cells are multipotent embryonic stem cells that migrate over long distances and give rise to various tissues in vertebrates, such as neurons, glia, cartilage, skeleton and pigment cells (Szabó and Mayor, 2018). Thus, NC cells represent an excellent model system to investigate cell-cell communication and evolutionary conserved signaling pathways involved in cell migration. Moreover, NC cells and metastatic tumor cells exhibit shared mechanisms in gene expression and behavior. Both undergo an epithelial-mesenchymal transition (EMT) acquiring motile and invasive characteristics (Theveneau et al., 2010). Failure in NC cell migration can result in serious birth defects and multiorgan malformation syndromes, referred to as neurocristopathies (Pilon, 2021). Several mechanisms that control directional NC cell migration have been described, such as the confinement effect of surrounding tissues, collective chemotaxis and dynamic cell-cell interactions including contact inhibition of locomotion (CIL) (Szabó and Mayor, 2018). CIL describes the behavior of migratory NC cells that change their polarity and directionality upon cell-cell contact (András Szabó and Roberto Mayor; Barriga and Mayor, 2015; Szabó and Mayor, 2018). It has been shown that CIL is regulated by non-canonical planar cell polarity (PCP) Wnt signaling (Matthews et al., 2008). The accumulation of ligands like Dishevelled at cell-cell contacts upregulates the activity of the small GTPase RhoA. While the small GTPase Rac1 is inhibited at the cell-cell contact, its activity is critical at the cell front. Thus, the spatiotemporal regulation of these GTPases is crucial for directional cell migration (Carmona-Fontaine et al., 2008). Although NC cell migration is known to be regulated by several mechanisms and a number of molecular interactors, the underlying molecular dynamics, downstream effectors and how cell-cell contact information leads to cell polarity, cytoskeletal rearrangement and directional migration remain poorly understood (Theveneau and Mayor, 2012). A well-suited downstream effector of these signaling pathways, that is required for NC cell migration, is the Rho GEF (guanine nucleotide exchange factor) Trio, which is able to regulate both Rac1 and RhoA activity via its two GEF domains (Debant et al., 1996; Kratzer et al., 2019; Kratzer et al., 2020). The Trio GEF1 domain activates Rac1 and RhoG, while the Trio GEF2 domain activates RhoA exclusively (Schmidt and Debant, 2014). Furthermore, several pathogenic missense or nonsense variants of *TRIO* have been described in patients resulting in a variety of clinical features, including developmental delay, microcephaly, macrocephaly, skeletal problems and variable facial features (Gazdagh et al.,

2023). Consequently, it is of great interest to understand the function of Trio in cell migration processes, which will also shed more light on the clinical picture of individuals with *TRIO* gene mutations and may provide treatment options involving cellular and molecular approaches.

1.1. Relevance of Trio in disease and cancer progression

Multiple studies have demonstrated that dysfunction of TRIO can lead to neurodevelopmental disorders (NDDs) (Barbosa et al., 2020), including autism spectrum disorder (ADS) (Sadybekov et al., 2017) and schizophrenia (Singh et al., 2022). To date, there are more than 50 published cases of patients with a *TRIO* gene mutation and the number is continuously increasing (Ba et al., 2016; Barbosa et al., 2020; Gazdagh et al., 2023; Kloth et al., 2021; Kolbjer et al., 2021; Liu et al., 2022; Sadybekov et al., 2017; Schultz-Rogers et al., 2020). These patients have missense, truncating or nonsense variants (Fig. 1A) of *TRIO* and display multisyndromic phenotypes, including brain malformations, developmental delay, learning disabilities, microcephaly, macrocephaly, seizures, behavioral problems, skeletal problems, dental problems and varying facial features (Gazdagh et al., 2023). Recently, it has been shown that - depending on the region of mutation - the clinical features of patients can be subdivided into two clusters: Missense variants in the *TRIO* spectrin repeats and GEF1 domain (cluster 1) or missense variants only in the GEF1 domain (cluster 2) (Barbosa et al., 2020; Bonnet et al., 2023; Gazdagh et al., 2023). Cluster 1 *TRIO* mutations are characterized by Rac1 hyperactivation and patients show severe developmental delay, macrocephaly, skeletal and facial dysmorphism (Fig. 1B). These phenotypes can be explained by the autoinhibitory function of the TRIO spectrin repeats (Bircher et al., 2022). Physiologically, TRIO GEF1 activity is tightly controlled by the N-terminal spectrin repeats. These undergo an intramolecular binding and form a ring surrounding the GEF1 domain, preventing potential interaction partners from binding, which would induce Rac1 activation (Bircher et al., 2022; Bonnet et al., 2023). If specific amino acid residues in the spectrin repeats or the GEF1 domain are mutated, the folding of the spectrin ring structure is impaired and/or binding to the GEF1 domain is disrupted (Fig. 1.5). This prevents the autoinhibitory function of the spectrin repeats and leads to hyperactivation of Rac1 (Bonnet et al., 2023). Cluster 2 *TRIO* mutations are defined by a defective activation of Rac1 and patients exhibit mild intellectual disability, microcephaly and characteristic skeletal and facial dysmorphisms (Fig. 1C) (Barbosa et al., 2020; Gazdagh et al., 2023). Patients harboring a mutation or truncation affecting the *TRIO* GEF2 domain show similar phenotypes to cluster 2 patients (Gazdagh et al., 2023). However, the underlying molecular mechanism causing these phenotypes is not clear. So far, most of the literature focused on TRIO GEF1-mediated Rac1 activation (Tao et al., 2019b), and the molecular mechanism explaining the *TRIO* mutation phenotypes described above is based solely on Rac1 misregulation (Barbosa et al., 2020; Gazdagh et al., 2023). Furthermore, *TRIO* GEF2 mutations occur much rarer in the literature. This raises the question of whether the GEF2 domain is less important for the function of TRIO during developmental processes, or whether

the GEF2 domain plays an essential role so that loss-of-function mutations in the GEF2 domain would be lethal. Katrancha et al. described a case with a single de novo mutation in the GEF2 domain that increased GEF2 exchange activity and was associated with bipolar disorder, demonstrating the need for precise regulation of not only Rac1 but also RhoA during developmental processes (Katrancha et al., 2017).

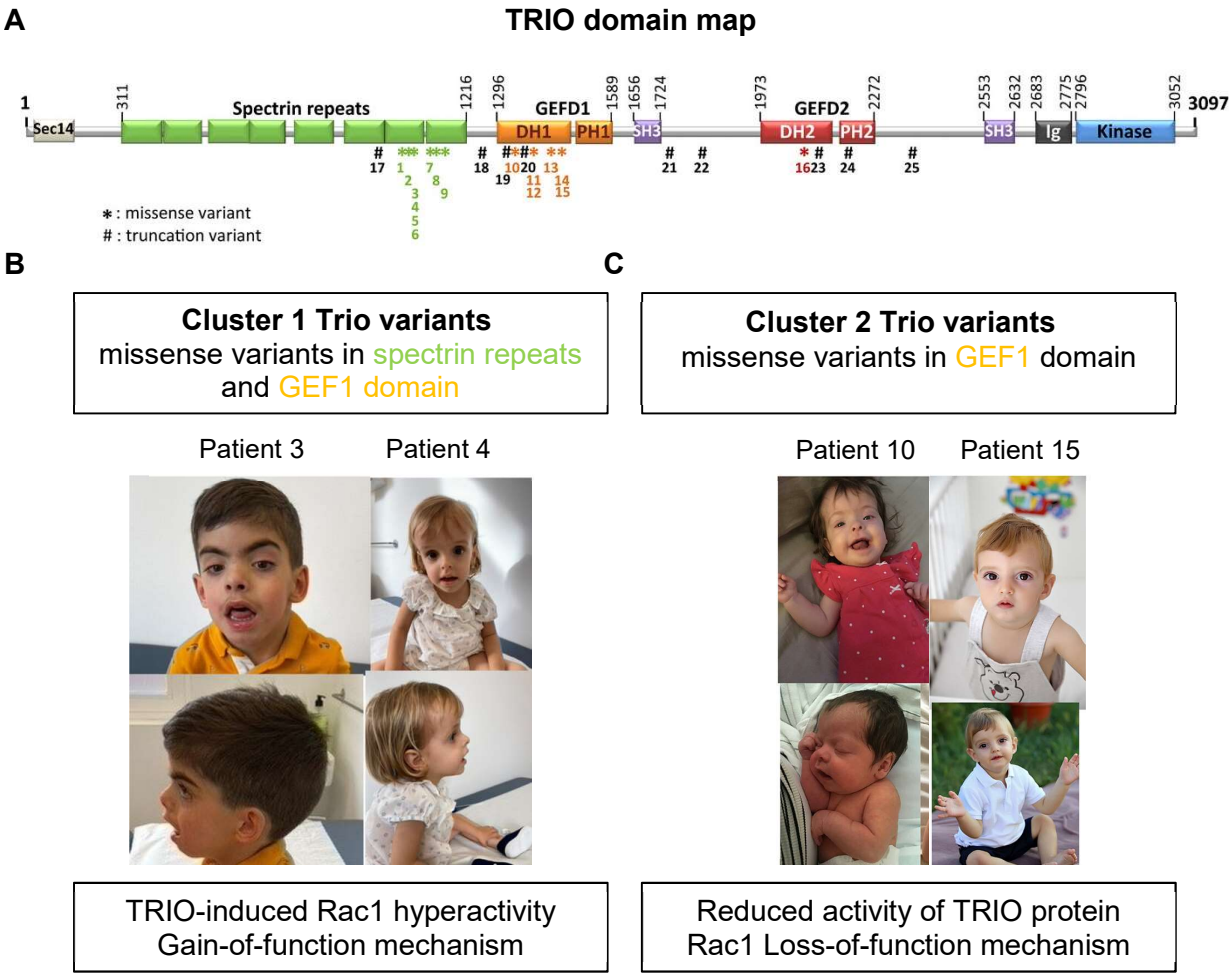

Figure 1.1 Pathogenic Trio mutations. **(A)** TRIO domain map displaying the position of missense and truncation variants in patients described in (Gazdagh et al., 2023). **(B)** Patients with cluster 1 Trio variants. Cluster 1 variants exhibit mutations in either the spectrin repeats or the GEF1 domain, resulting in hyperactivation of Rac1, which induces macrocephaly and severe developmental delays in affected patients. **(C)** Patients affected by cluster 2 *TRIO* variants, which feature mutations in the GEF1 domain, result in reduced Rac1 activity and are associated with microcephaly and mild intellectual disability. Figure modified after (Gazdagh et al., 2023).

TRIO has also been identified as a contributing factor in cancer progression (reviewed in (Schmidt and Debant, 2014)). Increased *TRIO* gene expression and protein levels are found in a variety of cancer types leading to enhanced cancer invasiveness (reviewed in (Bircher and Koleske, 2023; Kempers et al., 2021)). As Trio is a major regulator of cell migration, it is not surprising that mutations and upregulation of Trio are found in several types of cancer

(Kempers et al., 2021). In patients with breast cancer, glioblastoma and hepatocellular carcinoma, higher TRIO expression correlates with poor prognosis (Lane et al., 2008; Salhia et al., 2008; Wang et al., 2015). In colorectal cancer, TRIO GEF2 induced RhoA activation enhanced cancer cell migration, while Rac1 levels were not affected (Sonoshita et al., 2015). Furthermore, TRIO expression is elevated in osteosarcoma cells and promotes proliferation and invasiveness via Rac1 and RhoA activation (Wang et al., 2021).

In order to understand human diseases associated with Trio mutations and defective Trio protein regulation, it is of great interest to investigate the molecular functions of Trio in fine-tuning Rac1 and RhoA activity during cell migration processes. Ultimately, this will be an important step in the discovery of novel therapeutics for the treatment of Trio-related diseases.

1.2 Rho GEF Trio protein family and domains

Among the large family of Rho GEF proteins only the Trio protein family is known to feature two guanine nucleotide exchange factor (GEF) domains. In vertebrates, the paralogs Trio and Kalirin exist, while in invertebrates, the orthologs UNC-73 in *Caenorhabditis elegans* and dTrio in *Drosophila melanogaster* are known (Fig. 1.2) (Schmidt and Debant, 2014). The protein family is named Trio as their members display three catalytic domains, including the two GEF domains (GEF1 and GEF2) and a serine/threonine kinase domain. The GEF1 domain activates both GTPases Rac1 and RhoG, whereas the GEF2 domain exclusively activates RhoA (Bellanger et al., 2003; Debant et al., 1996). Furthermore, Trio family proteins harbor additional domains with slight variations among species, including a CRAL-Trio/Sec14 motif, multiple spectrin-like repeats, one or two Src homology 3 (SH3) motifs and zero to one Immunoglobulin (Ig) and Fibronectin (FnIII) domains. The Trio protein structure is highly conserved in different organisms (Schmidt and Debant, 2014). Variations in protein structure occur after the second GEF domain, where only vertebrate Trio and Kalirin feature a kinase domain. Trio proteins can be alternatively spliced, leading to different isoforms (Fig. 1.3). The expression profile of these isoforms varies between tissues and developmental stages. The full-length Trio protein is expressed ubiquitously, while shorter isoforms, which differ in their C-terminus, appear to be specifically expressed in the nervous system. These isoforms feature either one or both GEF domains, suggesting their potential in regulating Rac1 and RhoA activity in varying ways (Bircher and Koleske, 2023; Rabiner et al., 2005; Schmidt and Debant, 2014). Additionally, an oncogenic isoform of Trio (Tgat) has been identified in patients with adult T-cell leukemia. Tgat features only the GEF2-DH domain and a short C-terminal peptide and has been shown to promote tumor formation (Yoshizuka et al., 2004).

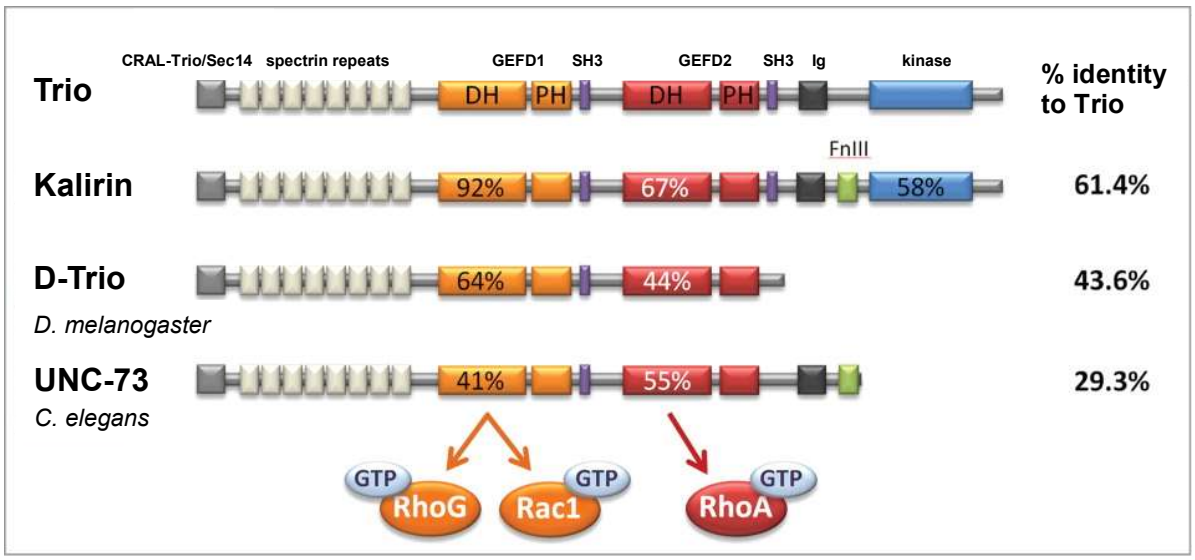

Figure 1.2 Trio protein family. The name Trio refers to the three catalytic domains: GEF1, GEF2 and serine/threonine kinase domain. Furthermore, Trio features additional domains: CRAL-Trio/Sec14 motif, multiple spectrin-like repeats, one or two SH3 motifs and zero to one Ig and FnIII domains. The Trio family consists of the two vertebrate paralogs, Trio and Kalirin, and the two invertebrate Trio orthologs, UNC-73 in *C. elegans* and dTrio in *D. melanogaster*. The protein structure is higly conserved among the different species. Percentage of protein sequence identity between Trio and other members is displayed (Schmidt and Debant, 2014).

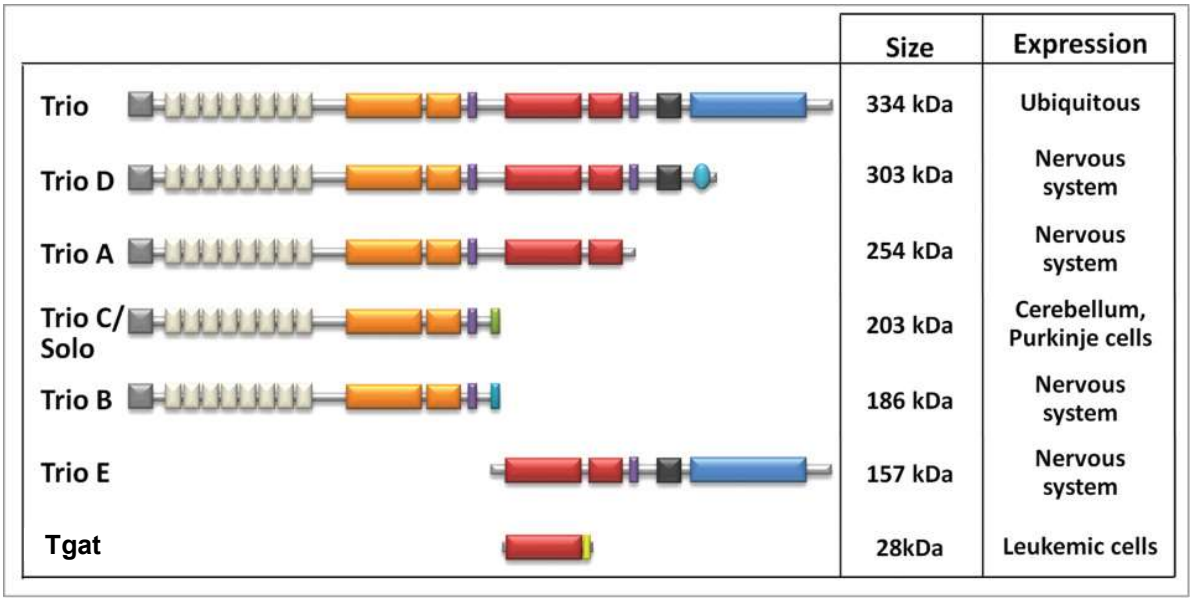

Figure 1.3 Trio isoforms. Known Trio isoforms that differ in the C-terminus, with one encoding only the C-terminal GEF2 and kinase domain (Trio E). Expression of these isoforms varies between tissues. In addition, an oncogenic Trio isoform, called Tgat, has been isolated in patients with adult T-cell leukemia (Schmidt and Debant, 2014).

1.3 Trio domains: function, catalytic activity and regulation

1.3.1 Trio GEF domains

In general, most of the literature is centered around the role of the two Trio GEF domains. Thereby, the majority focuses on the GEF1 domain, while there is less information available regarding the GEF2 domain (Rojas et al., 2007). The Trio GEF domains can activate the small Rho GTPases RhoG, Rac1 and RhoA (Blangy et al., 2000; Debant et al., 1996). Rho GTPases are molecular switches that alternate between an inactive state bound to GDP and an active state bound to GTP. Rho GEFs catalyze the exchange of GDP to GTP, thereby activating these small GTPases. This induces a conformational change of the GTPase, enabling the interaction with specific effectors, which leads to downstream signal transduction. Finally, it results in the regulation of numerous processes, such as cell adhesion, polarity and migration. GTPase activating proteins (GAPs) catalyze the hydrolysis of GTP, thereby inactivating the GTPase. Furthermore, the family of guanine dissociation inhibitors (GDIs) can form inactive complexes with GTPases and thereby segregate them to maintain their inactivity in the cytosol and prevent GDP/GTP cycling. These complexes also facilitate the rapid translocation of inactive GTPases to any membrane within the cell, thereby accelerating the response to specific signals (Etienne-Manneville and Hall, 2002; Hodge and Ridley, 2016; Wang et al., 2022).

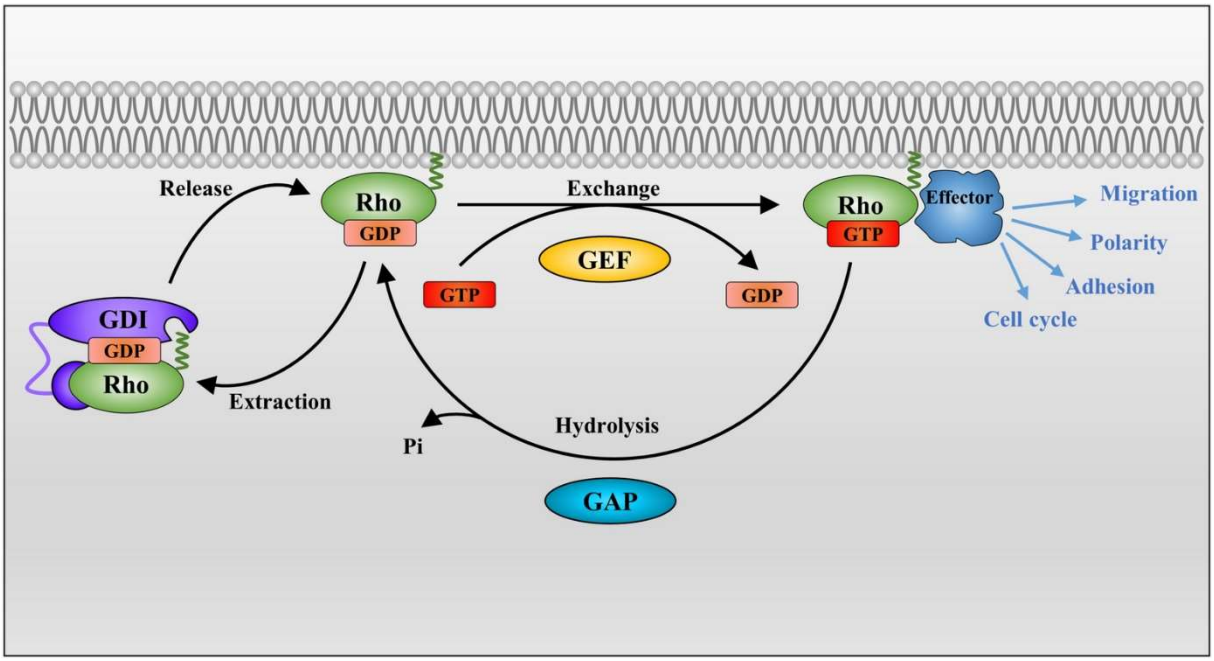

Figure 1.4 Rho GTPase cycle. Inactive GDP-bound Rho GTPases can be activated by Rho GEFs, that catalyze the exchange of GDP to GTP. The conformation of the Rho GTPase changes, thereby activating effectors and triggering biological processes such as cell polarity, adhesion and migration. Rho GAPs have the ability to bind activated Rho GTPases and facilitate the hydrolysis of GTP to GDP, leading to the inactivation of the Rho GTPase. Rho GDIs can bind Rho GTPases, restricting GDP/GTP cycling at the plasma membrane (Wang et al., 2022).

Rho-GEFs share a catalytic Dbl-Homology (DH) and a Pleckstrin Homology (PH) domain. While the DH domain functions as the catalytic active domain, the PH domain facilitates GTPase activation and promotes GEF localization to membrane structures via the binding to phosphoinositides or to membrane-associated proteins (Bellanger et al., 2003; Lemmon and Ferguson, 2000). For the Trio GEF1 domain, it has been demonstrated that the PH1 domain facilitates the DH1 domain binding to the Rho-GTPase Rac1. Subsequently, the DH1 domain can initiate the exchange from GTP to GDP to activate either Rac1 or RhoG (Bellanger et al., 2003). Recently, different groups have discovered a new regulatory mechanism for the GEF1 domain. The activity of GEF1 is autoinhibited by the nine N-terminal spectrin repeats, which cluster in a ring-like structure around the GEF1 domain. As a result of this interaction, GEF1 is incapable of binding Rac1 (Fig. 1.5). This suggests that Trio's spectrin repeats serve as a target for interaction partners. Those interaction partners could either engage Trio GEF1 mediated Rac1 activation by releasing the spectrin repeat ring formation or enhance the GEF1-spectrin repeat interaction to prevent Rac1 activation, resulting in spatiotemporal regulation of Rac1 activity (Bandekar et al., 2022; Bircher et al., 2022; Bonnet et al., 2023).

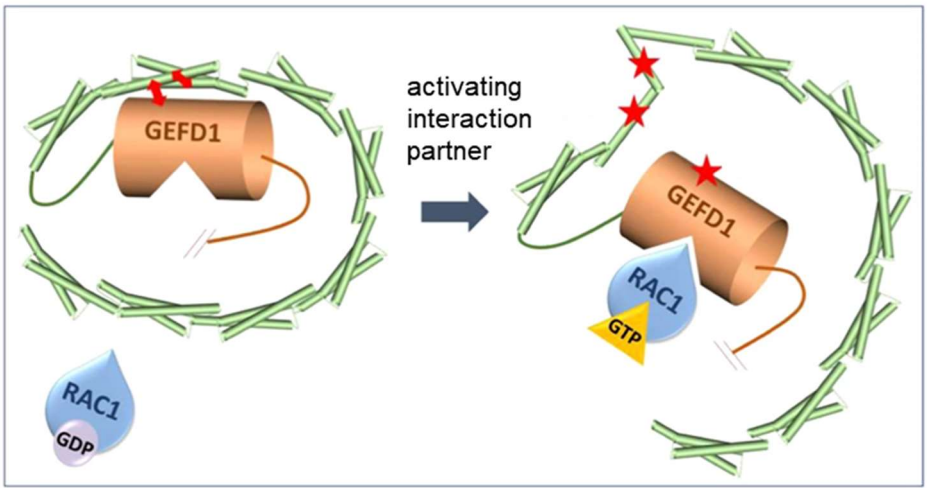

Figure 1.5 Structural model showing Trio GEF1 autoinhibition via spectrin repeats. Intramolecular folding of the spectrin repeats, that surround and bind the GEF1 domain, prevents GEF1 access to Rac1. Binding of an activating interaction partner possibly releases the intramolecular autoinhibition, allowing GEF1 access to Rac1. Red arrows indicate the amino acid position necessary to stabilize the binding of the spectrin repeats to the GEF1 domain. Red stars indicate positions of possible missense mutations that can lead to defective autoinhibition via the spectrin repeats and result in Rac1 hyperactivation (discussed in chapter 1.1). Figure modified after (Bonnet et al., 2023).

The Trio GEF2 domain consists of a DH2 and PH2 domain as well and selectively activates the Rho-GTPase RhoA (Debant et al., 1996). Unlike the GEF1-PH1 domain, the GEF2-PH2 domain acts as an inhibitory modulator of the DH2 domain and abolishes RhoA activation (Bellanger et al., 2003). Whether the PH2 domain completely prevents RhoA activation and how DH2-mediated RhoA activation is regulated still remains largely unclear. It was shown that

the heterotrimeric guanine nucleotide–binding protein (G protein) $G\alpha_q$ is an upstream regulator of the Trio GEF2 domain. $G\alpha_q$ binds to the PH2 domain and thereby prevents autoinhibition and stimulates RhoA activation via the GEF2-DH2 domain (Lutz et al., 2007; Williams et al., 2007). In general, an extracellular ligand can bind to membrane-bound $G\alpha_q$ leading to an $G\alpha_q$ activation, which in the end activates the Rho-GTPase at the plasma membrane (Kamato et al., 2017). However, which extracellular ligands could induce this signaling pathway is unknown. Thus, spatiotemporal regulation of the GEF2 domain may also be mediated via binding of interaction partners to relieve intramolecular autoinhibition.

1.3.2 Trio Kinase domain

In addition to the two GEF domains, Trio features a third catalytic domain at its C-terminal end, the serine/threonine kinase (STK) domain. So far it is still unclear whether this domain has catalytic activity (Schmidt and Debant, 2014). In support of a biological function of the kinase domain, it was shown that Trio binds the focal adhesion kinase (FAK) via its SH3, Ig and STK domains (Medley et al., 2003). Thereby, Trio activates FAK autophosphorylation, and bi-directional FAK phosphorylates the Trio STK domain. Furthermore, Trio and FAK co-localize at the cell periphery, suggesting a possible role for Trio in focal adhesion dynamics and cell motility (Medley et al., 2003). Overexpression of the kinase domain of the Trio paralog Kalirin has been shown to enhance neurite outgrowth. In contrast, a predicted catalytically inactive Kalirin kinase domain mutant blocked neurite extension (Yan et al., 2015). These findings suggest a physiological role for the STK domain, but its regulation, interaction partners and target substrates remain unknown.

1.3.3 Additional Trio domains

CRAL-Trio/Sec14 domains have the ability to bind small lipophilic molecules and are often found in multidomain proteins that activate small GTPases (Saito et al., 2007). The Sec14 domain of Kalirin was shown to have a unique ligand binding groove, suggesting an important role for protein-lipid interactions (Li et al., 2023).

Downstream of the Sec14 domain, Trio contains 9 spectrin repeats (Bircher et al., 2022). These are found in many proteins associated with the actin cytoskeleton (Djinovic-Carugo et al., 2002). Additionally to the inhibitory intramolecular regulation described above, spectrin repeats are thought to act as scaffolding domains for signaling complexes (Djinovic-Carugo et al., 2002). For example, the myosin II regulatory protein Supervillin has been reported to directly interact with the spectrin repeat region of Trio and Kalirin (Son et al., 2015).

SH3 domains are often found in close proximity to GEF PH-DH domains (Yohe et al., 2008). Trio possesses two SH3 domains, located directly behind the GEF1 and GEF2 domain (Schmidt and Debant, 2014). SH3 domains bind to polyproline motifs, mediate protein-protein interactions and might bind intramolecular to mediate conformational changes (Kurochkina and Guha, 2013).

At the C-terminal end, Trio has an immunoglobulin (Ig) domain that is located right before the STK domain (Schmidt and Debant, 2014). Ig domains primarily function as sites for protein-protein interactions in the context of the actin cytoskeleton (Otey et al., 2009). According to one study, the Ig domain of Trio has the ability to bind to the prenylated form of RhoA-GTP (Medley et al., 2000). In that model, Trio GEF2 generates RhoA-GTP, which anchors Trio to the plasma membrane via the Ig domain, suggesting that RhoA activity is involved in mediating Trio localization and coordinating Trio signaling.

In summary, Trio encompasses several domains that engage in protein and lipid binding, together with regulatory domains that impact the function of both GEF domains. Taken together, this suggests that Trio is precisely designed to control Rho GTPase activity in a spatiotemporal manner. This may be mediated not only through the GEF domains, but also via the multiple domains contained in the large protein.

1.4 Relevance of Trio in different tissues and associated interaction partners

Trio plays a crucial role in a variety of tissues, particularly during embryonic development (reviewed in (Bircher and Koleske, 2023)). During neuronal development, Trio is essential for axon outgrowth and guidance, dendritic spine morphogenesis and brain development (DeGeer et al., 2015; van Haren et al., 2014; Vanderzalm et al., 2009). Furthermore, Trio is involved in the regulation of E-Cadherin expression in epithelial adherens junctions (Yano et al., 2011) and supports the formation of the characteristic restrictive endothelial barrier by VE-Cadherin recruitment to adherens junctions (Kruse et al., 2019). Mediated through M-Cadherin, Trio-induced activation of Rac1 appears to participate in skeletal myogenesis (Charrasse et al., 2007). During the process of cell migration, Trio plays a crucial role in coordinating cytoskeletal structures, including actin and microtubules (Bellanger et al., 2000; van Haren et al., 2014). Regarding these cytoskeletal rearrangements, several upstream signaling binding partners have been described that regulate the activity of RhoA and Rac1 via the distinct Trio GEF domains (Tab. 1). In addition, Trio has an effect on cellular adhesion, which is required for proper cell spreading (Son et al., 2015). Furthermore, Trio is important for NC cell migration (Tab. 1), which will be outlined in detail in the subsequent sections. Table 1 summarizes the majority of identified Trio interaction partners. The interaction partners are categorized according to their role in Trio signaling in various physiological processes, and their biological relevance is briefly described. In conclusion, this demonstrates various ways in which Trio activity can be regulated in different biological contexts and tissues to precisely control Rho GTPase activity in a spatiotemporal manner.

Table 1 Summary of Trio interaction partners relevant for neuronal development, endothelial junctions, epithelial invagination, skeletal myogenesis and cell migration.

Neuronal development			
Interaction partner	**Binding site**	**Biological relevance**	**Reference**
Neuron Navigator 1 (NAV-1)	NAV-1 binds Trios N-terminal Sec14 domain and spectrin repeats	TRIO is recruited to microtubule plus-ends by both NAV-1 and EB1. The resulting NAV-1-TRIO complexes serve to stimulate Rho GTPase signaling locally, acting at the interface between microtubule dynamics and remodeling of the actin cytoskeleton in neuronal growth cones.	(van Haren et al., 2014)
EB1	Trio binds EB1 via its first SxIP motif	TRIO is recruited to microtubule plus-ends via NAV-1 and EB1. Dynamic microtubules regulate formation and localization of the NAV-1-TRIO complex and trigger Rac1 activation essential for proper neurite outgrowth.	(van Haren et al., 2014)
Myosin X	Trio binds Myosin X via the N-terminal SH3 domain	Interaction between Trio and Myosin X mediates the adhesion of migrating neurons to radial glial fibers by regulating the membrane localization of N-Cadherin.	(Wei et al., 2022)
CARMIL (capping protein, Arp2/3, myosin I linker)	CRML-1 and UNC-73 (*C. elegans* homolog of Trio) form a complex *in vivo*	CRML-1 (*C. elegans* homolog of CARMIL) controls cell and axon migrations by inhibiting Trio and, consequently, Rac1 signaling.	(Vanderzalm et al., 2009)
Abelson tyrosine kinase (Abl)	No direct binding shown	In the embryonic central nervous system, *Drosophila trio* and *Abl* work together to regulate axon outgrowth.	(Forsthoefel et al., 2005; Liebl et al., 2000)

Slit2	Slit2 may mediate Trio RhoA activity via Robo, no direct interaction	Trio signaling downstream of Slit2 activates RhoA, playing a crucial role in embryonic development by facilitating axon outgrowth and pathfinding and neuronal migration.	(Backer et al., 2018)
Molecular chaperone heat shock cognate protein 70 (Hsc70)	Hsc70 is dynamically associated with the Trio GEF1 domain	Hsc70 is required for netrin-1 mediated axon growth via Trio mediated Rac1 activation.	(DeGeer et al., 2015)
Rabin 8	Trio binds Rabin 8 via spectrin repeats	TRIO interacts with and activates RABIN8, which is required for proper trafficking of membrane vesicles from the neuronal soma to the growth cone.	(Tao et al., 2019a)
Endothelial adhesion			
Interaction partner	**Binding site**	**Biological relevance**	**Reference**
VE-Cadherin	Trio interacts via its N-terminal region, but not the GEF1 domain, with a region in the intermediate domain of VE-Cadherin, proximal to the β-catenin-binding domain	Trio GEF1 promotes Rac1 activation, resulting in the recruitment of VE-Cadherin to adherens junctions, while Trio GEF2 activates RhoA, leading to increased intracellular tension that reinforces Rac1 activation. This facilitates the formation of VE-Cadherin junctions and the characteristic restrictive endothelial barrier.	(Kruse et al., 2019; Timmerman et al., 2015)
N-Cadherin	Trio is recruited to N-Cadherin complexes via its N-terminus	N-Cadherin-Trio complex formation triggers Rac1 activation, subsequently stimulating the formation of VE-Cadherin junctions.	(Kruse et al., 2019)

Epithelial adhesion			
Interaction partner	**Binding site**	**Biological relevance**	**Reference**
Shroom3	unknown if Trio binds to Shroom3	Trio RhoA signaling is necessary for Shroom3-dependent apical constriction in MDCK cells and in the lens pit. Possibly, a complex comprising Trio, RhoA, Shroom3 and Rock1/2 stimulates the contractile actin-myosin network, resulting in apical constriction.	(Plageman et al., 2011)
E-Cadherin	Trio binds the cytoplasmatic domain of E-Cadherin	Trio mediated Rac1 activation is inhibited by Tara in epithelial cells to maintain E-Cadherin levels.	(Yano et al., 2011)
Skeletal myogenesis			
Interaction partner	**Binding site**	**Biological relevance**	**Reference**
M-Cadherin	Trio and Rac1 form a complex with M-Cadherin during the initiation of myoblast fusion	M-Cadherin–dependent Rac1 activation via Trio positively regulates myoblast fusion.	(Charrasse et al., 2007)
Cell migration			
Interaction partner	**Binding site**	**Biological relevance**	**Reference**
LAR protein tyrosine phosphatase	Trio-Ig-STK domain interacts with LAR-D2 PTPase domain	LAR-Trio complex may coordinate cytoskeletal rearrangements like actin polymerization and actin stress fiber and focal adhesion formation.	(Debant et al., 1996)

Focal adhesion kinase (FAK)	Trio binds via its SH3-Ig-like region and kinase domain to the FAK N-terminal portion including the kinase domain	Trio enhances FAK kinase activity by inducing FAK autophosphorylation, while FAK phosphorylates Trio. Trio-FAK interaction may be involved in regulating focal adhesion dynamics and cell motility.	(Medley et al., 2003)
Tara (Trio-associated repeat on actin)	Tara binds the Trio GEF1 domain	Tara directly binds and stabilizes F-actin trough Tara-Trio complexes to coordinate actin remodeling.	(Seipel et al., 2001)
ICAM-1 (Intercellular adhesion molecule 1)	ICAM-1 interacts with the Trio GEF1 domain	Mediated by ICAM-1, Trio facilitates the trans endothelial migration of leukocytes by activating Rac1 and RhoG in a filamin-dependent manner, leading to the formation of an endothelial docking structure.	(van Rijssel et al., 2012)
Supervillin 4	Trio binds Supervillin 4 directly via the spectrin repeats 6 and 7	Supervillin 4, recruited to focal adhesions through myosin II, induces Trio-mediated Rac1 activation and disassembly of cell-substrate adhesions to promote cell spreading.	(Son et al., 2015)
Filamin A	Trio PH1 domain binds to Filamin A	Trio-Filamin A interaction recruits Trio to actin structures, which is required for actin cytoskeleton remodeling.	(Bellanger et al., 2000)

$G\alpha_{q/11}$	$G\alpha_{q/11}$-GTP binds to the GEF2-DH-PH domains to activate RhoA	$G\alpha_{q/11}$-GTP activates Trio by relieving the autoinhibitory function of the PH2 domain. This leads to RhoA activation via the GEF2 domain. It is suggested that TrioC exists in an equilibrium of autoinhibited and active conformations. Trio mutations shift this equilibrium to the active state and lead to cancer progression.	(Bandekar et al., 2019)
NC cell migration			
Interaction partner	**Binding site**	**Biological relevance**	**Reference**
Cadherin-11	Trio binds to the intermediate domain in Cadherin-11	Trio is required for Cadherin-11-mediated protrusive activity during NC cell migration. In addition, Trio acts downstream of Cadherin-11 to activate Rac1 in migratory breast cancer cells.	(Kashef et al., 2009; Li et al., 2011)
Dishevelled	Trio GEF2 domain interacts with the Disheveled DEP domain	Trio promotes NC protrusion formation via interaction with Dishevelled, that leads to Rac1 activation. Trio/DVL/Rac1 signaling likely functions downstream of xCadherin-11.	(Kratzer et al., 2020)
Par3	Trio and Par3 co-localize in NC cells, binding site is unknown	Par3 controls CIL by inhibiting Trio-mediated activation of Rac1 at cell-cell contacts.	(Moore et al., 2013)
Myosin heavy chain 9 (Myh9)	Trio interacts with the Myh9 head domain via its GEF1 domain	Trio promotes NCC migration by interacting with Myh9 at cell-cell contacts and cell protrusions.	(Guo et al., 2021)

1.5 Function of Trio in cell migration

Given its ubiquitous expression and two GEF domains capable of regulating Rac1 and RhoA activity, it is not surprising that Trio plays a crucial role in cell migration (Bircher and Koleske, 2023; Grubisha et al., 2022). In general, cell migration is an essential mechanism involved in physiological processes such as development, immune response and wound healing (Mayor and Etienne-Manneville, 2016), whereby Rac1 and RhoA are key regulators of the dynamically organized cytoskeleton (Warner et al., 2019).

1.5.1 RhoA and Rac1 signaling

Several studies have demonstrated that it is not absolute levels of activity, but rather strict spatiotemporal regulation of Rac1 and RhoA that is required to achieve coordinated cytoskeletal modulations (Benink and Bement, 2005; Fritz et al., 2013; Machacek et al., 2009; Rajnicek et al., 2006; Woo and Gomez, 2006). This special precision can coordinate multiple GTPases in subcellular pools to operate with temporal synchrony regulating different events (Grubisha et al., 2022). In order to control these specific activity patterns, Trio provides a unique design with two GEF domains to precisely modulate the Rac1/RhoA balance in a spatiotemporal manner (Grubisha et al., 2022). Depending on the interactions between the upstream GEFs or, in the case of Trio, between the GEF1 or GEF2 domain and the downstream effectors, distinct subcellular localizations of these macromolecular clusters can coordinate GTPase-induced cytoskeletal behavior (Mertens et al., 2005; Pegtel et al., 2007). For example, during cell migration, RhoA controls cell contractility at the trailing edge via ROCK (Spiering and Hodgson, 2011), whereas at the leading edge, RhoA activity functions in microtubule stabilization via mDia (Pertz et al., 2006) and is also required to promote filopodia formation via the formin FHOD3 (Paul et al., 2015). Rac1 has a prominent function at the leading edge of cells, where it takes part in the formation of lamellipodia and filopodia through actin nucleation (Warner et al., 2019). In detail, Rac1 activates the WAVE regulatory complex (WRC) to stimulate Arp2/3 complex-mediated actin polymerization, which is essential for the establishment of the leading edge (Campellone and Welch, 2010). Furthermore, Rac1 enables microtubule stabilization via PAK1-dependent phosphorylation and inactivation of stathmin, a protein that induces microtubule catastrophe (Wittmann and Waterman-Storer, 2001).

1.5.2 Microtubule organization and dynamics

Microtubules are one of the major components of the cytoskeleton and they control directional migration via a number of coordinated processes (reviewed in (Etienne-Manneville, 2013)). Microtubules are dynamic polymers consisting of α-tubulin and β-tubulin heterodimers. These tubulin dimers are built in a head-to-tail fashion generating intrinsic polarity. This polarity facilitates directed movement of motor proteins on the microtubule surface and enables directed transport of vesicles, proteins and RNAs. Furthermore, this polarity leads to different kinetics of subunit addition and loss at the two microtubule ends, defined as plus end (faster

growing) and minus end (slower growing). Microtubules undergo dynamic instability, meaning they exhibit cycles of growth, shortening and regrowth. These microtubule dynamics have been shown to regulate actin dynamics, Rho GTPase signaling and focal adhesion turnover. Furthermore, microtubules enable signaling functions depending on the formation and release of the microtubule +TIP (microtubule plus-end tracking protein) complex. This complex assembles at the growing microtubule plus-end and is a dynamic network of proteins, regulating microtubule dynamics and interactions (reviewed in (Akhmanova and Steinmetz, 2010)). The core +TIP network is formed by the end-binding proteins EB1, EB2 and EB3 (also named MAPRE (microtubule associated protein member 1-3). These built a binding platform for a large number of proteins via specific +TIP localization motifs. While MAPRE1 and MAPRE3 are required for microtubule growth and stabilization (Komarova et al., 2009), MAPRE2 plays a role in the reorganization of microtubules during early apical-basal differentiation in epithelia, regulation of cell adhesion and mitotic progression (Goldspink et al., 2013; Iimori et al., 2016; Yue et al., 2014). Trio also acts as a +TIP by interacting with EB1 via a SxIP (Ser-x-Ile-Pro) motif (van Haren et al., 2014), which serves as microtubule plus-end localization signal (Honnappa et al., 2009). The recruitment of Trio to microtubules is required for neurite outgrowth and stabilization of the microtubule network in neurons (van Haren et al., 2014). It was shown that the +TIP Navigator 1 forms a complex with Trio at microtubule plus-ends, operating at the interface between microtubule dynamics and actin cytoskeleton remodeling by a local Trio-mediated Rac1 activation in neuronal growth cones (van Haren et al., 2014). Furthermore, it was shown, that EB1 recruits the CLIP-170-mDia1 complex to microtubule plus-ends to trigger actin polymerization and lamellipodia formation (Henty-Ridilla et al., 2016). In addition, Rho GEF-mediated activation of RhoA controls mDia induced detyrosination of microtubules, a marker of stable microtubules (Palazzo et al., 2001). Another major effect of microtubules on the actin network is the regulation of Rac1 and RhoA activation by microtubule polymerization and depolymerization (Palazzo and Gundersen, 2002; Waterman-Storer et al., 1999). At the leading edge, microtubules are involved in focal adhesion dynamics, mediated via GEF induced RhoA activation (Fig. 1.6) (Seetharaman and Etienne-Manneville, 2019).

1.5.3 Focal adhesion dynamics

Migrating cells are in constant communication with the extracellular matrix (ECM) (reviewed in (Etienne-Manneville, 2004)). This communication is mediated by adhesion complexes that include integrin receptors and focal adhesions physically linking the cell with the ECM. Focal adhesions connect the ECM with the cell cytoskeleton, thereby facilitating the migration of cells on the surrounding tissue. Focal adhesions are highly dynamic and a precise control of their turnover is essential for effective forward translocation of the cell body and persistent motility. Actin-myosin stress fibers are anchored at focal adhesions and RhoA promotes the formation of both to increase cell contractility (reviewed in (Etienne-Manneville, 2004)). Microtubules

precisely target focal adhesions, where their growth is paused and switches to shortening (Kaverina et al., 1998). This growth-to-shortening transition is seven times higher at focal adhesions than elsewhere and involves the focal adhesion component paxillin (Efimov et al., 2008). Furthermore, paxillin is phosphorylated by FAK, which also regulates microtubule stability (Palazzo et al., 2004) and is required for microtubule-mediated focal adhesion disassembly (Schober et al., 2007). Here, Trio may also play a role in regulating focal adhesion dynamics, as it localizes to microtubule plus-ends via EB1 binding, thereby initiating the transport of Trio to focal adhesion sites. Furthermore, Trio localizes to paxillin-positive focal adhesions (Müller et al., 2020) and enhances the activity of FAK (Medley et al., 2003). To regulate focal adhesion turnover, there is a bidirectional crosstalk between stress fibers located at focal adhesions and microtubules. This crosstalk is guided by Rho-GTPase signaling. Microtubule-mediated transport of Rho regulators may be critical for the establishment of Rho GTPase activity zones, which have been shown to be necessary at focal adhesion sites and at the leading edge (Müller et al., 2020; Stehbens and Wittmann, 2012). Initially, stress fibers guide microtubules towards focal adhesions. Contact of microtubules with focal adhesions mediates microtubule stabilization. Microtubule stability is regulated by RhoA and its effector mDia. In addition, RhoA activity is required for stress fiber formation and focal adhesion assembly. Thereby, stress fibers create a positive feedback loop, by generating a contractile force, which leads to focal adhesion formation. In contrast, microtubules generate a negative feedback loop, as they are targeted to focal adhesions via actin fibers, leading to focal adhesion disassembly (Figure 1.6). In conclusion, the coexistence of stress fibers and stable microtubules at focal adhesions provides the cell with a sensitive adhesion system and shows the relevance for a fine-tuned regulation of Rho GTPases at focal adhesion sites (reviewed in (Etienne-Manneville, 2004)).

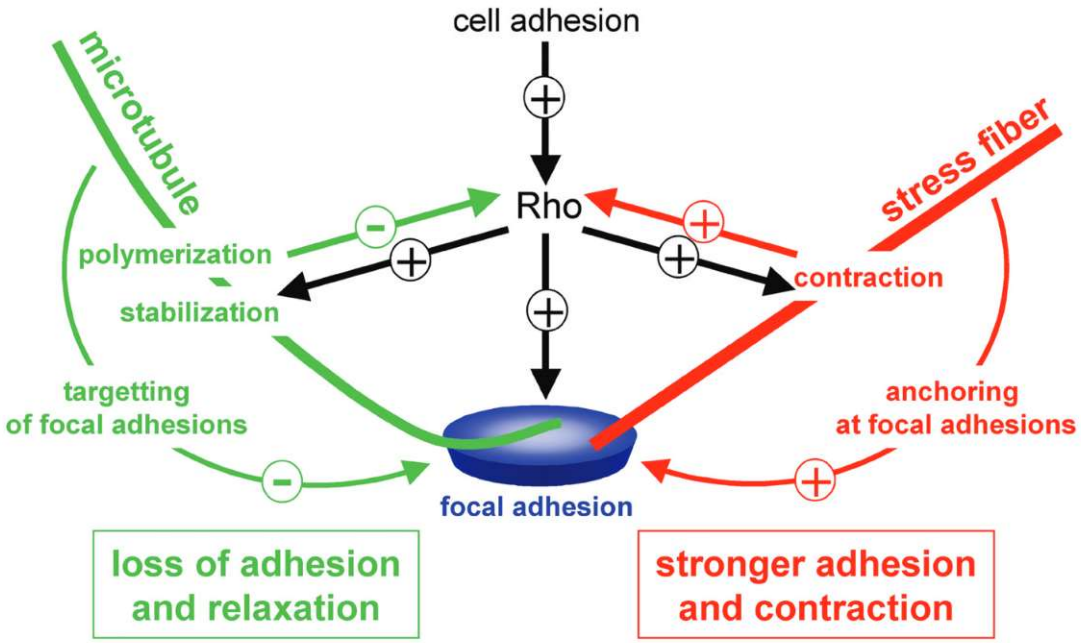

Figure 1.6 Actin and microtubule crosstalk regulates focal adhesion turnover. Integrin-mediated cell adhesion to the ECM results in the activation of RhoA and the formation of focal adhesions (blue). RhoA promotes the formation of contractile stress fibers. Through a positive feedback loop, the constriction of stress fibers and activation of RhoA results in the enlargement of focal adhesions (red). Furthermore, RhoA facilitates microtubule stabilization, while actin bundles guide microtubules towards focal adhesions. Microtubule polymerization towards focal adhesions locally inhibits RhoA and induces focal adhesion disassembly (green) (Etienne-Manneville, 2004).

1.6 The role of Trio in development and neural crest cell migration

As described in chapter 1.1, Trio has an evolutionary conserved role in the development of the nervous system. Furthermore, Trio is required for NC cell migration during development of the embryo (Kashef et al., 2009; Kratzer et al., 2020; Moore et al., 2013). After migration, cranial NC cells contribute to craniofacial structures, such as the bones and cartilage of the face, muscles and connective tissues of the ear and eye, teeth, and blood vessels (reviewed in (Mayor and Theveneau, 2013)). In addition, they generate pigment cells and contribute to the development of the peripheral nervous system in the head, brain growth and patterning, and certain aspects of cardiac development. Trunk NC cells give rise to pigment cells, the dorsal root, sympathetic ganglia and endocrine cells in the adrenal gland. The enteric NC cells are necessary for the development of the gastrointestinal tract and the enteric nervous system, which regulates digestive tract function (Figure 1.7). Thus, defects in the process of NC cell migration can lead to multiorgan syndromes (Pilon, 2016), which have already been observed in patients with *TRIO* mutations (Gazdagh et al., 2023).

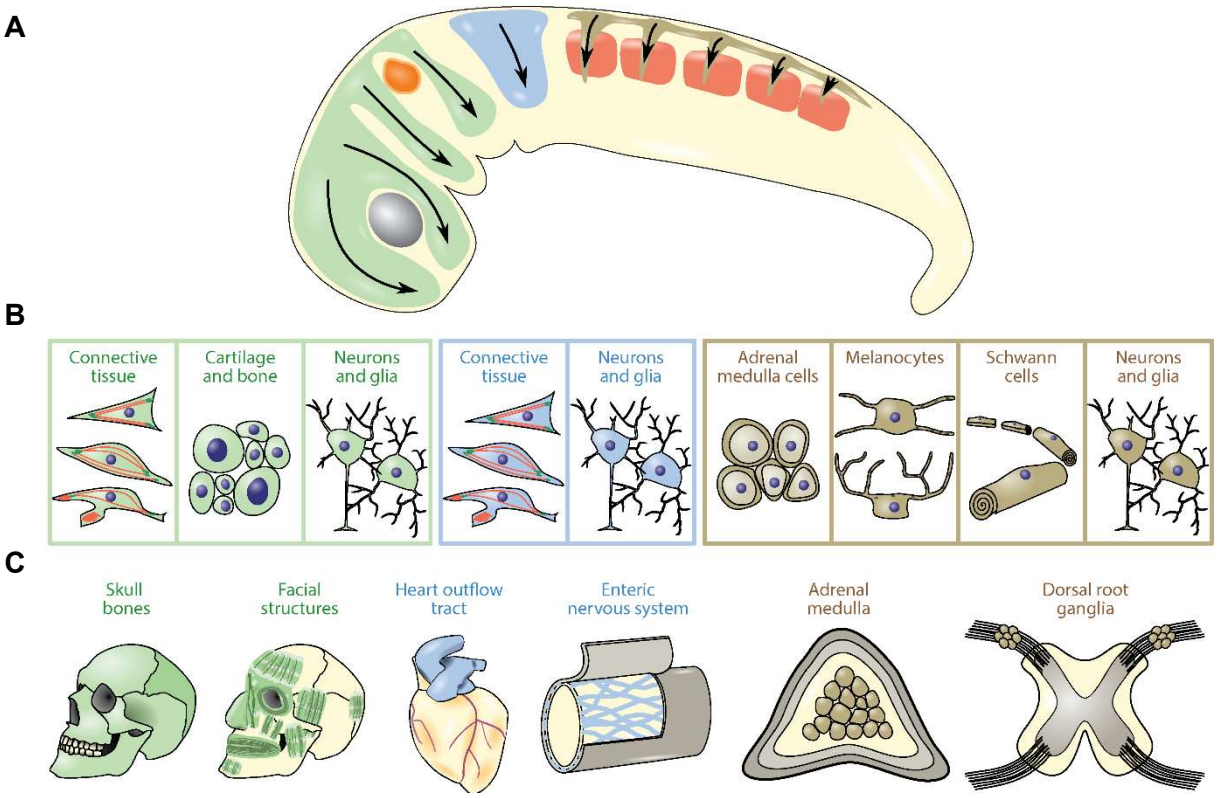

Figure 1.7 Neural crest cell delamination and differentiation. (A) The timing of delamination varies depending on the position, with thick streams delaminating simultaneously in cranial regions and thin streams delaminating progressively in the trunk along the anterior-posterior axis. **(B)** Examples of tissues that arise from the cephalic (green), vagal (blue) and trunk (brown) neural crest cells. **(C)** Examples of organs that originate from neural crest cells.

In *Xenopus* cranial NC cells, Trio is necessary for the formation of cell protrusions, cell migration, and development of the craniofacial cartilage (Kratzer et al., 2020). Thereby, filopodia and lamellipodia formation is controlled cell-autonomously via Trio-mediated Rac1 and RhoA activity (Kratzer et al., 2020). At cell protrusions, Trio interacts with Cadherin-11, which is likewise required for NC cell migration (Kashef et al., 2009). Cadherin-11 co-localizes with paxillin at focal adhesions and promotes cellular adherence to fibronectin via Syndecan-4 (Langhe et al., 2016). This adherence is necessary for NC cell spreading and adhesion to the extracellular matrix. Trio may also be involved in cell matrix adhesion, as described in chapter 1.5.3. Moreover, Cadherin-11 is required for contact inhibition of locomotion, maintaining collective cell migration via its adhesive function (Becker et al., 2013). It is hypothesized that Trio may play an important role in RhoA activation via Cadherin-11 at cell-cell contacts (Becker et al., 2013), as Trio was observed to be present at this location (Moore et al., 2013). Thus, Trio likely has different functions in NC cell migration depending on its subcellular localization. Supporting this hypothesis, Trio was shown to interact with the polarity protein Par3, which promotes CIL by inducing microtubule catastrophe through inhibition of Trio-induced Rac1 activation (Moore et al., 2013). In addition, Trio interacts with myosin heavy chain 9 (Myh9) at NC cell-cell contacts and cell protrusions, which is required for cell

contraction as well as cell migration (Guo et al., 2021). In general, Myh9 is known as a regulator of cytoskeletal reorganization and cell polarity, adhesion and migration (reviewed in (Wang et al., 2019)). Furthermore, Trio interacts via the GEF2 domain with Dishevelled, a known regulator of the Wnt signaling pathway (Kratzer et al., 2020). It was shown, that Dishevelled is able to restore Rac1 activity levels in Trio deficient *Xenopus* embryos. In conclusion, Trio seems to have different subcellular functions, and spatiotemporal regulation of Rac1 or RhoA activity may depend on its various interaction partners. Thereby, many cellular functions are regulated by Trio signaling, including cytoskeletal rearrangement, cell migration, axon outgrowth and pathfinding, and cell adhesion (reviewed in (Bircher and Koleske, 2023)). Furthermore, Trio plays a critical role in development and cancer metastasis. Recently, it was described that the spectrin repeats have an autoinhibitory effect on the Trio GEF1 domain (Bonnet et al., 2023). Specific interaction partners could either enhance inhibition or induce Rac1 activity. For the Trio GEF2 domain, only the inhibitory effect of the PH domain is currently known (Bellanger et al., 2003). Since previous research has primarily focused on the Trio GEF1 domain, it is worth further analyzing the molecular mechanisms regulating the activity of the Trio GEF2 domain, especially since the GEF2 domain is sufficient to restore NC cell migration (Kratzer et al., 2020).

Chapter 2

The end binding protein MAPRE2 is a regulator of craniofacial development

2. Introduction

MAPRE2 (microtubule associated protein member 2) is a member of the evolutionary conserved family of microtubule end binding (EB) proteins (Su and Qi, 2001). EB proteins bind to microtubule plus-ends and recruit additional +TIPs to regulate the microtubule-mediated interactions with diverse cellular structures (Galjart, 2010). MAPRE2 was shown to be necessary for the regulation of cell adhesion, mitotic progression and genome stability (Iimori et al., 2016; Liu et al., 2015; Yue et al., 2014), while MAPRE1 and MAPRE3 are required for the stabilization and persistent growth of microtubules (Komarova et al., 2009).

2.1 *MAPRE2* mutations induce craniofacial malformations in CSC-KT syndrome

Patient mutations in *MAPRE2* occurred within the calponin homology domain, which is required for microtubule plus-end binding (Isrie et al., 2015). Comparable to patients with *TRIO* gene mutations, individuals with *MAPRE* mutations display intellectual disability, microcephaly, and facial dysmorphism. Additionally, they exhibit symmetrical limb skin creases, a median cleft palate, and short stature (Isrie et al., 2015). These phenotypes were categorized as circumferential skin creases, Kunze type (CSC-KT) (Wouters et al., 2011), and *MAPRE2* as well as *TUBB* were identified as the genetic factors responsible for the condition (Isrie et al., 2015). *TUBB* is a beta-tubulin-encoding gene that is prominently expressed in the developing central nervous system (Sferra et al., 2020). A functional analysis of *TUBB* mutations utilizing fibroblasts revealed deficiencies in the polymerization of microtubules, vesicle trafficking and cell migration. The craniofacial malformations observed in CSC-KT patients are caused by misregulated NC cell migration (Isrie et al., 2015; Thues et al., 2021). Xenotransplantation of MAPRE2 loss-of-function neural crest cells into early developing chicken embryos demonstrated negligible migration (Thues et al., 2021). Although a knock-in patient mutation increased NC cell migration speed, the clinical features remained indistinguishable. Furthermore, focal adhesions are enlarged in MAPRE2 knock-out cells, while they are smaller and fewer in the knock-in mutant, suggesting a role for MAPRE2 in the crosstalk of microtubules with focal adhesions. In addition, like TRIO, MAPRE2 is involved in the migration and invasion of certain types of cancer (Abiatari et al., 2009). In summary, mutations in *MAPRE2*, *TUBB* and *TRIO* exhibit similar phenotypes and play a role in microtubule dynamics and focal adhesion formation during NC cell migration.

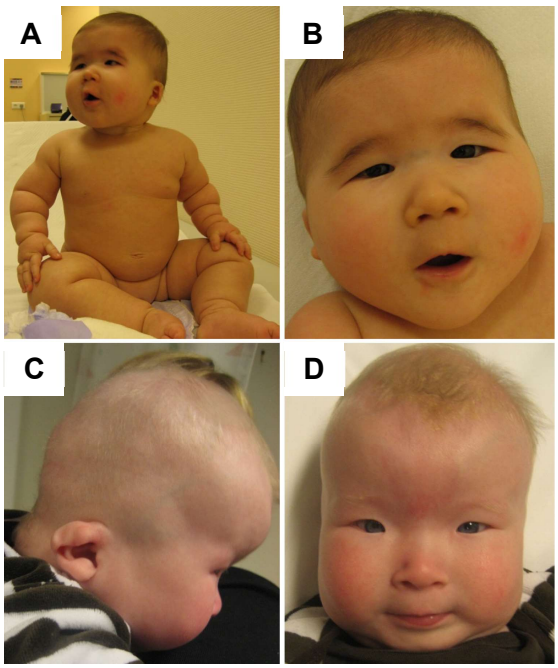

Figure 2 Clinical phenotypes of the CSC-KT syndrome. Clinical characteristics of affected individuals with a *MAPRE2* **(A-B)** or *TUBB* mutation **(C-D),** modified after (Isrie et al., 2015).

3. Aim of this study

The Rho GEF Trio features three catalytic domains, comprising two GEF domains and a kinase domain, is required for NC cell migration and promotes cell protrusion formation via the regulation of the small GTPases Rac1 and RhoA (Kratzer et al., 2020). We showed previously that the Trio GEF2 domain is sufficient to restore Trio loss-of-function induced NC cell migration defects in *Xenopus* embryos. Furthermore, our observations in explanted NC cells revealed a dynamic intracellular localization of the Trio GEF2 domain, which is possibly co-localizing with microtubules. Therefore, this study aims to investigate the localization and functions of the different Trio domains, with focus on the GEF2 domain, via live-cell imaging using different deletion constructs. To further determine Trio's role in NC cell migration, *in vivo* and *in vitro* migration assays will be employed. In addition, it will be analyzed, by applying live-cell imaging and immunostaining, if Trio knockdown affects focal adhesions in migrating NC cells, as Trio and Cadherin-11, a known interactor of Trio (Kashef et al., 2009), co-localize to paxillin-positive focal adhesions (Langhe et al., 2016; Müller et al., 2020). The influence of Trio loss-of-function on its interactors will also be analyzed.

TRIO gene mutations have been demonstrated to cause neurodevelopmental disorders and facial dysmorphism in patients (Gazdagh et al., 2023). Similar clinical features were observed in patients with mutations in the *MAPRE2* and *TUBB* genes. In this study, we will test if the defects induced through loss of Mapre2 and Tubb can be phenocopied in *Xenopus* embryos using translation-blocking morpholino oligonucleotides. Additionally, *in situ* hybridization using NC cell markers will be performed. In summary, the experiments in this study aim to uncover the molecular mechanisms underlying Trio, Mapre2 and Tubb in NC cell migration, possibly contributing to the development of future therapeutics.

4. Material and Methods

4.1 Molecular biology methods

4.1.1 Transformation of competent *E. coli* cells

First, competent *E. coli* cells were thawed on ice. 50 µL of the *E. coli* suspension were gently mixed with 2.5 µL of plasmid DNA and incubated on ice for 30 min, followed by a heat shock at 42 °C for 35 s. The cells were incubated for additional 2 min on ice and afterwards mixed with 1 mL LB medium. Subsequently, the suspension was incubated for 1 h at 37 °C at 180 rpm. Next, the cells were centrifuged for 3 min at 3,000 rpm, 1 mL of the supernatant was discarded and the cells were resuspended in the remaining liquid. The suspension was plated on an agar plate with the appropriate antibiotic (ampicillin or kanamycin). The plate was incubated at 37 °C for 12–16 h. Agar plates with transformed E. coli cells were closed tightly with parafilm and stored for 1–3 months at 4 °C.

4.1.2 Isolation of plasmid DNA from *E. coli* cells

A single colony was transferred from an agar plate into a falcon tube with 6 mL LB medium and 100 µg/mL antibiotic. The mixture was incubated at 37 °C and 180 rpm for 16–18 h. The following plasmid isolation was performed using the “GeneJET Plasmid Miniprep Kit”. The plasmid DNA was eluted with nuclease free water. The DNA concentration was determined using the NanoDrop 2000 UV-Vis spectrophotometer.

4.1.3 Restriction digestion

The restriction digestion was performed according to the following scheme:

Table 4.1 Restriction digestion

Component	25 µL reaction	10 µL reaction
Plasmid DNA	5 µg	0.5 µL
Buffer	2.5 µL	1 µL
Enzyme	1 µL	0.2 µL
Nuclease free water	to 25 µL	to 10 µl

All reagents were mixed on ice and the restriction enzyme was added as last component to the reaction. The reaction mixture was incubated at 37 °C for 30–60 min. The purification was performed using the “Gene Jet PCR Purification Kit”. Gel extraction was used for purification, when a specific restriction product was required and/or the remaining piece of DNA was larger than 100 bp. Therefore, the “GeneJET Gel Extraction Kit” was used. In both variants, the DNA fragment was eluted with nuclease free water. Restriction analysis to test cloned plasmids was performed using a 10 µL reaction mixture. Immediately after incubation, the samples were loaded onto an agarose gel.

4.1.4 Agarose gel electrophoresis

For agarose gel electrophoresis, 1 % agarose gels were used. Therefore, agarose was melted in 1x TAE buffer and 0.05 µL/mL GelRed were added. 1 µL of DNA/RNA sample was mixed with 1 µL Loading Dye (6x) and 4 µL H_2O and loaded onto the gel. Additionally, 1 µL DNA ladder mixed with 4 µL H_2O was loaded as DNA size marker. The electrophoresis was performed in 1x TAE buffer at 100 V for 40–60 min. Afterwards, the gel was imaged using the Odyssey® Fc Imaging System.

4.1.5 PCR amplification

PCR reactions were performed using the following protocol:

Table 4.2 PCR reaction

Component	100 µL reaction
Template DNA	20 ng
dNTPs (10 mM)	2 µL
Forward primer (10 µM)	5 µL
Reverse primer (10 µM)	5 µL
Phusion Buffer	20 µL
Phusion DNA Polymerase	1 µL
Nuclease free water	to 100 µL

All components were mixed on ice, the DNA polymerase was added as last component. The PCR was performed in a Thermo Cycler using the following program:

Table 4.3 PCR program

Step	Temperature [°C]	Time	Cycles
Initial denaturation	98	30 s	1
Denaturation	98	10 s	30
Annealing	58-72	30 s	
Extension	72	30 s	
Final extension	72	10 min	1
Hold	4	∞	1

The PCR reaction was analyzed on a 1 % agarose gel. If the PCR product was cloned into a vector with the same resistance as the template vector, 1 µL DpnI was added to the PCR mixture and a digestion was performed at 37 °C for 1 h, followed by a heat shock at 80 °C for 20 min. The PCR was purified using the “GeneJET PCR Purification Kit”.

4.1.6 Ligation Cloning

For ligation cloning, a plasmid restriction digestion was performed with two restriction enzymes to prepare the plasmid backbone. In addition, the insert was prepared via PCR or also via restriction digestion. When using PCR, primers were designed including the appropriate restriction enzyme sites to create compatible overhangs for the following ligation reaction. Furthermore, six random base pairs were added to the 5’ end of the primers, so that after PCR

the obtained DNA fragments could be efficiently digested with the chosen restriction enzymes. Afterwards, the ligation was performed using the following protocol. The amount of required insert was calculated with the NEBioCalculator (formula: required mass insert (g) = desired insert/vector molar ratio x mass of vector (g) x ratio of insert to vector lengths).

Table 4.4 Ligation reaction

Component	20 µL reaction
Backbone DNA	50 ng
Insert DNA	3:1 insert:vector ratio
T4 Ligation Buffer	2 µL
T4 Ligase	1 µL
Nuclease free water	to 20 µl

The reaction mixture was incubated for 1–2 h at RT. Afterwards, 2.5 µl of reaction mixture were used for plasmid transformation.

4.1.7 Site-directed mutagenesis

Site-directed mutagenesis was performed after (Liu and Naismith, 2008). Therefore, the primer-primer complementary (overlapping) sequences at the 5' end were 15–20 bp long. The non-overlapping sequences at the 3' end were 15–25 bp long. The melting temperature of the non-overlapping sequences was designed to be 5 to 10 °C higher than the melting temperature of the primer-primer complementary sequences. The mutation site was placed in the middle of the complementary region. The PCR was performed as described in section 4.1.5. Deviating from this, 20 cycles of denaturation, annealing and extension were used.

4.1.8 *In vitro* transcription of sense RNA

For capped sense mRNA synthesis, the SP6 or T7 mMessage mMachine kit was used. The reaction was performed after the following protocol:

Table 4.5 sense RNA synthesis

Component	20 µL reaction
Linearized template DNA	6 µl
2x NTP/CAP	10 µl
10x Reaction Buffer	2 µL
Enzyme Mix	2 µL

The reaction mixture was incubated at 37 °C for 2–3 h. Afterwards, 1 µl TURBO DNase was added and the mixture was incubated at 37 °C for another 15 min. The sense mRNA was purified using the Ilustra RNAspin Mini RNA Isolation Kit (GE Healthcare). The mRNA was eluted with nuclease free water, checked on a 1% agarose gel (100 V, 7 min) and its concentration was determined using the NanoDrop 2000 UV-Vis spectrophotometer.

4.1.9 *In vitro* transcription of labeled antisense RNA

Digoxigenin labeled antisense RNA was synthesized using the following protocol:

Table 4.6 antisense RNA synthesis

Component	25 µL reaction
Linearized template DNA	1 µg
5x Transcription buffer	5 µl
Digoxigenin-mix	4 µL
0.75 M DTT	1 µL
RNase Out	1 µL
T3/T7/SP6 RNA Polymerase	1 µL
RNase free water	to 25 µL

The reaction mixture was incubated at 37 °C for 2 h. Afterwards, 1 µL Turbo DNaseI was added and the mixture was incubated at 37 °C for another 15 min. The antisense RNA was purified using the Illustra RNAspin Mini RNA Isolation Kit (GE Healthcare). The RNA was eluted with nuclease free water and checked on a 1% agarose gel (100 V, 7 min). Hybmix was added depending on the amount of synthesized RNA and the solution was stored at -20 °C.

4.2 Cell biology methods

4.2.1 Cultivation of MDCK cells

The cultivation of MDCK cells was performed in cell culture flasks. The cells were grown until 80–90 % cell confluence. First, the old medium was discarded and the cells were washed two times with PBS. To detach the cells, 2 mL Trypsin was added and the dish was incubated for 10–30 min at 37 °C and 5 % CO_2 until all cells were detached. Afterwards, Trypsin was inactivated by adding 8 mL MDCK medium. A single cell suspension was produced by multiple up and down pipetting. The cells were split 1:5 if cultivated for four days. The cell suspension was always filled up to 10 mL with MDCK medium. The cells were incubated for 2–5 days at 37 °C, 5 % CO_2 and ≥ 95 % humidity.

4.2.2 Long time storage of MDCK cells

MDCK cells were cultured until 80–90 % cell confluence. Subsequently, the medium was discarded, the cells were washed with PBS and treated with 2 mL Trypsin for 10–30 min at 37 °C and 5 % CO_2. Afterwards, 8 mL MDCK medium were added and the cells were resuspended by pipetting up and down several times. The suspension was centrifuged for 5 min at 800 rpm at RT. The supernatant was discarded and the cell pellet was transferred into a cryotube and mixed with 1 mL MEM medium containing 20 % FBS and 10 % DMSO. Immediately, the cryotubes were placed inside the freezing container and stored for one day at -80 °C. Afterwards, the cryotubes were transferred into liquid nitrogen.

4.2.3 Thawing of MDCK cells

Frozen cells were thawed quickly at 37 °C and resuspended in 5 mL MDCK medium. The cell suspension was centrifuged at 800 rpm for 3 min. The resulting pellet was resuspended in 10 mL MDCK medium and plated on a cell culture dish. The cells were split the next day.

4.2.4 Transient transfection with plasmid DNA

For the transient transfection, the required number of cover slips was placed in a 24 well plate and 8 x 120,000 cells were plated in 1 mL MDCK medium on top of each cover slip. Afterwards, cover slips were attached to the dish using a pipette tip so that the cells could grow on top of it. The cell number per mL was calculated using a Neubauer counting chamber. The cells were incubated at 37 °C and 5 % CO_2 for one day. 3 µL Lipofectamine and 100 µL OptiMEM per 1 µg plasmid DNA were mixed and incubated for 5 min at RT. The Lipofectamine-OptiMEM solution was added to the prepared amount of plasmid DNA and again incubated for 20 min at RT. Afterwards, the DNA solution was added dropwise to the MDCK cells. The cells were incubated at 37 °C and 5 % CO_2 for two days.

4.2.5 Immunostaining of transfected cells

First, media was discarded and cells were washed twice with PBS. Cells were fixed with 0.5 mL 4 % PFA for 20 min on ice and under the hood. All incubation steps were performed in the dark. Subsequently, the cells were washed two times with PBS. Thereafter, cells were permeabilized with 0.5 mL 0.2 % TritonX/PBS for 20 min. Cells were washed three times with PBS. Afterwards, cells were treated with blocking solution (1 % BSA in PBS) for 1 h at RT. Cover slips were transferred in a humid chamber on top of a parafilm layer. 30 µL of primary antibody diluted in blocking solution were added and cover slips were incubated for 2 h at RT or overnight at 4 °C. Cells were washed four times with PBS and subsequently incubated with the secondary antibody diluted in PBS for 1 h at RT. Again, cells were washed four times with PBS. For nucleus staining, DAPI (1:1000 in PBS) was added and cells were incubated for 30 min at RT. Afterwards, cover slips were fixed on top of microscopy slides using mounting medium and kept in the dark at RT.

4.3 Xenopus laevis methods

4.3.1 Testis extraction

For testis extraction, a male frog was sacrificed in accordance with animal welfare. Therefore, the male frog was euthanized in 0.05 % benzocaine for 20–25 min at 18 °C. In addition, the cervical spine was cut through using a sharp knife. The abdominal cavity was opened using sharp scissors and both testes were cut out. Testes were cleaned in 1x MBS and stored up to two weeks in 1x MBS at 4 °C.

4.3.2 *In vitro* fertilization and jelly coat removal

For *in vitro* fertilization of *Xenopus* oocytes, an appropriate amount of testis was macerated in

a petri dish, 1x MBS was added and the suspension was stored on ice. *Xenopus* female frogs were injected with 500 units of chorionic gonadotropin (Ovogest, MSD) into the dorsal lymph sac using insulin syringes approximately 16 h before egg laying. Eggs from female frogs were collected in a petri dish and fertilized with 50–300 µl testes suspension diluted 1:10 with H_2O bidest. After fertilization, 0.1x MBS was added and embryos were stored at 14–18 °C. For jelly coat removal, embryos were gently swirled in 2 % L-cysteine (pH 8.0) at 18 °C in a beaker for 3–5 min. Afterwards, embryos were washed three times in 0.1x MBS and cultivated at 14–18 °C until the desired developmental stage, defined according to (Nieuwkoop and Faber, 1994).

4.3.3 Microinjections

Injection needles were prepared using glass capillaries and a needle puller (Magnetic Glass Microelectrode Horizontal Needle Puller, Narishige PN-13). For microinjections, a micromanipulation system (PV820 Pneumatic Pump, M3301 Micromanipulator, World Precision Instruments) was used. The needle was adjusted for 4 or 10 nL injection volume. Therefore, the diameter of the droplet size was measured with a micrometer scale and set to the desired injection volume. Before injection, embryos were kept in injection buffer at 14 °C. For microinjection, embryos were transferred into a small petri dish containing a grid. Embryos were oriented with the animal pole to the top and the injection buffer was completely removed. Embryos were injected with 10 nL in the one-cell stage and in one blastomere of the two-cell stage. For eight-cell stage injections, 4 nL of injection volume were used. After injection of all embryos, injection buffer was added and embryos were stored in it for at least 30 min. Subsequently, embryos were washed three times with 0.1x MBS and cultivated at 14–18 °C in 0.1x MBS.

4.3.4 Fixation and X-Gal staining

Embryos were fixed in MEMFA for 20–45 min. Subsequently, they were washed tree times in 1x PBS for 5 min. If *β-galactosidase* (*lacZ*) RNA was co-injected as lineage tracer, embryos were incubated in X-gal solution in the dark until a blue staining was visible. Embryos were washed again three times with 1x PBS and re-fixed in MEMFA for 1 h or overnight. For long term storage or for in-situ hybridization, embryos were transferred into 100 % ethanol.

4.3.5 Whole mount *in situ* hybridization

The whole mount in situ hybridization protocol was adapted from standard protocols (Harland, 1991). First, the embryos were rehydrated after the following protocol:

Table 4.7 Rehydration of embryos

Solution	Incubation time
75 % Ethanol	5 min
50 % Ethanol in H2O	5 min
25 % Ethanol in PTw	5 min
1 x PTw	4 x 5 min

Next, embryos were treated with Proteinase K (1:4000 in PTw). Temperatures and times were applied depending on the developmental stage following incubation.

Table 4.8 Proteinase K treatment

Developmental stage	Incubation time	Temperature
9–10.5	5 min	RT
14–36	7 min	RT
20–25	7 min	RT
40–44	5 min	37 °C

This was followed by an acetylation reaction described in the following table:

Table 4.9 Acetylation of embryos

Solution	Incubation time
0.1 M Triethanolamine (fresh)	2 x 5 min
3 mL 0.1 M Triethanolamine + 9.4 µL acetic anhydride	5 min
+ 9.4 µL acetic anhydride	5 min
1 x PTw	2 x 5 min
1 x PTw + 4% Formaldehyde	20 min
1 x PTw	5 x 5 min

Afterwards, hybridization of embryos was performed in a water bath at 65 °C according to the following table. All used solutions were prewarmed.

Table 4.10 Hybridization of embryos

Solution	Incubation time (65 °C)
0.5 mL 1x PTw + 0.5 mL Hybmix	10 min
1 mL Hybmix	3–4 h
1 mL Antisense probe in Hybmix	Overnight
1 mL Hybmix	10 min

Hybridization was followed by multiple washing steps summarized in table 4.11.

Table 4.11 Washing steps to remove unbound RNA

Solution	Incubation time	Temperature
2 x SSC	2–3 x 5 min	65 °C
2 x SSC	3 x 15 min	65 °C
2 x SSC/ RNaseA /Rnase T1-Mix (1:10000)	1 h	37 °C
2 x SSC	2 x 5 min	RT
0.2 x SSC	2 x 30 min	65 °C
1 x MAB	12 x 5 min	RT

Following steps were performed for the antibody reaction:

Table 4.12 Blocking and antibody reaction

Solution	Incubation time
MAB/ 2 % BR	15 min
MAB/ 2 % BR/ 20 % horse serum	40 min
MAB/ 2 % BR/ 20 % horse serum/ 1:50000 α-DIG antibody	overnight at 4 °C

Solutions were used up to 30 times.

The staining reaction was performed according to the following table:

Table 4.13 Staining reaction

Solution	Incubation time
1 x MAB	2 h (replaced every 10 min)
APB (fresh)	2 x 5 min
APB/ NBT/BCIP	Up to three days at 4 °C
MEMFA	1 h / overnight at 4 °C

Embryos were transferred to 100 % ethanol in case of strong background staining or for long-term storage.

Embryos with strong pigmentation were bleached before imaging using the following protocol:

Table 4.14 Bleaching of embryos

Solution	Incubation time
1 x PTw	3 x 5 min
0.5 x SSC	2 x 5 min
Bleaching solution	20–120 min on a light source
1 x PTw	3 x 5 min
MEMFA	1 h / overnight at 4 °C

4.3.6 Cranial neural crest cell explants

For cultivation of explanted NC cells, a two, four or eight well chambered microscopy dish was covered with fibronectin (1:100 in 1 x PBS) for 1 h at RT. Afterwards, the chambers were washed and filled with 0.8 x MBS. Cranial NC cells were explanted at stage 18/19 in 0.8 x MBS in a petri dish coated with 1 % agarose in 0.8 x MBS. Embryos were sorted according to their fluorescence signal to determine the injected side. First, the vitelline membrane was carefully removed using sharp forceps. In the next step, the epidermis was gently opened at the region of cranial NC cells and NC cells were extracted by cutting them out with two sharp forceps. Explanted cells were then cut in small pieces using an eyelash knife and transferred to the fibronectin coated chamber slides for 1–2 h at RT. Afterwards imaging or immunostaining was performed.

4.3.7 Immunostaining of neural crest cells

For immunostaining, NC cells were cultivated on cover slips as described above. First, NC cells were fixed with MEMFA/ 4 % PFA or Glyoxal for 20 min. During this step, it was crucial that NC cells never came into contact with air. Afterwards, cells were washed three times with 1x PTw for 5–10 min. Blocking was performed using blocking solution (10 % FBS + 1 % PenStrep in PTw) for 1 h at RT or overnight at 4 °C. The primary antibody was diluted in blocking solution and 30 µl were placed in a humid chamber on parafilm. The cover slips were placed on top of the primary antibody droplets, with the cells on top of the antibody solution and incubated for 4 h at RT or overnight at 4 °C. Afterwards, cover slips were transferred back into the 24 well plate and washed three times with PTw for 5–10 min. The secondary antibody was diluted in blocking solution and added to the coverslips. Cells were incubated for 3 h at RT or overnight at 4 °C. The cells were washed three times with 1 x PTw for 5–10 min. If needed, Phalloidin staining was performed for 1 h at RT. DAPI staining was performed for 30 min at RT. Afterwards, cover slips were fixed on top of microscope slides using mounting medium and kept in the dark at RT.

4.4 Image analysis

In general, image processing was performed using ZEN,Fiji and Imaris.

4.4.1 Delaunay triangulation

The dispersion of NC cells was measured by Delaunay triangulation using the dispersion tool plugin in ImageJ. Dispersion was quantified for each explant after 5 h of cultivation by calculating the mean triangle size between individual nuclei of NC cells.

4.4.2 Imaris based tracking

For tracking analysis, the Imaris particle tracking tool was used. For microtubule plus-end tracking the same rectangle size and time frame were chosen and the following program settings were used:

Table 4.15 Imaris particle tracking settings

Option	Setting
Estimated XY Diameter	1.33
Max Distance	1
Max Gap	0
Autoregressive motion	-
Track duration	5

4.4.3 Focal adhesion formation tracking

For focal adhesion formation tracking, images were taken each minute for 40 min. Tracking was performed using the Focal Adhesion Analysis Server (FAAS) (Berginski and Gomez, 2013). Settings listed in the following table were used:

Table 4.16 FAAS settings

Option	Setting
Threshold	adjusted for each image
Min Phase Length	2
Min Adhesion Size	2

4.5 Chemicals and solutions

Table 4.17 Chemicals and solutions

Name	Company
Agarose	Roth
Ampicillin	Roth
Benzocaine	Sigma-Aldrich
DAPI (1mg/ml)	Roth
DNA Ladder 1kb Plus	Thermo Fischer Scientific
Digoxiginin-11-UTP	Sigma-Aldrich
dNTP Mix (10 mM)	Thermo Fischer Scientific
DTT (Dithiolthreitol)	Thermo Fischer Scientific
Fibronectin	Sigma-Aldrich
FBS (fetal bovine serum)	Sigma-Aldrich
Gel Red® Nucleic Acid Gel Stain	VWR
H_2O_2 (30 %)	Sigma-Aldrich
Kanamycin	Roth
L-Cysteine hydrochloride	Roth
Loading Dye (6x)	Thermo Fischer Scientific
Fluorescent mounting medium	Dako
Gibco™ MEM	Thermo Fischer Scientific
NBT/BCIP Stock Solution	Roche Diagnostics
Ovogest	MSD
Penicillin (10,000 U/mL)/ Streptomycin (10 mg/mL)-solution	Sigma-Aldrich
Alexa Fluor™ 594 Phalloidin	Thermo Fischer Scientific
X-gal (5-Bromo-4chloro-3indolyl α-D-galactopyranoside)	Roth

4.6 Media and buffers

Table 4.18 Media and buffers

Name	Ingredients
APB (alkaline phosphatase-buffer)	100 mM Tris (pH 9.5) 50 mM $MgCl_2$ 100 mM NaCl 0.1 % Tween-20

Bleaching solution	3.0 % (v/v) H_2O_2 10 % (v/v) Formamide 80 % Ethanol
Cysteine buffer	2 % L-Cysteine, pH 8.0
Denhardts (100x)	2 % BSA 2 % Polyvinylpyrrolidon (Sigma) 2 % Ficoll 400 in ddH_2O
Glyoxal fixation solution	2.835 ml H_2O 0.789 mL 100 % Ethanol 0.313 ml 40% Glyoxal 0.03 ml acetic acid pH 4.5 (NaOH)
Hybridization-Mix (Hybmix)	50 % Formamide (v/v) 5x SSC 1 mg/mL Torula RNA 100 µg/mL Heparin 1x Denhardt's 0.1% Tween-20 (v/v) 0.1% CHAPS (w/v) 10 mM EDTA
Injection buffer	1 x MBS 2 % (w/v) Ficoll 400
LB-Agar	1.5 % (w/v) agar-agar (Roth) in LB-medium
Luria-Bertani (LB)- Medium	1 % (w/v) Bacto-Trypton (Roth) 0.5 % (w/v) yeast extract (Roth) 1 % (w/v) NaCl pH 7.5
MAB (Maleic acid buffer) (5x)	0.5 M maleinacid (Roth) 0.75 M NaCl pH 7.5
MBS (Modified Barth´s Solution) (5x)	10 mM Hepes (Roth), pH 7.0 88 mM NaCl 1 mM KCl 2.4 mM $NaHCO_3$ 0.82 mM $MgSO_4$ 0.41 mM $CaCl_2$ 0.66 mM KNO_3
MDCK cells media	MEM, Gibco 5 % FCS 2 mM glutamine 100 U/mL penicillin 100 mg/mL streptomycin for $MDCK_{TTL\text{-}GFP}$ add 0.5 mg/mL Geniticin (G418)
MEM (Modified Eagle solution) (10x):	1 M MOPS (Roth) 20 mM EGTA (Roth) 10 mM $MgSO_4$ heat and light sensitive
MEMFA	1 x MEM 3.7 % (v/v) Formaldehyd (Roth/Merck)
PBS (Phosphate bufferd saline) (10x)	1.37 M NaCl 27 mM KCl

	100 mM Na_2HPO_4 18 mM KH_2PO_4 pH 7.4
Penicillin/Streptomycin/PBS (Pen/Strep/PBS)	100 U/mL Penicillin, 100 µg/mL Streptomycin, 1x PBS
Proteinase K-solution (Merck)	Stock solution 600 U/mL 0.25 µL/mL in PTw
PTw (1x)	1x PBS 0.1 % Tween-20
PTw (1x) + FA	4 % Formaldehyd in PTw
SSC (20x)	0.3 M Sodium citrate 3 M NaCl pH 7.0
SSC (2x)/ RNase	2 mg/mL RNase A, 5,000 U/mL RNaseT1 (Thermo Scientific); 1:10,000 in 2 x SSC
TAE (10x)	2 M Tris 100 mM EDTA (Roth) pH 7.7 with acetate
Transfer buffer (10x):	250 mM Tris 1.9 M glycine 20 % methanol
Triethanolamin (0.1 M):	1.86 % (w/v) Triethanolamin-Hydrochlorid pH 7.5
X-gal staining solution	1 mg/mL X-Gal (Roth) 5 mM $K_3Fe(CN)_6$ (Roth) 5 mM $K_4Fe(CN)_6$ (Roth) 2 mM $MgCl_2$ 1 x PBS

4.7 Kits

Table 4.19 Kits

Name	Company
GenJet Gel Extraction Kit	Thermo Fischer Scientific
GenJet PCR Purification Kit	Thermo Fischer Scientific
GenJet PCR Purification Kit	Thermo Fischer Scientific
illustraTM RNAspin Mini RNA Isolation Kit	GE Healthcare
SP6 mMESSAGE mMACHINE	Ambion
T7 mMESSAGE mMACHINE	Ambion
ZymocleanTM Gel DNA Recovery Kit	Zymo Research

4.8 Competent cells

Table 4.20 Competent cells

E. coli strain	Source
XL1-Blue	Stratagene
Top10	Life Technologies

4.9 Cell lines

Table 4.21 Cell lines

Cell line	Organism	Tissue	ATCC-Nr.	Source
MDCKWT/MDCK$_{\Delta TTL}$/ MDCK$_{TTL\text{-}GFP}$	*Canis familiaris,* dog	Kidney (epithelial)	CCL-34	(Müller et al., 2021)

4.10 Enzymes

Table 4.22 Enzymes

Name	Company
BamHI (FastDigest®)	Thermo Fischer Scientific
ClaI (FastDigest®)	Thermo Fischer Scientific
CutSmart™ Buffer	New England Biolabs
DraIII HF®	New England Biolabs
EcoRI (FastDigest®)	Thermo Fischer Scientific
FastDigest® Buffer (10x)	Thermo Fischer Scientific
HindIII (FastDigest®)	Thermo Fischer Scientific
NotI (FastDigest®)	Thermo Fischer Scientific
Phusion High-Fidelity DNA Polymerase (2 U/µL)	Thermo Fischer Scientific
Proteinase K	Merck Millipore
RNase A/T1 Mix	Thermo Fischer Scientific
RNase OUT Ribonuclease Inhibitor	Thermo Fischer Scientific
T4 DNA Ligase (5 U/mL)	Thermo Fischer Scientific
T7 RNA Polymerase (20 U/µL)	Thermo Fischer Scientific
DreamTaqTM DNA Polymerase	Thermo Fischer Scientific
XbaI (FastDigest®)	Thermo Fischer Scientific
XhoI (FastDigest®)	Thermo Fischer Scientific

4.11 Vectors

Table 4.23 Vectors

Name	Vector	Insert	Application/ RNA synthesis	Citation/ Cloning
AP-2α	pCS2+	*X. laevis* AP-2α	antisense probe, HindIII, T7	(Winning et al., 1991)
Twist	pGEM-T	*X. laveis* twist	antisense probe, EcoRI, T7	(Hopwood et al., 1989)
H2B-mCherry	pCS2+	Histone 2B-mCherry	sense RNA, NotI, SP6	(Kashef et al., 2009)
lacZ	pCS2+	Bacterial β-galactosidase	sense RNA, NotI, SP6	(Smith and Harland, 1991)
pCS2+-GFP	pCS2+	eGFP	Cloning	(Wehner et al., 2011)

membrane-GFP	pCS2+	GAP43-GFP	sense RNA, NotI, SP6	(Moriyoshi et al., 1996)
membrane-RFP	pCS2+	myristoylation/palmitylation motif from the Lck tyrosine kinase- RFP	sense RNA, NotI, SP6	(Megason and Fraser, 2003)
membrane-CFP	pSP64 TBx	Glycosylphosphatidylinositol-CFP	sense RNA, EcoRI, SP6	(Stanganello et al., 2015)
EMTB-tomato	pCS2+	microtubule binding domain of ensconsin-tomato	sense RNA, NotI, SP6	(Revenu et al., 2014)
EB3-mCherry	pcDNA3.1+	End-binding protein3-mCherry	sense RNA, DraIII, T7	Jubin Kashef
EB3-GFP	pCS2+	End-binding protein3-GFP	sense RNA	Ligation cloning; backbone: pCS2+-GFP was cut with BamHI, insert: EB3 was cut out of EB3-mCherry with BamHI
Paxillin-mCherry	pCS2+	Paxillin-mCherry	sense RNA, KpnI, SP6	Ligation cloning, backbone: pCS2+-GFP was cut with ClaI and XbaI, insert was PCR amplified out of pmCherry-paxillin (Addgene plasmid # 50526) using primer 1+2 (Tab. 4.24)
TRIO-GFP	pEGFP-C1	full-length human TRIO	DNA injection	(Debant et al., 1996)
TRIO-SRNN	pEGFP-C1	full-length human TRIO including SRNN mutation	DNA injection	(van Haren et al., 2014)
TRIO-dead-GEF1	pEGFP-C1	full-length human TRIO including GEF1 mutation, leading to catalytic dead GEF1	DNA injection	(Cannet et al., 2014)
TRIO-dead-GEF2	pEGFP-C1	full-length human TRIO including GEF2 mutation, leading to catalytic dead GEF2	DNA injection	(Cannet et al., 2014)
xGEF1-GFP	pCS2+	*X. laevis* Trio-GEF1 domain -GFP	sense RNA, XhoI, SP6	cloned by Marie Kratzer
xGEF2-GFP	pCS2+	*X. laevis* Trio-GEF2 domain -GFP	sense RNA, XhoI, SP6	cloned by Marie Kratzer
xGEF2-SRNN	pCS2+	*X. laevis* Trio-GEF2 domain -GFP including SRNN mutation	sense RNA, XhoI, SP6	Cloning via site-directed mutagenesis using XGEF2-GFP and primer 3+4 (Tab.4.24)
xGEF2-SSNN	pCS2+	*X. laevis* Trio-GEF2 domain -GFP including SSNN mutation	sense RNA, XhoI, SP6	Cloning via site-directed mutagenesis using XGEF2-GFP and primer 5+6

				(Tab.4.24)
xTrio-IG-STK-GFP	pCS2+	*X. laevis* C-terminal Trio-Ig and STK domains-GFP	sense RNA, NotI, SP6	Ligation cloning: backbone: xGEF1-GFP cut with ClaI and XhoI, insert: was PCR amplified out of *X. laevis* cDNA using primer 7+8 (Tab.4.24)
xDsh-GFP	pCS2+	*X. laevis* Dishevelled2-GFP	sense RNA	(Yang-Snyder et al., 1996)

4.12 Primer

Table 4.24 Primer

Nr.	Name	Sequence 5'→ 3'
1	fdw_ClaI_mCherry-Pax	TCATCGATCGATATGGACGACCTCGACGCC
2	rev_XbaI-mCherry-Pax	TTACTATCTAGACTCGAGCCTAGCAGAAGAG
3	GEF2-SRNN_fw	CTCTCGGAATAACCAGCCCGTCAGACACCACTCTCCAGTCCTGG
4	XGEF2-SRNN_rv	CGGGCTGGTTATTCCGAGAGGGCCTGCTTCGGCTGGAGC
5	XGEF2-SSNN_fw	GAGCTCAAATAACGGATCTCCAGCCAGCCGGCCTG
6	XGEF2-SSNN_rv	GAGATCCGTTATTTGAGCTCCAAAAAGAGCCTTTTTGAAGGGGAC
7	ClaI_xTrio-IG-STK-GFP_fw	TCATCGATCGATATGGTATCGGTTAAGCTCCTG
8	XhoI-xTrio-IG-STK-GFP_rv	TTACTACTCGAGCTGGTGTTTACGACGTTC
9	ClaI_mCherry-Pax_fw	TCATCGATCGATATGGTGAGCAAGGGCGAG
10	XbaI_mCherry-Pax_rv	5'TTACTATCTAGACTCGAGCCTAGCAGAAGAG

4.13 Morpholino oligonucleotides

Table 4.25 Morpholino oligonucleotides

Name	Sequence 5'→ 3'	Citation
Co MO	CCTCTTACCTCAGTTACAATTTATA	-
Trio MO1	AAAAAAAGTCGACATCGATACGCGT	(Kratzer et al., 2020)
Trio MO2	ATCCTTAGAGTTCCCCAACCCTCCA	(Kratzer et al., 2020)
Mapre2 MO1	TCCGAACAGAGTCAATGGGAGAAT	this thesis
Mapre2 MO2	TTGACCGCCATTCCCCAA	this thesis
Tubb MO	TCATGGTTCAGGCGTAATAGAT	this thesis

4.14 Antibodies

Table 4.26 Antibodies

Name	Description	Dilution IF	Company
anti-α-tubulin	Mouse Primary Monoclonal IgG	1:100	Calbiochem
anti-acetylated- α-tubulin	Mouse Primary Monoclonal IgG2b	1:100	Sigma-Aldrich
anti-β-integrin	Mouse Primary Monoclonal IgG	1:100	DSHB
anti-Digoxiginin-alkaline phosphatase	Sheep Primary Polyclonal IgG	-	Roche
anti-Rac1-GTP	Mouse Primary Monoclonal IgM	1:100	Biomol
anti-RhoA-GTP	Mouse Primary Monoclonal IgM	1:100	Biomol
anti-phospho-paxillin	Rabbit Primary Polyclonal IgG	1:50	Abcam
anti-mose Alexa 488	Goat Secondary Polyclonal IgG	1:400	Life Technologies
anti-mouse Alexa 594	Goat Secondary Polyclonal IgG	1:400	Life Technologies
anti-rabbit Alexa 488	Goat Secondary Polyclonal IgG	1:400	Life Technologies
anti-rabbit Alexa 594	Donkey Secondary Polyclonal IgG	1:400	Life Technologies

4.15 Microscopes

Table 4.27 Microscopes

Name	Version
Spinning disk microscope Zeiss	Zeiss AxioObserver.Z1
Nikon stereo microscope SMZ18	SMZ18

4.16 Software

Table 4.28 Software

Name	Version	Producer
ApE-A plasmid Editor	v3.1.4	Wayne Davis
Fiji	(ImageJ) 1.54f	NIH
Graphpad Prism	8	GraphPad Software
Image Studio™	5.5.4	(LI-COR® Biotechnology)
NanoDrop 2000/2000c	1.6.198	Thermo Fisher Scientific
NIS-Elements	5.21.03	Nikon
Office	2019	Microsoft
ZEN	blue	Zeiss

5. Results

5.1 The Trio-GEF2 domain dynamically localizes to microtubule plus-ends

Since Trio appears to have different functions depending on its subcellular localization, we examined whether localization studies could provide additional insight into Trio's essential role in NC cell migration. Therefore, *Xenopus* embryos were injected with either full-length-TRIO-GFP DNA, *xTrio-GEF1-GFP* RNA, *xTrio-GEF2-GFP* RNA, *xTrio-IG-STK-GFP* RNA or *membrane-GFP* RNA as control. NC cells were explanted at stage 18 and cultivated on fibronectin-coated microscopy slides. Localization of the different Trio constructs was analyzed using spinning disk microscopy (Fig. 5.1 A). Full-length-TRIO-GFP was detected in small intracellular spots and at the plasma membrane. Comparably, the *Xenopus* Trio GEF2 (xTrio-GEF2) construct, consisting of the DH2, PH2, and SH3 domain, dynamically localized to intracellular spots, tracking from the cell center to the plasma membrane. In contrast, uniform cytoplasmic expression was observed for the *Xenopus* Trio GEF1 construct (xTrio-GEF1), encoding the DH1, PH1 and SH3 domain. The *Xenopus* construct comprising the C-terminal Trio Ig domain and the serine/threonine kinase domain (xTrio-IG-STK) as well showed an even distribution within the cytoplasm, while membrane-GFP localized at the cell membrane as expected (Fig. 5.1 A). Since van Haren et al. showed that the C-terminal part of the Trio protein including the GEF2 domain binds to the end binding protein EB1 and functions as a +TIP in neurons (van Haren et al., 2014), we further tested whether Trio also co-localizes with microtubular structures in migrating *Xenopus* NC cells. Therefore, embryos were injected with *xGEF1-GFP* RNA, *xGEF2-GFP* RNA or *membrane-GFP* RNA in combination with the microtubule marker *EMTB* (microtubule binding domain of ensconsin)-*tomato* (Bulinski et al., 2001) or the +TIP marker *EB3-mCherry* (Stepanova et al., 2003). NC cells were explanted at stage 18 und cultivated on fibronectin-coated slides. Life cell imaging showed that xGEF2 was dynamically localized at microtubules (Fig. 5.1 B, supplemental movie 1). Furthermore, xGEF2-GFP consistently co-localized with EB3-mCherry at microtubule plus-ends, while xGEF1-GFP and membrane-GFP did not (Fig. 5.1 C-E, Fig. 5.2). In conclusion, the Trio GEF2 domain undergoes microtubule-mediated transport during NC cell migration by binding to microtubule plus-ends, which is consistent with previously published data in neurons (van Haren et al., 2014).

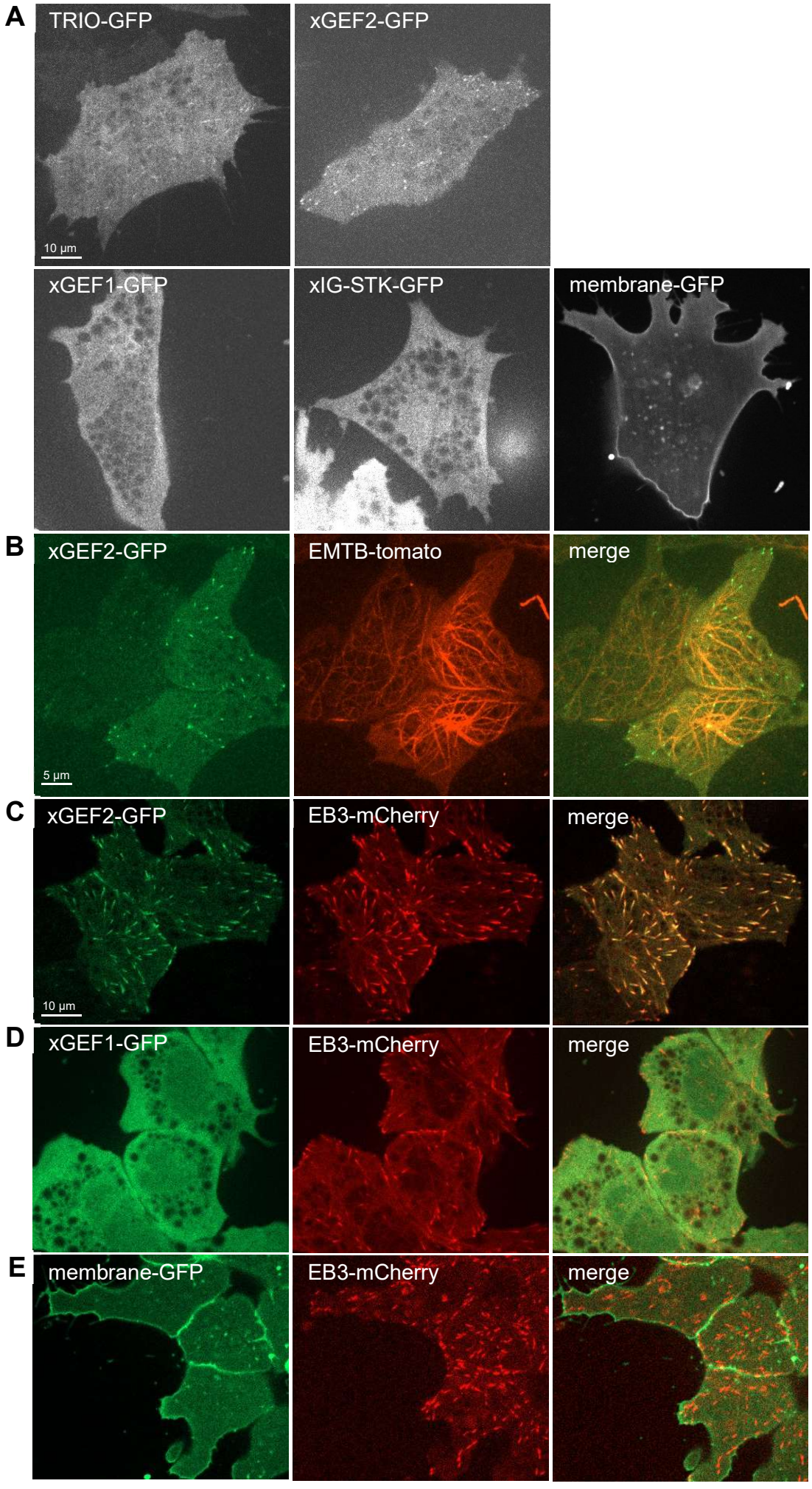
A
TRIO-GFP
xGEF2-GFP
10 µm
xGEF1-GFP
xIG-STK-GFP
membrane-GFP
B
xGEF2-GFP
EMTB-tomato
merge
5 µm
C
xGEF2-GFP
EB3-mCherry
merge
10 µm
D
xGEF1-GFP
EB3-mCherry
merge
E
membrane-GFP
EB3-mCherry
merge

Figure 5.1 The Trio-GEF2 domain co-localizes with microtubule plus-ends in migrating NC cells. **(A-E)** NC cells were explanted at stage 18 and protein localization was analyzed using spinning disk microscopy. **(A)** Full-length-TRIO-GFP and xGEF2-GFP localized in small intracellular dots within the cytoplasm, while xGEF1-GFP and xIG-STK-GFP were evenly distributed throughout the cytosol and membrane-GFP localized at the plasma membrane. Embryos were injected in one blastomere at the two-cell stage with 200 pg full-length-TRIO-GFP DNA, *xGEF2-GFP* RNA, *xGEF1-GFP* RNA, *xIG-STK-GFP* RNA or 150 pg *membrane-GFP* RNA**.** Scale bar = 10 µm **(B)** xGEF2-positive spots co-localized at EMTB-tomato-positive microtubules in NC cells explanted from embryos injected with 200 pg *xGEF2-GFP* RNA and 250 pg *EMTB-tomato* RNA. Scale bar = 5 µm. **(C)** xGEF2-positive spots co-localized with the +TIP marker EB3-mCherry in NC cells explanted from embryos injected with 200 pg *xGEF2-GFP* RNA and 300 pg *EB3-mCherry* RNA. Scale bar = 10 µm. **(D, E)** xGEF1-GFP uniformly localized in the cytoplasm and membrane-GFP was localized at the plasma membrane. Both do not show co-localization with EB3-mCherry in NC cells explanted from embryos injected with 200 pg *xGEF1-GFP* RNA or 150 pg *membrane-GFP* RNA in combination with 300 pg *EB3-mCherry* RNA. Scale bar = 10 µm.

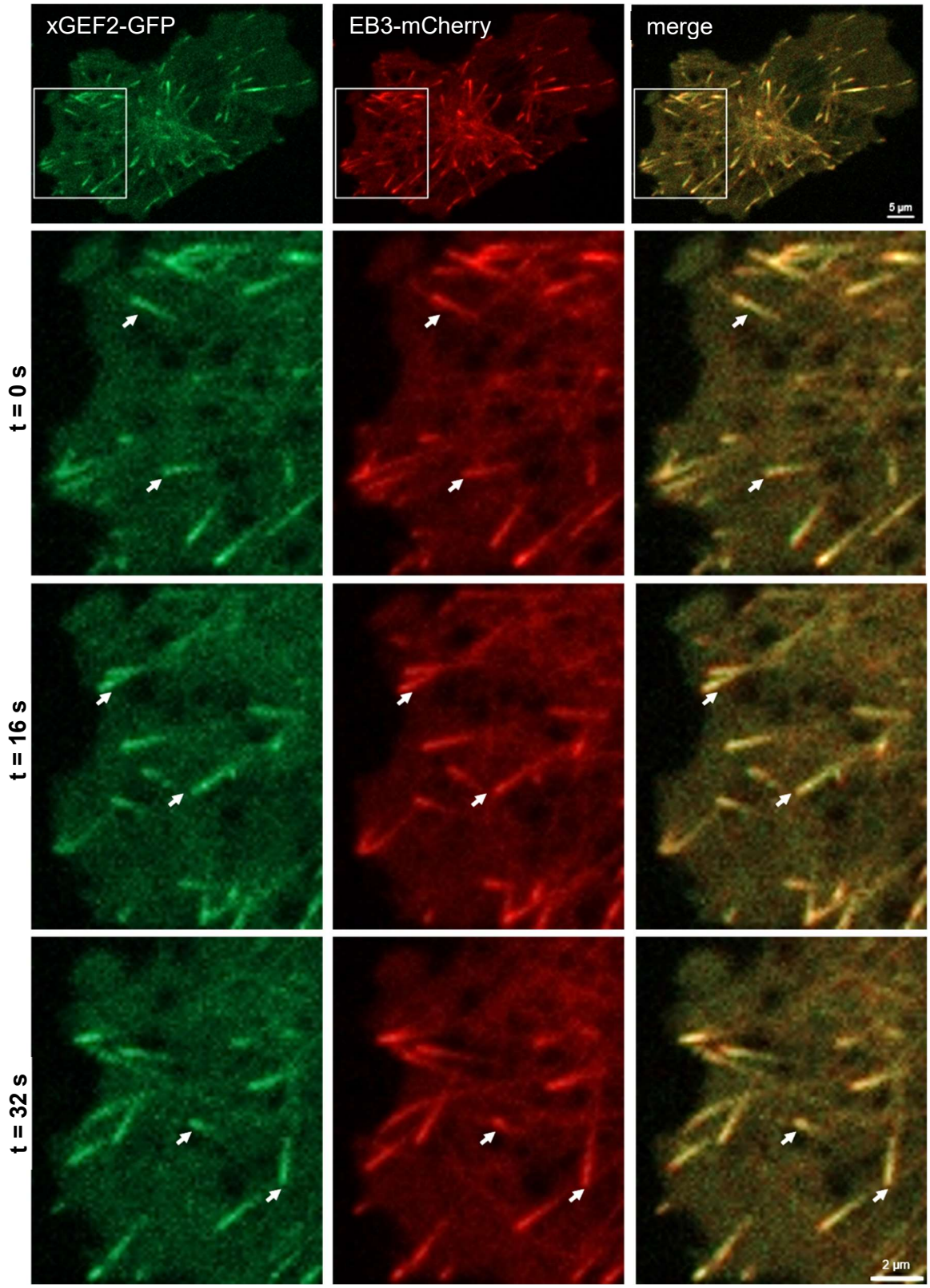

Figure 5.2 xGEF2-GFP co-localizes with EB3-mCherry at microtubule plus-ends in NC cells. xGEF2-GFP and EB3-mCherry display co-localization in migrating NC cells at all imaged time points. Analyzed NC cells were explanted from embryos injected with 200 pg *xGEF2-GFP* RNA and 300 pg *EB3-mCherry* RNA. Time points are indicated at 0, 16 and 32 seconds of imaging. Scale bar first row = 5 µm, following rows = 2 µm.

5.2 Microtubule plus-end mediated transport of Trio is required for its function in NC cell migration

In previous studies, we showed that Trio loss-of-function induces NC migration defects and that the Trio GEF2 domain is sufficient to rescue these phenotypes. To address the question whether microtubule plus-end binding of the GEF2 domain is important for the function of Trio during NC cell migration, a xGEF2 mutant was cloned, that does not bind to microtubule plus-ends. Multiple +TIPs contain the small amino acid motif Ser-x-Ile-Pro (SxIP), that serves as EB1-dependent microtubule plus-end binding motif (Honnappa et al., 2009). Trio contains two SxIP motifs between the GEF2-PH2 and SH3 domain: An SRIP motif and an SSIP motif. Using site-directed mutagenesis, either the first SRIP motif was mutated into SRNN or the second SSIP motif was mutated into SSNN (illustrated in Fig 5.3 A), as Honnappa et al. showed that substitution of the apolar isoleucine and proline to polar residues (asparagines or serines) abrogates binding to EB1 and tracking of microtubule ends in multiple +TIPs (Honnappa et al., 2009). Here, we show that mutation of the first SRIP motif to SRNN completely abolished microtubule plus-end binding of the *Xenopus* Trio GEF2 domain in NC cells, while mutation of the second SSIP motif to SSNN did not (Fig. 5.3, supplemental movies 2–4). These findings were previously demonstrated in neuronal cells for full-length TRIO by (van Haren et al., 2014). To analyze if microtubule plus-end binding is required for Trio function, we performed *in vivo* rescue experiments using the xGEF2-SRNN mutant. Therefore, *Xenopus* embryos were injected with Trio morpholino (Trio MO) in combination with *wild type xGEF2-GFP* RNA *or xGEF2-SRNN-GFP* RNA in one blastomere at the eight-cell stage. Control morpholino (Co MO) injection served as control and co-injection of *lacZ* RNA in all conditions was used as lineage tracer. NC cell migration was analyzed at tailbud stages by *AP2-α in situ* hybridization. As expected, Trio morphant embryos showed defects in NC migration (Fig. 5.4 A), while Co MO-injected embryos showed a normal pattern of migrating NC cells (Fig. 5.4 B). Co-injection of increasing concentrations of wild type xGEF2 rescued the Trio morphant NC migration defects at all concentrations analyzed (Fig. 5.4 C, E). In contrast, the xGEF2-SRNN mutant was not as efficient in rescuing the Trio MO induced NC migration defects (Fig. 5.4 D, E) and failed to restore NC migration at low concentrations. At higher concentrations of xGEF2-SRNN, a rescue effect was observed, however, it was weaker compared to wild type xGEF2. At these high concentrations, the GEF2 domain may already be provided to all functional sites, potentially eliminating the need for microtubule plus end-mediated transport.

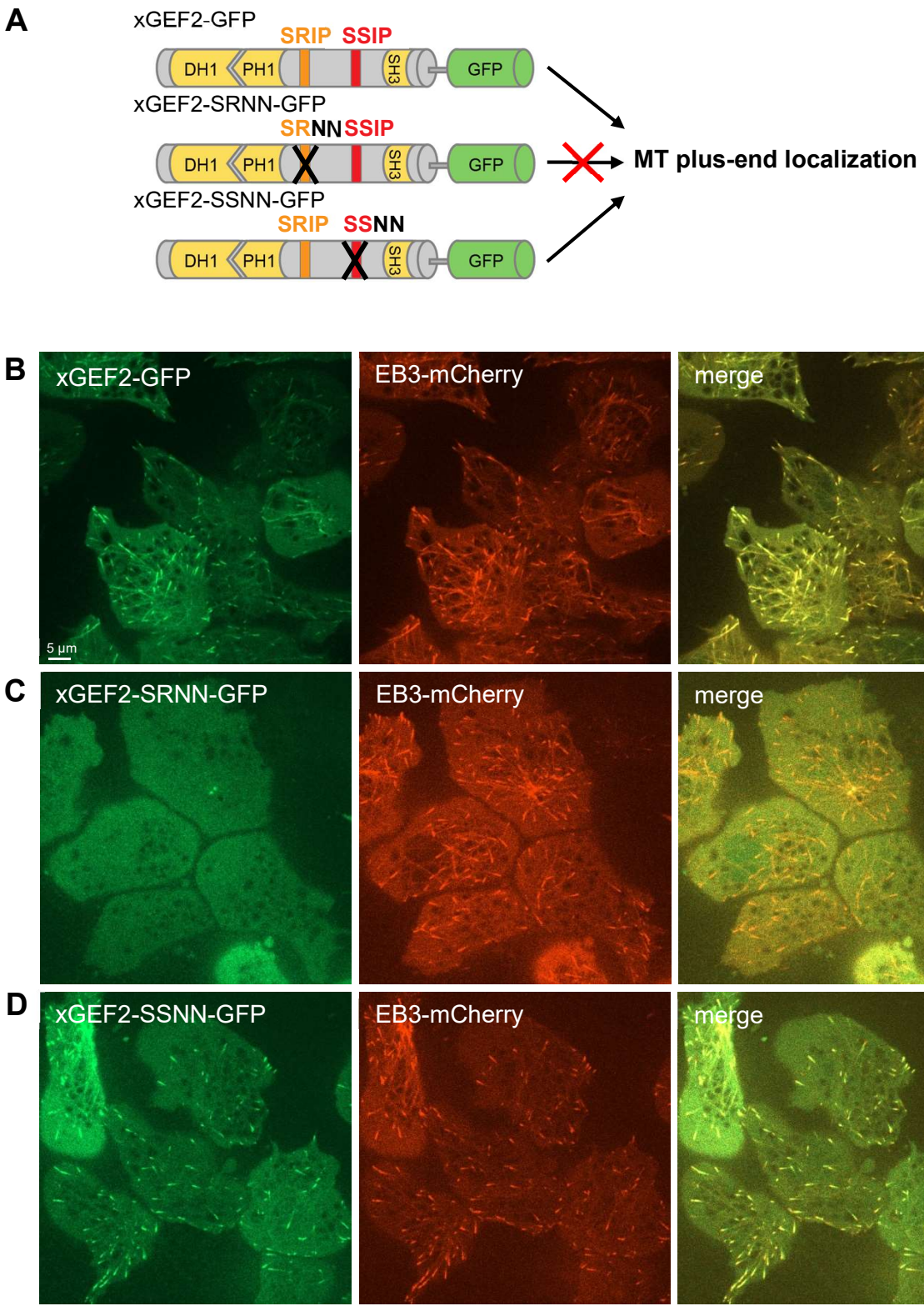
A
xGEF2-GFP
SRIP SSIP
DH1 PH1 SH3 GFP
xGEF2-SRNN-GFP
SRNN SSIP
DH1 PH1 SH3 GFP
xGEF2-SSNN-GFP
SRIP SSNN
DH1 PH1 SH3 GFP
MT plus-end localization
B
xGEF2-GFP
EB3-mCherry
merge
5 µm
C
xGEF2-SRNN-GFP
EB3-mCherry
merge
D
xGEF2-SSNN-GFP
EB3-mCherry
merge

Figure 5.3 The xGEF2-SRNN mutant abolished co-localization to microtubule tips. (A) Schematic structure of xGEF2 constructs. The wild type xGEF2-GFP construct consists of the PH1, DH1 and SH3 domains and two SXIP motifs (SRIP and SSIP) that can act as microtubule plus-end localization signals (Honnappa et al., 2009). **(B-D)** Mutation of the first SRIP motif into SRNN completely abolished microtubule plus-end binding, while mutation of the second SSIP motif into SSNN did not. Embryos were injected in one blastomere at the two-cell stage with 200 pg *xGEF2-GFP* RNA, *xGEF2-SRNN-GFP* RNA or *xGEF2-SSNN-GFP* RNA in combination with 300 pg *EB3-mCherry* RNA. NC cells were explanted at stage 18 and protein localization was analyzed using spinning disk microscopy. Scale bar = 5 µm.

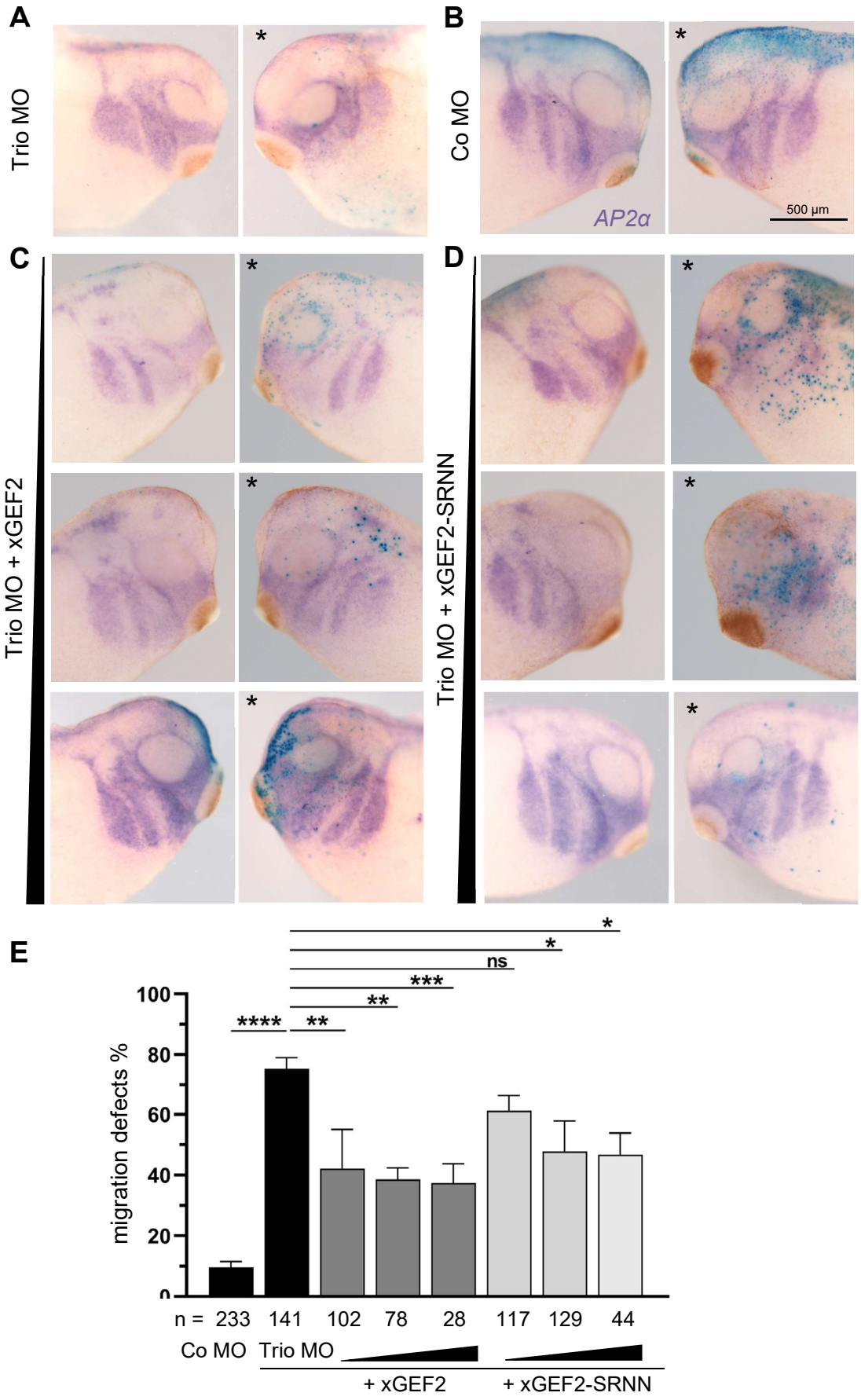
A
Trio MO
B
Co MO
AP2α
500 µm
C
Trio MO + xGEF2
D
Trio MO + xGEF2-SRNN
E
migration defects %
100
80
60
40
20
0
****
**
**
***
ns
*
*
n = 233 141 102 78 28 117 129 44
Co MO
Trio MO
+ xGEF2
+ xGEF2-SRNN

Figure 5.4 Microtubule plus-end localization of Trio is required for NC cell migration. (A-D) Embryos were injected with 4 ng Trio MO or a control MO in combination with 50, 75 or 100 pg *wild type xGEF2-GFP* or *xGEF2-SRNN-GFP* RNA together with 75 pg *lacZ* RNA as lineage tracer in one blastomere at the eight-cell stage. NC cell migration was analyzed at stage 26 by *AP2-α in situ* hybridization. The injected side is marked with an asterisk. Scale bar = 500 µm. **(A, B)** Trio morphant embryos showed NC cell migration defects compared to control embryos. **(C)** Co-injection of wild type xGEF2 rescued the Trio loss-of-function NC cell migration defects at all used concentrations. **(D)** The xGEF2-SRNN mutant failed to restore NC migration at low concentrations. **(E)** Graph summarizing the percentage of embryos with NC cell migration defects in at least three independent experiments. +s.e.m. and the number of analyzed embryos are indicated for each condition. **** $p<0.0001$, *** $p<0.001$, ** $p<0.01$, * $p<0.05$, ns = not significant (one-way ANOVA).

To further analyze the need for microtubule-based transport of Trio during NC cell migration, *in vitro* migration assays were performed. *Xenopus* embryos were injected with Co MO or Trio MO together with *H2B-mCherry* RNA and *membrane-CFP* RNA (to mark the membrane and the nucleus, respectively) in combination with either *xGEF2-GFP* RNA or *xGEF2-SRNN-GFP* RNA in one blastomere at the eight-cell stage. NC cells were explanted at stage 18, followed by cultivation on fibronectin-coated microscopy slides. Live-cell imaging was performed directly after NC cells were attached to the fibronectin-matrix using spinning disk microscopy. NC cell dispersion was analyzed after 5 h by determining the dispersion area via Delaunay triangulation followed by calculation of the mean triangle size. NC cell dispersion was strongly reduced in Trio morphant explants compared to controls (Fig. 5.5). Co-injection of wild type xGEF2 restored NC cell migration, while co-injection of the mutant xGEF2-SRNN did not. For all the Trio MO injected conditions, only a few explants were evaluable as most of the NC cells died within a few hours of imaging. Consequently, these results are not statistically significant, but support the *in vivo* result described above. Taken together, these data suggest that microtubule trafficking of Trio is important for its function in NC migration.

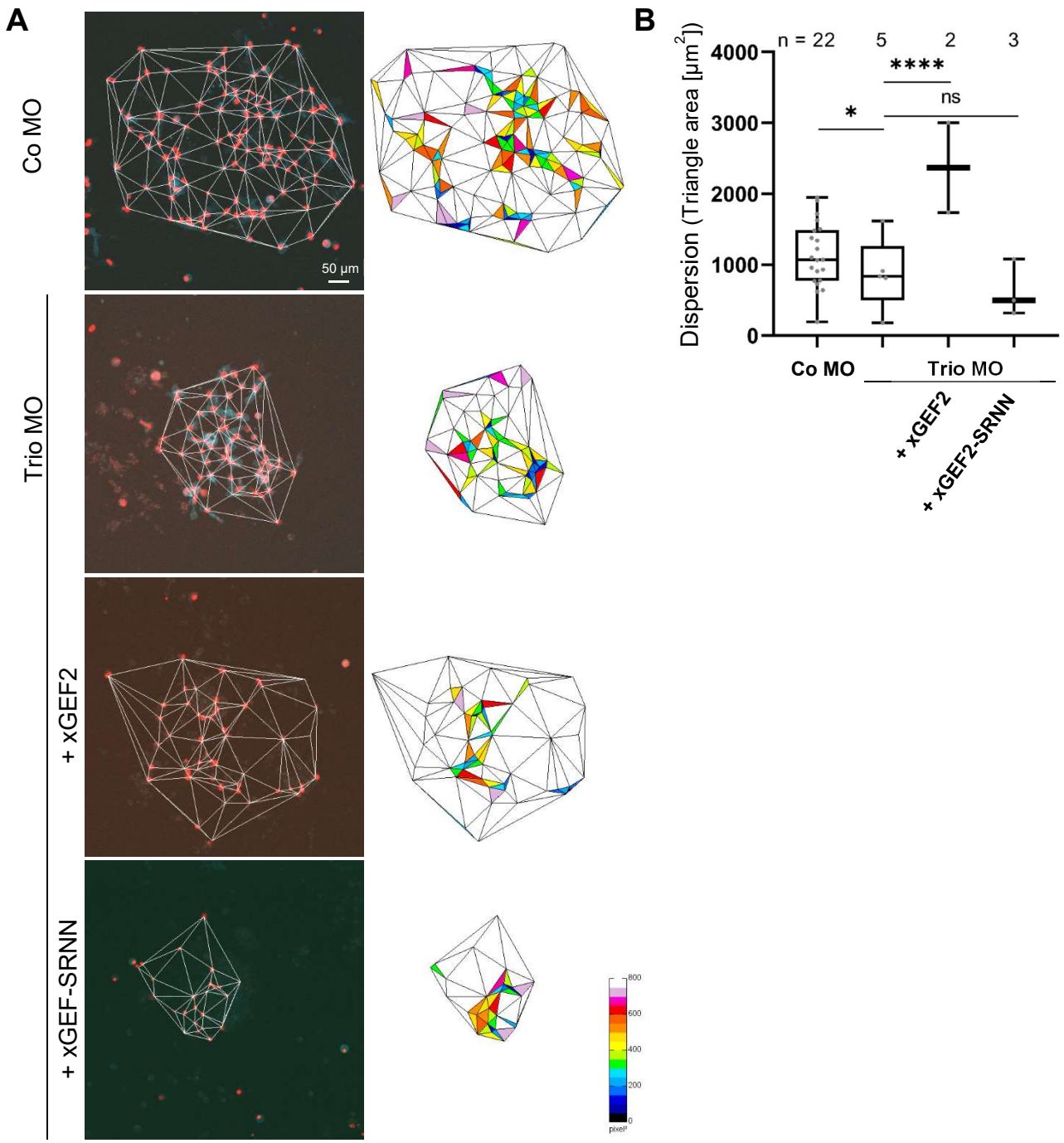

Figure 5.5 Microtubule trafficking of Trio is important for its function in NC cell dispersion. (A) Embryos were injected with 4 ng Co MO or 4 ng Trio MO together with 150 pg *H2B-mCherry* RNA and 250 pg *membrane-CFP* RNA in combination with either 50 pg *xGEF2-GFP* RNA or 50 pg *xGEF2-SRNN-GFP* RNA in one blastomere at the eight-cell stage. NC cells were explanted at stage 18 and cultivated on fibronectin-coated microscopy slides. Live-cell imaging was started after NC cells were attached to the fibronectin-matrix using spinning disk microscopy. NC cell dispersion was analyzed after 5 h by determining the dispersion area via Delaunay triangulation using ImageJ. Scale bar = 50 µm. **(B)** Graph summarizing NC cell dispersion defined as the mean triangle size per explant (µm^2) calculated by Delaunay triangulation after 5 h of cultivation in two independent experiments. NC cell dispersion was reduced in Trio morphant explants compared to controls. Co-injection of wild type xGEF2 rescued NC

cell migration defects, while co-injection of the mutant xGEF2-SRNN did not. Box plots show median, 25th to 75th percentiles and Whiskers from min to max. Single values for each explant are shown in gray, number of explants are indicated. **** p<0.0001, *p<0.05, ns = not significant (one-way ANOVA).

5.3 Trio loss-of-function disrupts microtubule dynamics in NC cells

Since microtubule plus-end based transport of Trio is important for NC cell migration, we further investigated if Trio loss-of-function affects microtubule dynamics. Therefore, microtubule plus-end tracking analysis of Trio morphant and control NC cells was performed. *Xenopus* embryos were injected with either Co MO or Trio MO together with *EB3-GFP* RNA or *EB3-mCherry* RNA. NC cells were explanted at stage 18 and cultivated on fibronectin-coated microscopy slides. Microtubule plus-ends were tracked at the cells leading edge during NC cell migration using the Imaris particle tracking tool. Consistent with our previous findings (Kratzer et al., 2020) control cells formed protrusions in the direction of migration, while Trio morphant NC cells displayed less protrusions and cellular blebbing (Fig. 5.6 A-D, supplemental movie 5, 6). To analyze microtubule dynamics at cell-cell contacts, explanted Trio morphant and control NC cells were placed in close proximity to facilitate cell-cell interaction. Microtubule plus-ends were tracked during the time of cell-cell contact (Fig 5.6 E, F, supplemental movie 7). Here, fluorescently labeled EB3 proteins were switched during the repetition of experiments to exclude any effect of the used fluorophores. Our findings showed that microtubule plus-ends at the leading edge of Trio morphant cells are less stable, as measured by the EB3 lifetime (Fig. 5.6 G), but grow significantly faster, as measured by the mean growth rate (Fig. 5.6 H), compared to control cells. At cell-cell contacts, however, Trio morphant NC cells display slower and more stable microtubules compared to control cells (Fig. 5.6 G, H). Thus, Trio loss of function impairs distinct microtubule functions critical for NC migration (Fig. 5.6 I). At the leading edge, microtubules are stabilized and are involved in the formation of actin structures and the formation of focal adhesions (Etienne-Manneville, 2004). On the contrary, at cell-cell contacts, NC cells undergo CIL and change their direction of migration (Szabó and Mayor, 2018). In order to establish cell retraction, microtubules depolymerize fast and facilitate the formation of actomyosin stress fibers (Moore et al., 2013). Taken together, these results suggest that Trio is important for the regulation of microtubule stability promoting stable microtubules at the leading edge and microtubule catastrophe at cell-cell contacts.

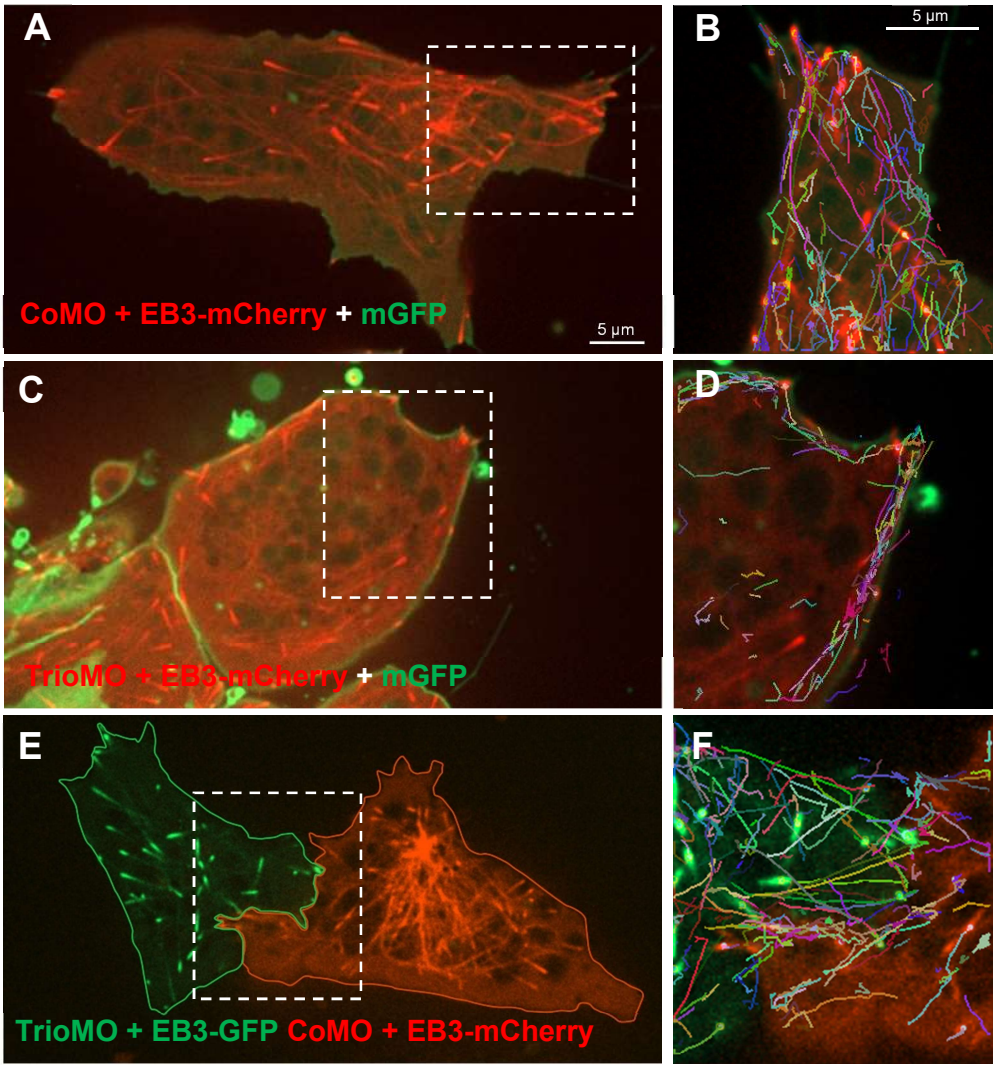
A
CoMO + EB3-mCherry + mGFP
5 µm
B
5 µm
C
TrioMO + EB3-mCherry + mGFP
D
E
TrioMO + EB3-GFP CoMO + EB3-mCherry
F

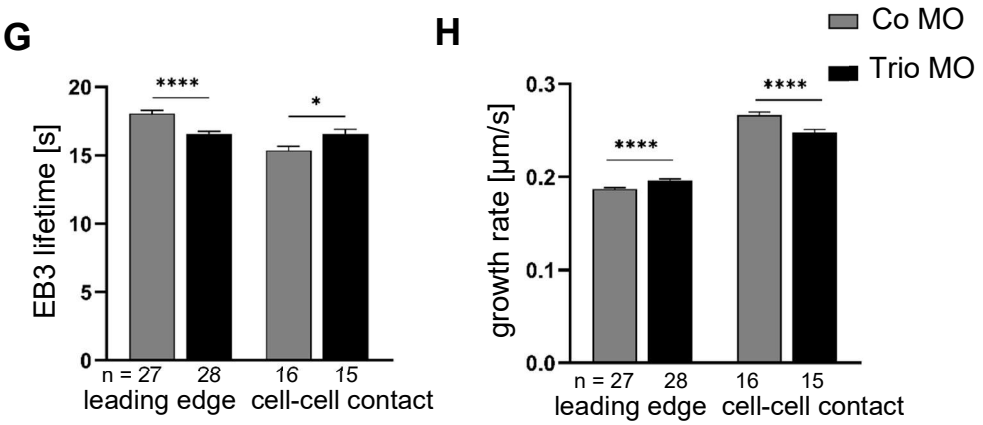
G
EB3 lifetime [s]
20
15
10
5
0
****
*
n = 27 28 16 15
leading edge cell-cell contact
H
Co MO
Trio MO
growth rate [µm/s]
0.3
0.2
0.1
0.0
****
****
n = 27 28 16 15
leading edge cell-cell contact

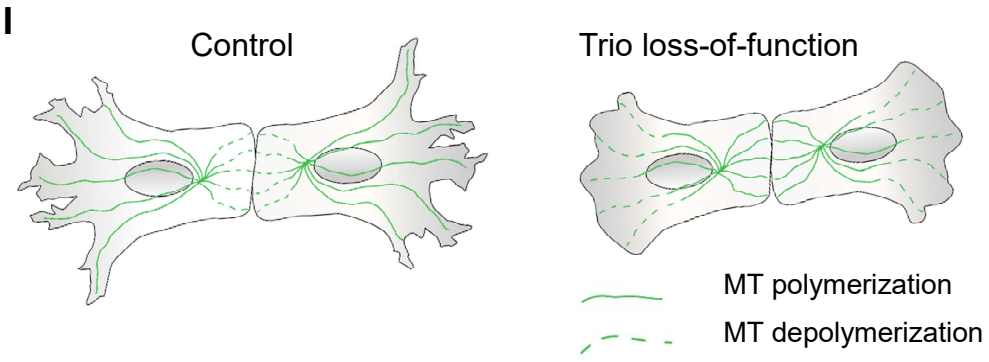
I
Control
Trio loss-of-function
MT polymerization
MT depolymerization

Figure 5.6 Trio affects microtubule plus-end dynamics at the leading edge and at cell-cell contact sites. (A-F) NC cells were explanted at stage 18 and migrating NC cells were imaged every two seconds for three minutes using spinning disk microscopy. Microtubule plus-ends were tracked using the Imaris particle tracking tool**.** Scale bar = 5 µm. **(A-D)** Embryos were injected with 6.5 ng Co MO or Trio MO in combination with 450 pg *EB3-mCherry* RNA and 300 pg *membrane-GFP* RNA in one blastomere at the two-cell stage. Microtubule plus-ends were tracked at the leading edge of NC cells using a specific square size, indicated by the white dashed line. Single tracks are indicated by distinct colors. **(E, F)** For microtubule tracking at cell-cell contact sites, embryos were injected with 4 ng Co MO or Trio MO in combination with 250 pg *EB3-mCherry* RNA or 150 pg *EB3-GFP* RNA in one blastomere at the eight-cell stage. The outer line of the cells was indicated by a green and red line. **(B**, **D, F)** Higher magnifications of the square shown in A, C and E, respectively. **(G)** Graph summarizing measured EB3 lifetime in seconds. **(H)** Graph summarizing microtubule plus-end growth rate in µm/s. **(G, H)** +s.e.m. and the number of analyzed cells are indicated for each condition in four independent experiments. ****p<0.0001, *p<0.05 (Mann-Whitney test). Trio loss-of-function disrupts microtubule dynamics in migrating NC cells. Microtubules demonstrate reduced stability and faster growth at cell protrusions, while displaying increased stability and slower growth at cell-cell contacts as compared to the control. **(I)** Trio loss of function impairs microtubule dynamics relevant for NC migration. In wild type NC cells, microtubules located at the leading edge are more stable (indicated by a solid green line) and contribute to the formation of protrusions, while microtubules at cell-cell contacts depolymerize rapidly (indicated by a dashed green line), leading to a change in cell directionality. Both of these functions are compromised in Trio morphant NC cells, with microtubules being stabilized at cell-cell contacts (solid green line) but display less stability at cell protrusions (dashed green lines) compared to the control.

Since microtubule stability is disturbed in Trio morphant NC cells, we started to analyze whether microtubule acetylation and cell matrix adhesion are also affected. Tubulin acetylation increases the stability and flexibility of microtubules against mechanical stress and enhances vesicle and protein-complex trafficking (Eshun-Wilson et al., 2019; Nekooki-Machida and Hagiwara, 2020). *Xenopus* embryos were injected at the eight-cell stage with Co MO or Trio MO in combination with either *xGEF2-GFP* RNA or *xGEF2-SRNN* RNA together with *membrane-GFP* RNA as lineage tracer. NC cells were explanted at stage 18 and microtubule acetylation and cell matrix adhesion were analyzed by immunostaining for acetylated-tubulin or β-integrin, respectively; DNA was stained with DAPI. Initial experiments suggest that acetylated tubulin appeared less frequently in Trio morphant NC cells compared to controls, which seems to be rescued by co-injection of wild type xGEF2 but not by the mutant xGEF2-SRNN construct (Fig. 5.7 A). Furthermore, cell-matrix adhesion appeared to be affected in Trio morphant NC cells, as analyzed by β-integrin immunostaining. While control NC cells exhibited β-integrin expression at the leading edge, Trio morphant NC cells showed a more diffuse signal. Integrin expression seemed to be restored by co-injection of wildtype xGEF2 but not by xGEF2-SRNN (Fig. 5.7 B). These results provide a first indication of Trio loss-of-function-induced defects in microtubule acetylation and cell-matrix adhesion, but require further analysis to draw meaningful conclusions.

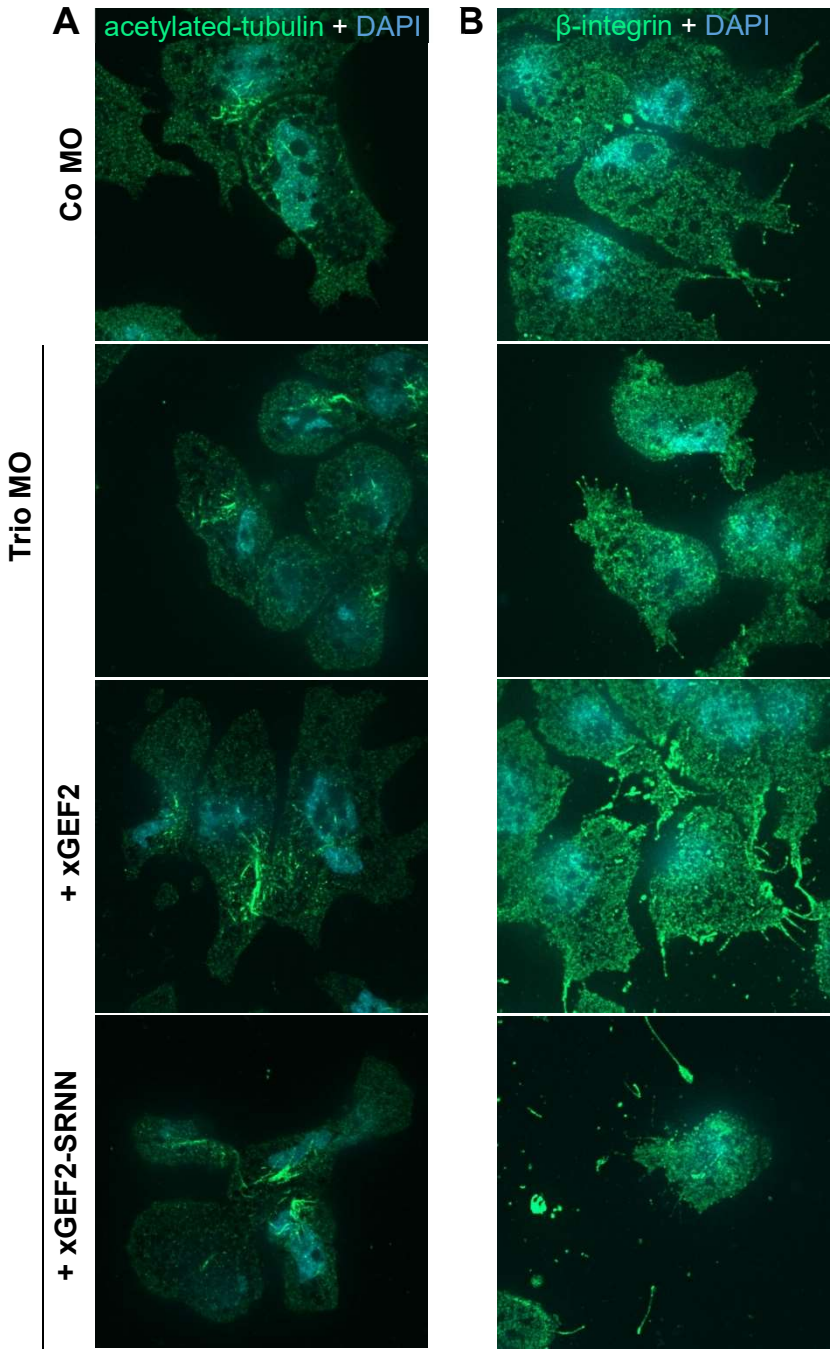

Figure 5.7 Microtubule acetylation and cell matrix adhesion in NC cells seem to be affected by Trio-loss-of-function. (A, B) Embryos were injected with 4 ng Co MO or Trio MO together with 50 pg wild type *xGEF2* RNA or *xGEF2-SRNN* RNA and 250 pg *membrane-GFP* RNA as lineage tracer in one blastomere at the eight-cell stage. NC cells were explanted at stage 18 and analyzed by immunostaining against acetylated-tubulin and β-integrin. **(A)** Acetylated tubulin seems to occur less frequently in Trio morphant NC cells compared to controls. Microtubule acetylation status of Trio morphant NC cells appears to be restored by co-injection of wild type xGEF2 but not by xGEF2-SRNN. **(B)** β-integrin expression seems to be affected in Trio morphant NC cells. While control NC cells exhibit β-integrin expression at the leading edge, Trio morphant NC cells show a more diffuse signal. Co-injection of wild type xGEF2 restored β-integrin expression patterns, while co-injection of xGEF2-SRNN did not.

5.4 Trio is required for focal adhesion dynamics in NC cells

Previously, we have shown that Trio morphant NC cells display migration defects, reduced cell protrusions, a diffuse actin cytoskeleton and a blebbing phenotype (Kratzer et al., 2020). Furthermore, these cells exhibit changes in microtubule stability and, possibly, cell adhesion. All these cellular components are involved in focal adhesion assembly and disassembly. Thus, to analyze if focal adhesion formation is affected by Trio loss-of-function, co-immunostaining for phospho-paxillin and α-tubulin was performed. *Xenopus* embryos were injected at the eight-cell stage with Co MO or Trio MO in combination with either *xGEF2-GFP* RNA or *xGEF2-SRNN-GFP* RNA together with *H2B-mCherry* RNA as lineage tracer. In addition, cell circularity of single cells was measured. NC cells were explanted at stage 18, cultivated on fibronectin-coated coverslips and fixed after 2 h. In control cells, microtubules were organized in radial asters and extended into cell protrusions. In contrast, Trio morphant NC cells displayed a disrupted microtubule network, with microtubules predominantly concentrated at the cell center, while cell protrusions were mostly absent (Fig. 5.8 A). These cells exhibited a rounder shape, measured by cell circularity (Fig. 5.8 B). Furthermore, phospho-paxillin staining revealed that focal adhesions in Trio loss-of-function NC cells are mislocalized towards the cell center. Co-injection of xGEF2 rescued these defects - NC cells were less circular and focal adhesions localized at cell protrusions - while xGEF2-SRNN failed to restore circularity and normal focal adhesion formation (Fig. 5.8 A, B). However, measurements of focal adhesion area showed no significant differences in focal adhesion size for all conditions (data not shown).

Since prominent mislocalization of focal adhesions was observed in Trio morphant NC cells, we sought to effectively determine whether Trio loss-of-function impairs focal adhesion formation in NC cells. Therefore, we turned to life-cell analysis using *Paxillin-mCherry* RNA to examine focal adhesion assembly and disassembly in detail. *Xenopus* embryos were injected with Co MO or Trio MO together with *Paxillin-mCherry* RNA and *membrane GFP* RNA in one blastomere at the two-cell stage. After explantation and cultivation on fibronectin-coated microscopy slides, migrating NC cells were imaged every minute for 40 minutes (Fig. 5.9 A, supplemental movie 8). Focal adhesion size and lifetime were determined using the focal adhesion analysis server (Berginski and Gomez, 2013). Trio morphant NC cells showed significantly larger focal adhesions compared to controls (Fig. 5.9 A, B). The lifetime of focal adhesions was slightly, but not significantly, increased (Fig. 5.9 C). During live-cell imaging, it was noted that focal adhesions exhibited high dynamics in control cells, whereas focal adhesions in Trio loss-of-function NC cells mostly maintained their position (supplemental movie 8). These findings indicate that Trio morphant NC cells display compromised focal adhesion size and dynamics, which could potentially be a factor contributing to their migration defects.

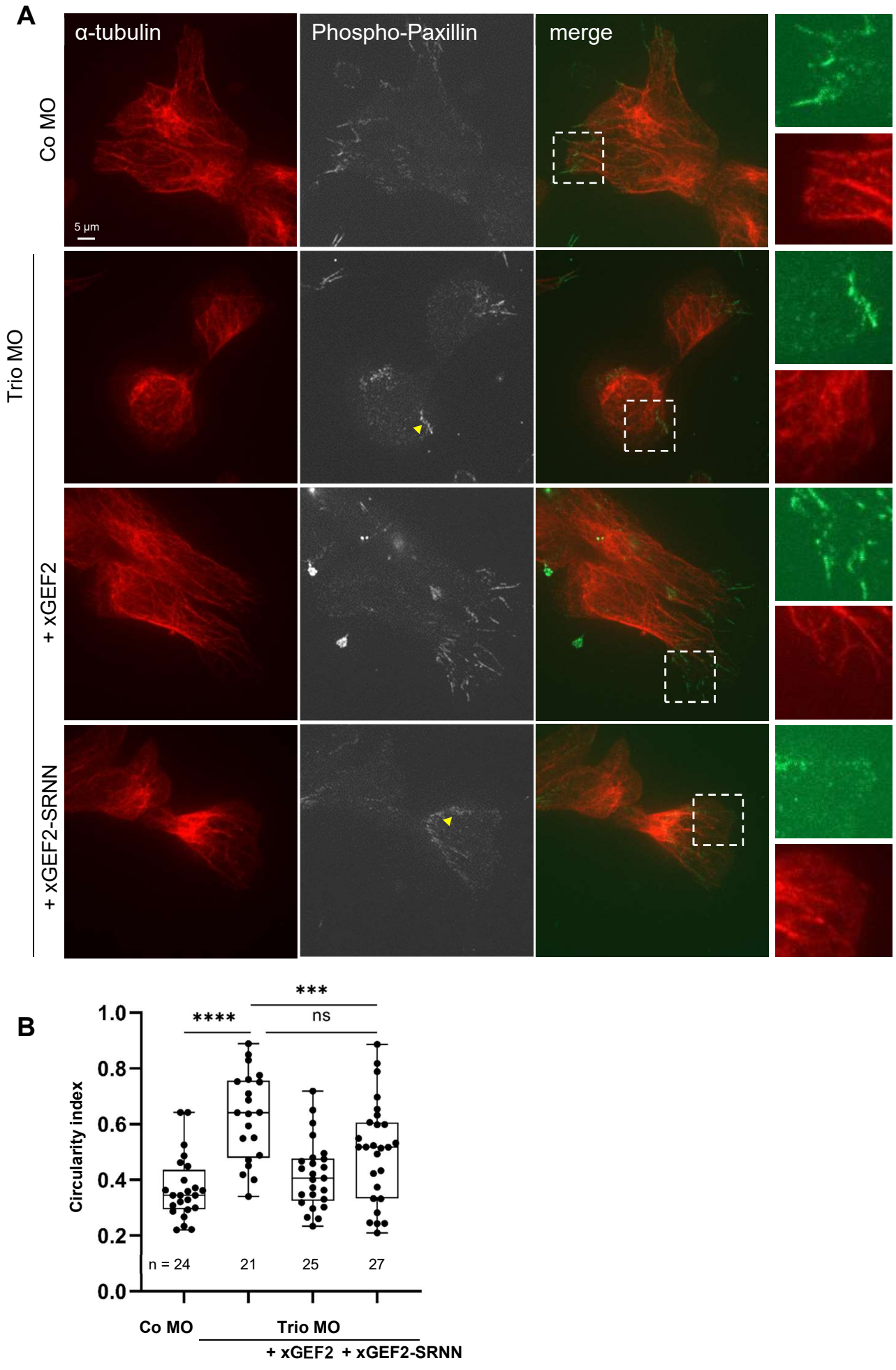
A
α-tubulin
Phospho-Paxillin
merge
5 µm
Co MO
Trio MO
+ xGEF2
+ xGEF2-SRNN
B
Circularity index
1.0
0.8
0.6
0.4
0.2
0.0
****
***
ns
n = 24
21
25
27
Co MO
Trio MO
+ xGEF2
+ xGEF2-SRNN

Figure 5.8 Trio loss-of-function disrupts microtubule network and focal adhesion formation. (A) Embryos were injected with 4 ng Co MO or Trio MO together with 50 pg *wild type xGEF2-GFP* or *xGEF2-SRNN-GFP* RNA and 300 pg *H2B-mCherry* RNA as lineage tracer in one blastomere at the eight-cell stage. NC cells were explanted at stage 18 and migrating NC cells were analyzed by immunostaining against α-tubulin and phospho-paxillin. α-tubulin staining revealed a dispersed arrangement of microtubules and mislocalization of focal adhesion clusters in Trio morphant NC cells. These phenotypes were also observed in the samples injected with *xGEF2-SRNN-GFP* RNA (yellow arrows). Co MO and *xGEF2-GFP* RNA injected samples showed normal α-tubulin and focal adhesion distribution. White rectangles show magnified areas of α-tubulin (red) and phospho-paxillin (green) staining. Scale bar = 5 µm **(B)** Graph showing cell circularity measured for imaged cells in three independent experiments. Trio loss-of-function leads to an increase in cell circularity, that can be rescued by co-injection of *xGEF2-GFP* RNA, but not by *xGEF2-SRNN-GFP* RNA. Box plots show median, 25th to 75th percentiles and Whiskers from min to max. Single values for each cell are shown in black. +s.e.m. and numbers of analyzed cells are indicated for each condition. **** p<0.0001, ***p<0.001, ns = not significant (Kruskal-Wallis test).

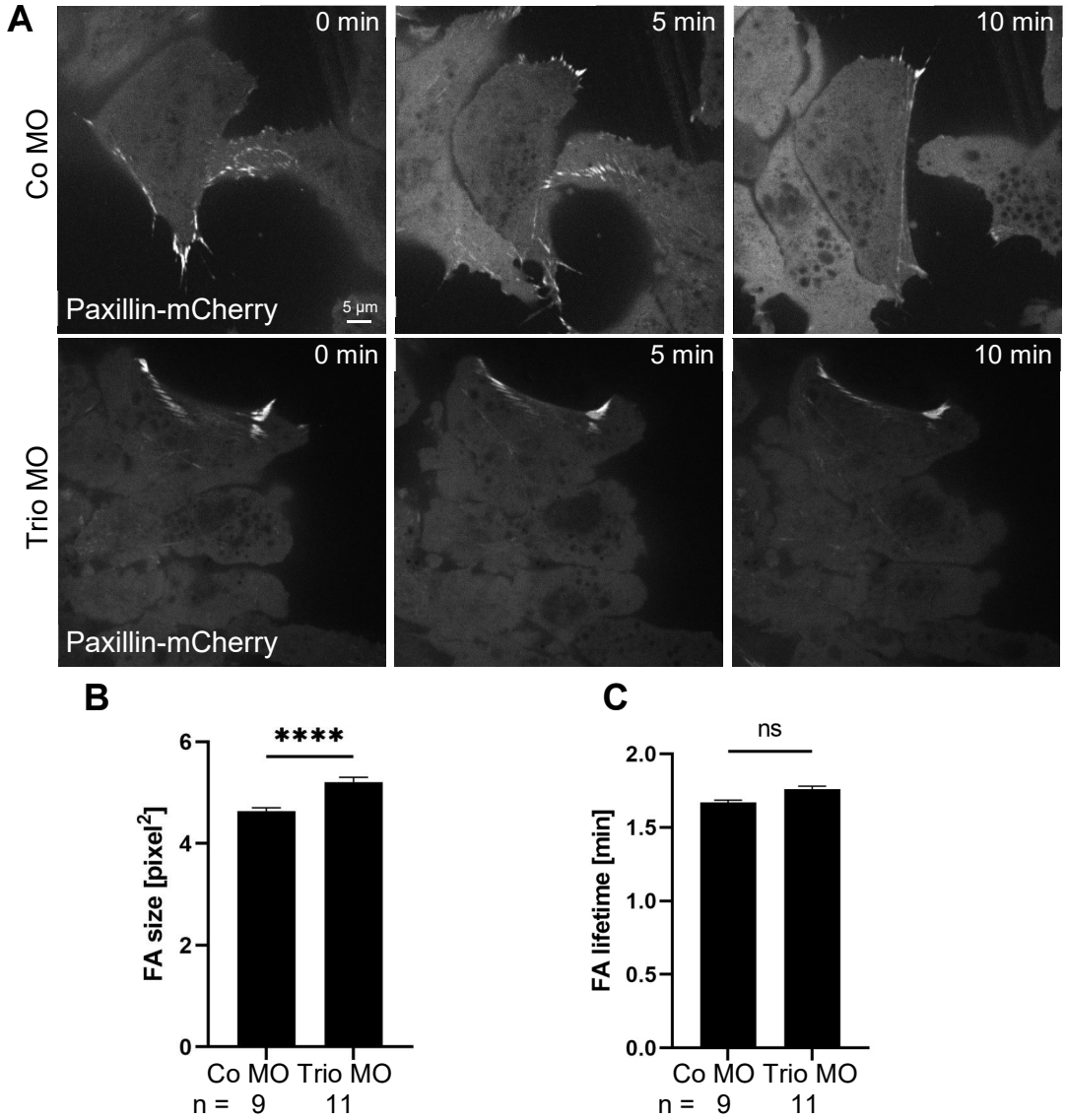

Figure 5.9 Trio loss-of-function affects focal adhesion size. (A) Embryos were injected with 6.5 ng Co MO or Trio MO together with 400 pg *Paxillin-mCherry* RNA and 250 pg *membrane-GFP* RNA in one blastomere at the two-cell stage. NC cells were explanted at stage 18 and cultured on fibronectin-coated microscopy slides. NC cells were recorded each minute for a 40 min time frame. Images after 0, 5 and 10 min are shown. Focal adhesions in control cells are highly dynamic, while focal adhesions in Trio loss-of-function NC cells remain mostly at their position. Scale bar = 5 µm **(B)** Graph showing focal adhesion size. **(C)** Graph showing focal adhesion lifetime. **(B, C)** Three independent experiments, +s.e.m. and numbers of analyzed cells are indicated for each condition. ****p<0.001, ns = not significant (Mann-Whitney test).

5.5 Loss of Trio affects Dishevelled trafficking in migrating NC cells

Previously, we showed that Dishevelled interacts with the Trio GEF2 domain and restores the Trio loss-of-function induced NC cell migration defects (Kratzer et al., 2020). Furthermore, Trio loss-of-function mediated Rac1 downregulation was rescued by Dishevelled expression. Dishevelled can interact with the GEF Tiam to activate Rac1 (Čajánek et al., 2013; Habas et al., 2003), but it is also a known regulator of Wnt signaling and RhoA activity (Gao and Chen, 2010). In addition, Dishevelled has been shown to affect microtubule stability in neurons (Ciani et al., 2004; Krylova et al., 2000). We further observed that co-expression of full-length-TRIO or TRIO-GEF2 together with Dishevelled recruits Trio to intracellular Dishevelled signalosomes (Kratzer et al., 2020). These intracellular vesicle-like organelles are known to be directionally transported along microtubules, as observed during embryonic cortical rotation establishing dorsal cell fates in *Xenopus* (Miller et al., 1999). Since Trio loss-of-function affects microtubule dynamics and Trio-Dishevelled interaction appears to be required for NC cell migration, we analyzed whether Trio loss-of-function affects Dishevelled trafficking in migrating NC cells. Therefore, *Xenopus* embryos were injected with Co MO or Trio MO together with *xDishevelled-GFP* RNA and *EB3-mCherry* RNA in one blastomere at the eight-cell stage. NC cells were explanted at stage 18 and cultivated on fibronectin-coated microscopy slides. Time lapse imaging was performed using spinning disk microscopy. Dishevelled was localized intracellular in small, dynamic dot-like structures (Fig. 5.11 A, supplemental movie 9). Each Dishevelled signalosome was tracked over time using the Imaris particle tracking tool. Interestingly, Trio morphant NC cells exhibited a reduced number of Dishevelled signalosomes per cell, measured by the track number (Fig. 5.11 B). Furthermore, the track length of Dishevelled signalosomes was significantly reduced in Trio morphant NC cells, measured by the track displacement length (Fig. 5.11 C). These preliminary findings indicate that impaired Trio function could affect Dishevelled trafficking in NC cells. Yet, conducting additional replicates is crucial to confirm the data. Thus, it remains to be investigated in future studies whether the decreased quantity of Dishevelled signalosomes and their compromised trafficking are a result of the microtubule stability defects due to Trio loss-of-function discussed earlier, or attributed to other factors.

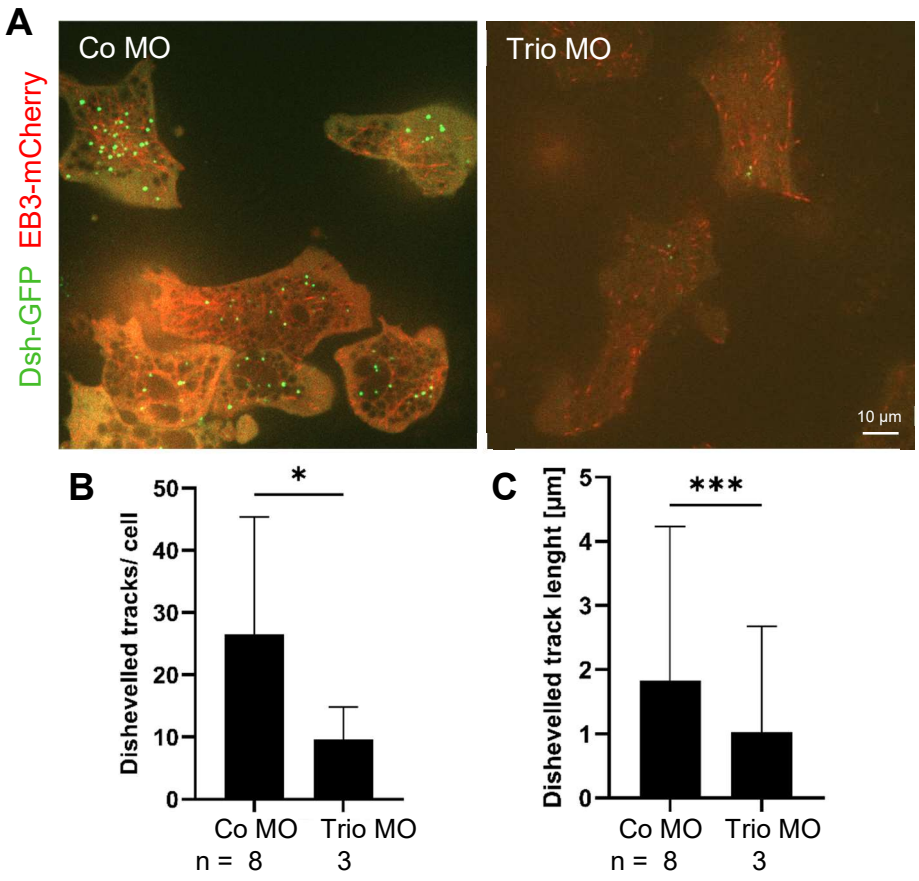

Figure 5.10 Dishevelled trafficking is impaired in Trio morphant NC cells. (A) *Xenopus* embryos were injected with 4 ng Co MO or Trio MO together with 200 pg *xDishevelled-GFP* RNA and *EB3-mCherry* RNA in one blastomere at the eight-cell stage. Life-cell imaging was performed using spinning disk microscopy. Dishevelled signalosomes were tracked over time using Imaris in one experiment. Scale bar = 10 µm **(B)** Trio morphant NC cells showed a reduced Dishevelled track number per cell, compared to controls. **(C)** In addition, the track length of Dishevelled signalosomes was significantly reduced in Trio morphant NC cells, measured by the track displacement length. **(B, C)** SD and number of analyzed cells are indicated for each condition. *p<0.05, ***p<0.001 (Mann-Whitney test).

5.6 Both Trio GEF domains play an important role in NC cell migration

We previously demonstrated that neural crest cell migration and protrusion formation rely on the Trio GEF2 domain, while the GEF1 domain appeared to be irrelevant in this context (Kratzer et al., 2020). Based on recent research, showing that the N-terminal spectrin repeats within the Trio protein autoregulate Trio GEF1 activity (Bircher et al., 2022; Bonnet et al., 2023), we repeated Trio loss-of-function rescue experiments, but instead of using constructs harboring only the respective GEF domains, we used full-length-TRIO constructs with catalytically dead GEF domains. These contain point mutations in either the GEF1 or GEF2 domain, which result in the elimination of their exchange activity (Cannet et al., 2014). Consequently, they are incapable of activating Rac1 (dead-GEF1) or RhoA (dead-GEF2). For rescue experiments, Trio MO was co-injected in *Xenopus* embryos with full-length-TRIO DNA,

TRIO-dead-GEF1 DNA or TRIO-dead-GEF2 DNA and *lacZ* RNA as lineage tracer. Co MO injection served as control condition. NC cell migration was analyzed at tailbud stages by *AP2-α in situ* hybridization. As expected, Trio MO injection resulted in severe NC migration defects (Kratzer et al., 2020; Moore et al., 2013), while control embryos displayed normal NC cell migration patterns (Fig. 5.11). Co-injection of full-length-TRIO DNA and TRIO-dead-GEF1 DNA restored *in vivo* NC migration. Surprisingly, injection of TRIO-dead-GEF2 DNA also prevented NC migration defects, although slightly less efficiently than the dead-GEF1 mutant, which possesses the functional GEF2 domain (Fig. 5.11). These results suggest that one GEF domain can substitute for the other. For example, Rac1, which is activated by the GEF1 domain, could potentially also be activated by the interaction between the GEF2 domain and Dishevelled, as previously discussed (Kratzer et al., 2020). Additionally, these findings indicate that the Trio GEF domains are not the only factors that are crucial for NC cell migration. The additional Trio domains, that influence its localization and binding to specific interaction partners, could also play an important role in regulating Trio's function during NC cell migration.

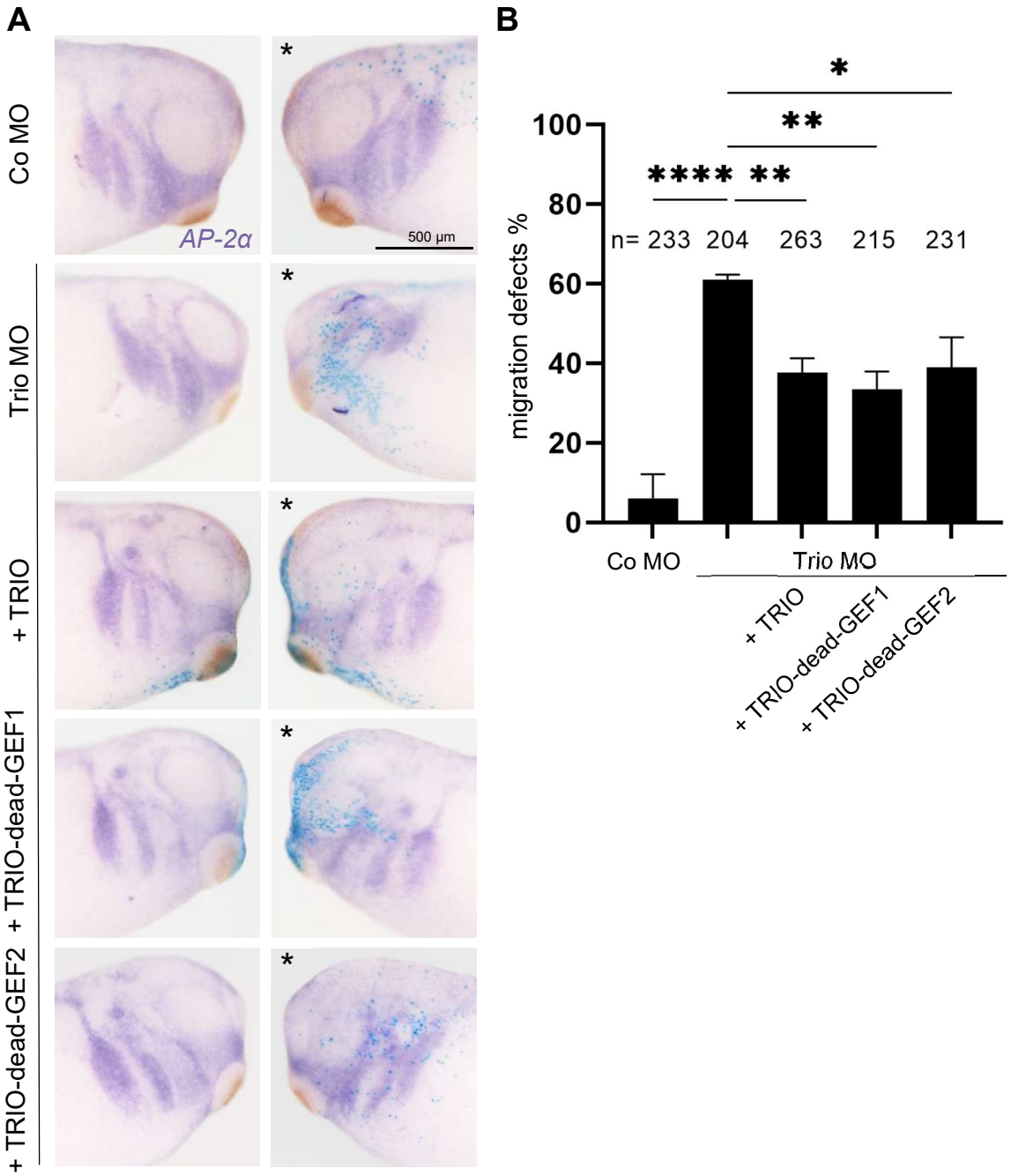

Figure 5.11 The Trio GEF1 and GEF2 domain play an important role in NC cell migration. (A) *Xenopus* embryos were injected with 4 ng Trio MO alone or in combination with 30 pg full-length TRIO-GFP DNA, 30 pg TRIO-dead-GEF1-GFP DNA or 30 pg Trio-dead-GEF2-GFP DNA and 100 pg *lacZ* mRNA as lineage tracer. Injection of 4 ng Co MO served as control condition and NC cell migration was analyzed at tailbud stages by *AP2-α in situ* hybridization. The injected side is marked with an asterisk. Scale bar = 500 µm. **(B)** Graph summarizing the percentage of embryos with NC cell migration defects in four independent experiments. +s.e.m. and the number of analyzed embryos are indicated for each condition. ****p<0.0001, **p<0.01, *p<0.05, ns = not significant (one-way ANOVA). As shown before (Kratzer et al., 2020), Trio MO injection caused severe NC migration defects. These were significantly reduced by co-injection of TRIO DNA, TRIO-dead-GEF1 DNA and TRIO-dead-GEF2 DNA.

5.7 Mapre2 and Tubb are required for craniofacial development in *Xenopus* embryos

Microtubule organization and dynamics as well as microtubule-based transport of vesicles and proteins are essential for cell migration (Etienne-Manneville, 2013). Here, we showed that the Rho GEF Trio functions via microtubule plus-end based transport and vice versa effects microtubule dynamics in migrating NC cells. Mapre2 is a member of the evolutionary conserved family of microtubule end binding proteins (Su and Qi, 2001) and was shown to be necessary for the regulation of cell adhesion, mitotic progression and genome stability (Iimori et al., 2016; Liu et al., 2015; Yue et al., 2014). Tubb encodes for a beta-tubulin and is highly expressed during central nervous system development (Sferra et al., 2020). To investigate a disease-related association between Trio, Mapre2 and Tubb and to comprehend their molecular function during NC cell migration, we performed initial loss-of-function experiments. First, we aimed to determine whether deficiencies in Mapre2's and Tubb's function in *Xenopus* embryos result in phenotypes like those observed in patients with mutations in the *MAPRE2* or *TUBB* genes. Individuals carrying *MAPRE2* mutations display intellectual disability, microcephaly and facial dysmorphism, reminiscent of those with *TRIO* gene mutations. Additionally, they exhibit symmetrical limb skin creases, a median cleft palate and short stature (Isrie et al., 2015). Further on, it was shown that mutations in the *TUBB* gene, lead to similar phenotypes (Isrie et al., 2015). To induce Mapre2 and Tubb loss-of-function in *Xenopus* embryos, translation-blocking morpholino antisense oligonucleotides were designed. For the *Xenopus mapre2* gene, there are five known transcript variants (Fisher et al., 2023) and both the L and S homeologs are expressed during development (Session et al., 2016). To target all possible *Mapre2* transcript variants, two Mapre2 morpholinos were designed (Fig 5.12 A). Mapre2 MO1 binds the 5' UTR of the L1 and S1 variants, while Mapre2 MO2 binds the 5' UTR and start codon region of the L2, S2 and S3 transcript variants, to ensure coverage for all potentially expressed Mapre2 isoforms. Since only the L homeolog of *Xenopus* Tubb is expressed during embryonic development (Session et al., 2016) and there is only one transcript variant described (Fisher et al., 2023), a single translation blocking Tubb MO was designed binding the 5' UTR and start codon region. For phenotypic analysis, embryos were injected with Mapre2 MO1, Mapre2 MO2, a combination of both or Tubb MO together with *lacZ* RNA as lineage tracer in one blastomere at the two-cell stage. Co MO injection served as control condition and embryos were analyzed at stage 44. Comparable to patient phenotypes, injection of Mapre2 MO2 and of the combination of Mapre2 MO1 and MO2 resulted in craniofacial malformation on the injected side (Fig. 5.12 B, C). Furthermore, embryos were shorter in length. In contrast, the injection of Mapre2 MO1 resulted in a slight increase in craniofacial defects, which did not reach statistical significance. This suggests that Mapre2 MO2 is more efficient than Mapre2 MO1. The embryos injected with Tubb MO also present craniofacial defects, including smaller eyes, shorter body length and impaired gut

development. In conclusion, these findings indicate that the used morpholinos lead to phenotypes similar to those observed in patients. This suggests that *Xenopus* can be used as a viable model organism for studying diseases associated with misregulation of Mapre2 and Tubb.

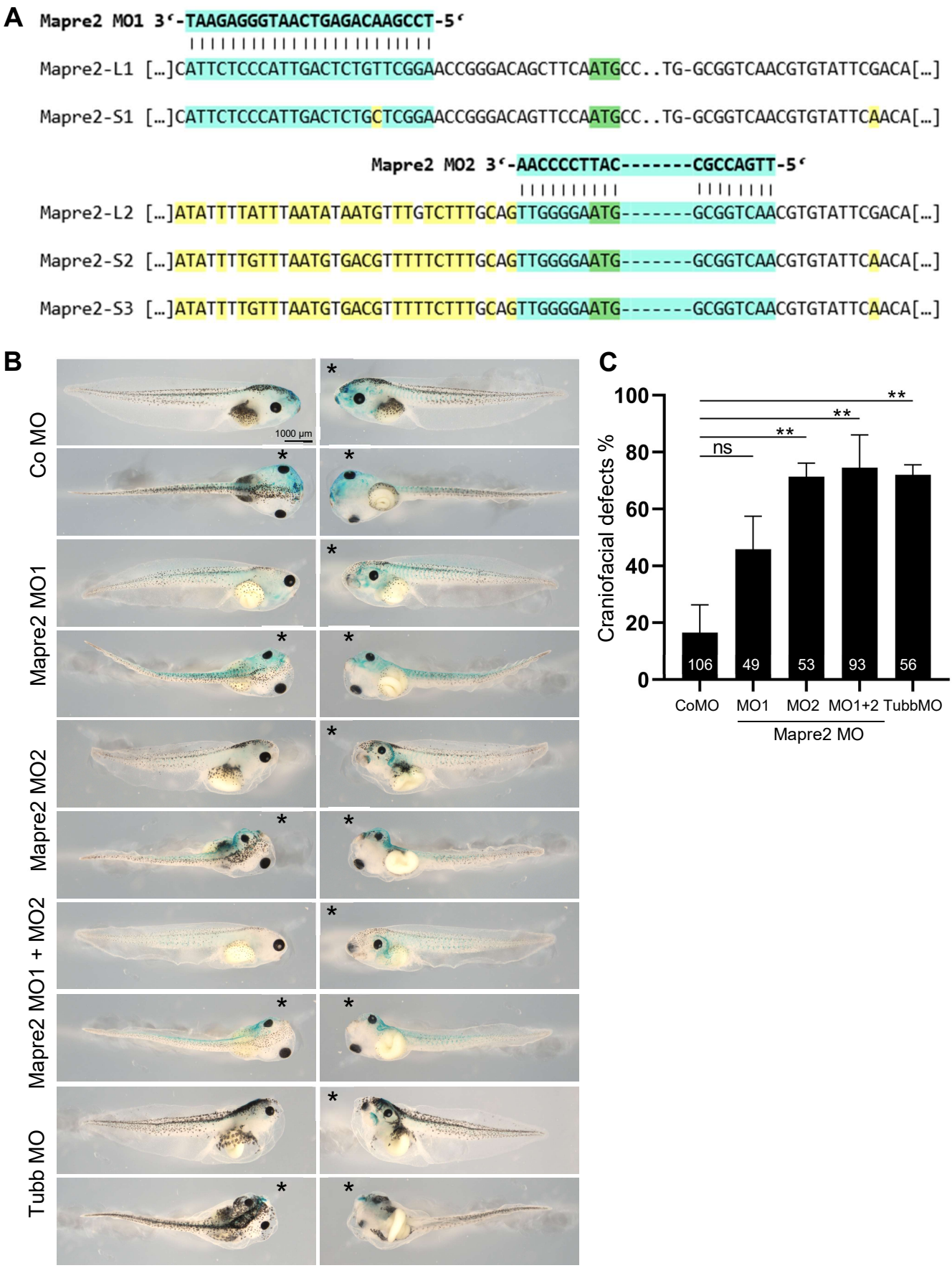
A
Mapre2 MO1 3'-TAAGAGGGTAACTGAGACAAGCCT-5'
Mapre2-L1 […]CATTCTCCCATTGACTCTGTTCGGAACCGGGACAGCTTCAATGCC..TG-GCGGTCAACGTGTATTCGACA[…]
Mapre2-S1 […]CATTCTCCCATTGACTCTGCTCGGAACCGGGACAGTTCCAATGCC..TG-GCGGTCAACGTGTATTCAACA[…]
Mapre2 MO2 3'-AACCCCTTAC-------CGCCAGTT-5'
Mapre2-L2 […]ATATTTTATTTAATATAATGTTTGTCTTTGCAGTTGGGGAATG-------GCGGTCAACGTGTATTCGACA[…]
Mapre2-S2 […]ATATTTTGTTTAATGTGACGTTTTTCTTTGCAGTTGGGGAATG-------GCGGTCAACGTGTATTCAACA[…]
Mapre2-S3 […]ATATTTTGTTTAATGTGACGTTTTTCTTTGCAGTTGGGGAATG-------GCGGTCAACGTGTATTCAACA[…]
B
Co MO
Mapre2 MO1
Mapre2 MO2
Mapre2 MO1 + MO2
Tubb MO
1000 µm
C
Craniofacial defects %
100
80
60
40
20
0
ns
**
**
**
106
49
53
93
56
CoMO
MO1
MO2
MO1+2
TubbMO
Mapre2 MO

Figure 5.12 Mapre2 and Tubb loss-of-function leads to craniofacial defects in *Xenopus* embryos. **(A)** Designed translation-blocking morpholino antisense oligonucleotides Mapre2 MO1 (3'-TAAGAGGGTAACTGAGACAAGCCT-5') and MO2 (3'-AACCCCTTACCGCCAGTT-5') (highlighted in blue). The respective *Mapre2* mRNA sequences are shown based on Xenbase (Fisher et al., 2023). Mapre2 MO1 is designed to target the transcript variants Mapre2-L1 and Mapre2-L2, binding to the 5' UTR. Mapre2 MO2 is designed to target the transcript variants Mapre2-L2, -S2 and -S3, binding to the 5' UTR and the start codon (ATG) regions (green). The morpholino binding regions are marked in blue. Yellow highlighted nucleotides show mismatches compared to the Mapre2-L1 sequence. Points (..) stand for the sequences of Mapre2-L1 and Mapre2-S1, that are hidden here. Hyphens (---) show that these sequence parts are missing in the Mapre2-L2, -S2 and S3 transcript variants. **(B)** *Xenopus* embryos were injected with 10 ng Co MO, Mapre2 MO1, Mapre2 MO2, a combination of 7.5 ng Mapre2 MO1 and MO2 each, or 10 ng Tubb MO (5'-TCATGGTTCAGGCGTAATAGAT-3') together with 100 pg *lacZ* RNA as lineage tracer in one blastomere at the two-cell stage. Developmental defects with focus on craniofacial malformations were analyzed at stage 44. The injected side is marked with an asterisk. Scale bar = 1000 µm. **(C)** Graph summarizing the percentage of embryos with craniofacial defects in three independent experiments. +s.e.m. and the number of analyzed embryos are indicated for each condition. **p<0.01, ns = not significant (one-way ANOVA). Injection of Mapre2 MO2 results in craniofacial defects, which were also observed with the combined injection of Mapre2 MO1 and MO2 and with the Tubb MO. Injection of Mapre2 MO1 alone did not result in significant craniofacial defects.

5.8 Mapre2 and Tubb loss-of-function induce early and late NC migration defects

Mutations in *MAPRE2* and *TUBB* have been demonstrated to cause defects in NC cell migration and, consequently lead to the observed patient phenotypes (Isrie et al., 2015). To analyze whether Mapre2 and Tubb loss-of-function induced craniofacial malformations are also caused by NC migration defects in *Xenopus*, embryos were injected with Mapre2 MO1, Mapre2 MO2, a combination of both or Tubb MO together with *lacZ* RNA as lineage tracer in one blastomere at the two-cell stage. Co Mo injection served as control condition. NC cell migration was analyzed at stage 21 and 26 by *twist in situ* hybridization. Mapre2 MO2 and Tubb MO injections caused severe NC migration defects in early and late migratory stages, compared to control embryos (Fig. 5.13). Again, Mapre2 MO1 injection did not induce any major defects (Fig. 5.13). Taken together, like in patients, loss of Mapre2 and Tubb results in impaired NC migration leading to craniofacial malformations in *Xenopus* embryos.

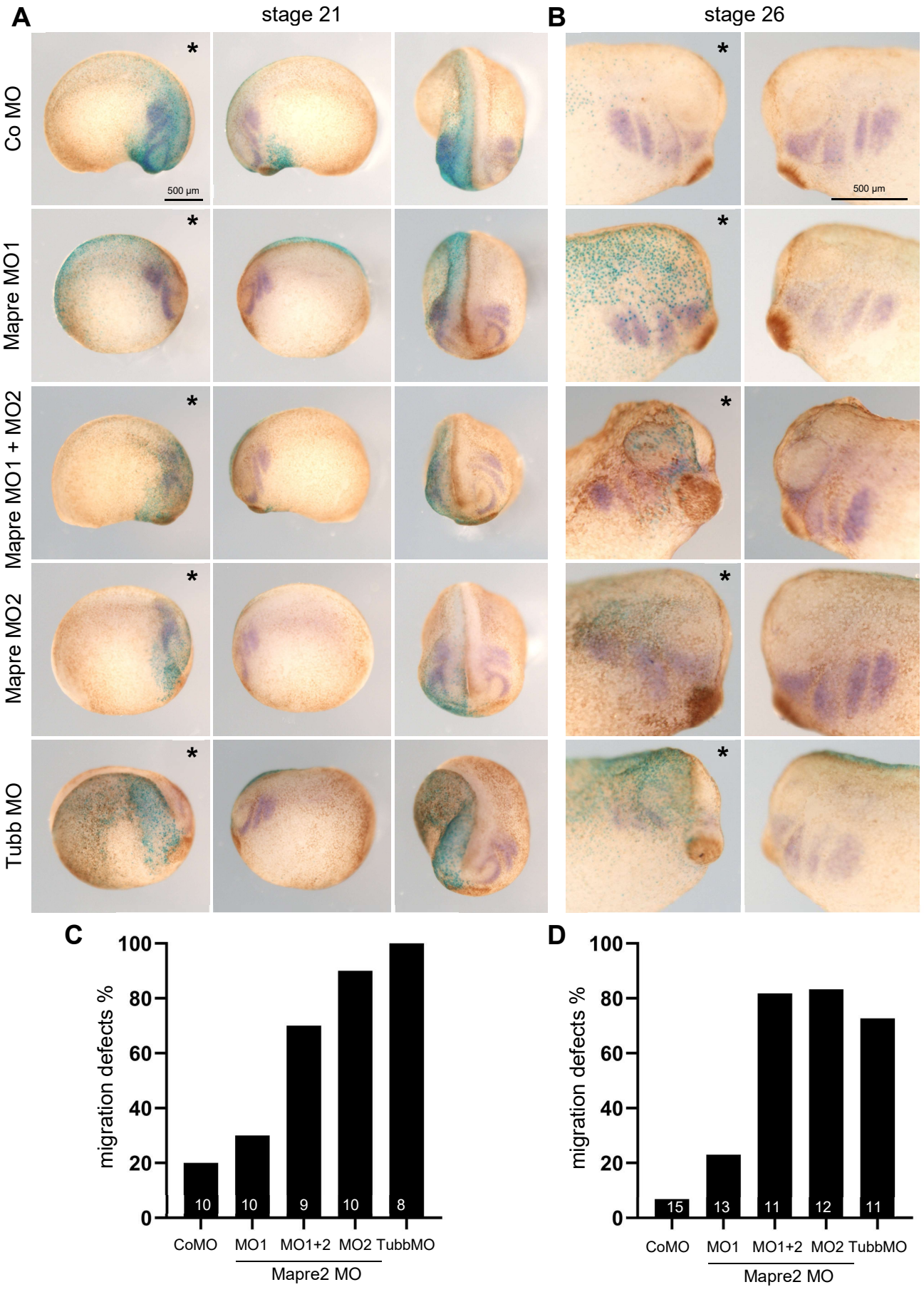
A
stage 21
B
stage 26
Co MO
Mapre MO1
Mapre MO1 + MO2
Mapre MO2
Tubb MO
500 µm
500 µm
C
migration defects %
100
80
60
40
20
0
10
10
9
10
8
CoMO
MO1
MO1+2
MO2
TubbMO
Mapre2 MO
D
migration defects %
100
80
60
40
20
0
15
13
11
12
11
CoMO
MO1
MO1+2
MO2
TubbMO
Mapre2 MO

Figure 5.13 Mapre2 and Tubb loss-of-function leads to early and late NC migration defects. *Xenopus* embryos were injected with 10 ng Co MO, Mapre2 MO1, Mapre2 MO2, a combination of 7.5 ng Mapre2 MO1 and MO2 each or 10 ng Tubb MO together with 100 pg *lacZ* RNA as lineage tracer in one blastomere at the two-cell stage. NC cell migration was analyzed at stage 21 **(A)** and 26 **(B)** by *twist in situ* hybridization. The injected side is marked with an asterisk. Scale bar = 500 µm. Graph summarizing the percentage of embryos with NC cell migration defects at stage 21 **(C)** and stage 26 **(D)** in one experiment. The number of analyzed embryos is indicated for each condition. Mapre2 and Tubb knockdown results in NC migration defects during early and late migratory stages, compared to control embryos. NC migration defects were mostly not observed following injection of Mapre2 MO1.

6. Discussion

The Rho GEF Trio is well suited to act as a downstream effector of several signaling pathways, that are involved in the regulation of cytoskeletal rearrangements and, thus, cell motility. During development, Trio is required for filopodia and lamellipodia formation and proper cell migration in NC cells (Kratzer et al. 2020). Loss of Trio results in a cell blebbing phenotype, in which NC cells fail to form protrusions and actin structures are disrupted. This blebbing phenotype is rescued by constitutively active Rac1 and RhoA, demonstrating that Trio activates both GTPases in NC cells (Kratzer et al., 2020). Additionally, a number of pathogenic *TRIO* missense or nonsense variants have been observed in patients, leading to various clinical manifestations, such as neurodevelopmental disorders, micro- or macrocephaly and distinct facial characteristics (Gazdagh et al., 2023). These findings provide further support for the existence of a defect in multipotent neural crest cells, which migrate long distances within the embryo during development and differentiate into various tissues and organs (Mayor and Theveneau, 2013). The literature provides evidence that Trio has distinct functions depending on its subcellular localization and interaction with different binding partners, resulting in temporal and spatial regulation of Rac1 and RhoA activity (Bellanger et al., 2000; Guo et al., 2021; Kashef et al., 2009; Kratzer et al., 2020; Kruse et al., 2019; Medley et al., 2003; Moore et al., 2013; van Haren et al., 2014). However, it is unclear how Trio is transported to different cellular compartments and whether additional cellular processes are affected, that lead to a defect in NC cell migration. Here, we show that Trio is transported by microtubules and participates in microtubule stability and focal adhesion dynamics - key mechanisms essential for cell migration.

6.1 Microtubule-mediated transport of Trio is required for its function in NC cell migration

In NC cells, Trio has been shown to have different functions depending on its subcellular localization. At cell protrusions, Trio interacts with Cadherin-11, which is required for NC cell migration (Kashef et al., 2009). Furthermore, Cadherin-11 plays a role in contact inhibition of locomotion (CIL), maintaining collective cell migration via its adhesive function. During CIL, Trio may play an important role in RhoA activation via Cadherin-11 at cell-cell contacts (Becker et al., 2013). In addition, Moore et al. showed that Trio co-localizes at NC cell-cell contacts with the polarity protein Par3. This interaction leads to an inhibition of the Trio GEF1 domain and, thereby, to a downregulation of Rac1 activity, facilitating microtubule depolymerization and cell retraction required for CIL (Moore et al., 2013).

Since Trio functions at specific subcellular sites, including cell-cell contacts and cell protrusions, it must be effectively and dynamically transported to these sites of action. Previously, it was shown that Trio interacts with the +TIP proteins EB1 and NAV1 and can itself act as +TIP via a specific microtubule plus-end localization motif (van Haren et al., 2014).

In neurons, this TRIO-NAV1 complex is important for neurite outgrowth. We find that Trio is likewise transported by microtubules in migrating NC cells, shown by co-localization studies using the microtubule marker EMTB and the +TIP marker EB3. Furthermore, using site-directed mutagenesis, we confirm that the amino acid motif SRIP, which is located immediately downstream of the GEF2 domain and has been shown to be required for EB1 binding in neurons (van Haren et al., 2014), is crucial for microtubule plus-end binding in NC cells as well. In addition, we showed that a GEF2 mutant, abolishing microtubule plus-end binding, was ineffective in rescuing the NC migration defects *in vivo* and *in vitro*. Furthermore, cell blebbing, measured by cell circularity, of Trio morphant NC cells was restored by wild type GEF2, but not by the GEF2 mutant. At higher concentrations of the GEF2 mutant, a rescue effect was observed, however, it was weaker compared to wild type GEF2. In this case, the GEF2 domain may be provided to all functional sites, potentially eliminating the need for microtubule plus end-mediated transport. To verify this concentration-dependent effect, western blotting could be used to test whether wild-type GEF2 and GEF2 mutant protein levels are the same in *Xenopus* embryo lysates. Furthermore, to support our findings, rescue experiments could be repeated using a full-length Trio construct containing the SRNN mutation. Taken together, these results demonstrate that microtubule-mediated trafficking of the Trio GEF2 domain is required for its function.

Another GEF, known as GEF-H1, has also been shown to bind directly to microtubules, which is inhibiting its function, while microtubule depolymerization leads to GEF-H1 mediated RhoA activation (Chang et al., 2008). It is currently unclear whether Trio or specific catalytic domains are inactive when transported on microtubule tracks. To analyze this, drugs like nocodazole, that affect microtubule stability and lead to depolymerization, or taxol, which induces microtubule polymerization, could be applied. For example, RhoA and Rac1 levels could be measured using FRET sensors in Trio morphant or Trio overexpressing NC cells treated with microtubule stability affecting drugs.

6.2 Trio is involved in regulating microtubule stability in migrating NC cells

Trio is not only transported by microtubules, but it also affects microtubule dynamics. Microtubule dynamics differ depending on their subcellular localization in migrating cells (reviewed in (Etienne-Manneville, 2013)). Consistent with the prior research shown for migrating NC cells (Moore et al., 2013; Villaseca et al., 2023), we observe differing microtubule dynamics at the cell's leading and trailing edges. At the leading edge, microtubules polymerize and facilitate the formation of protrusions, whereas at sites of cell-cell contact, microtubules undergo frequent catastrophes to retract protrusions, resulting in contact inhibition of locomotion. This gradient of microtubule stability is disturbed in Trio morphant NC cells. Microtubules at cell-cell contacts become more stable compared to controls, while at the leading edge, microtubule stability decreases, concluding that Trio is involved in maintaining

microtubule dynamics required for NC cell migration. Contrary to our findings, Moore et al. demonstrated that inhibition of Par3 results in an increase of Rac1 activity and stabilization of microtubules at NC cell-cell contacts, which can be rescued by co-injection of a Trio morpholino (Moore et al., 2013). Likely, Trio loss-of-function rescues the Par3 morphant phenotype, since loss of Trio also reduces Rac1 activity in NC cells (Kratzer et al., 2020), possibly offsetting the observed increase in Rac1 activity in Par3 morphant NC cells. In addition, it was shown that Par3 interacts with the GEF Tiam1, leading to Rac1 activation required for persistent migration of keratinocytes (Pegtel et al., 2007). Furthermore, Par3 depletion and Tiam1 deficiency reduced microtubule stability, shown by a decrease in microtubule acetylation. Possibly, like Trio, Par3 may have varying roles, that rely on its subcellular positioning and the linked interaction partners.

Additional to Trio and Tiam1, GEF-H1 was hypothesized to affect microtubule organization, since GEF-H1 overexpression showed abnormal circular microtubule morphology in COS7 cells (Yoshimura and Miki, 2011). Furthermore, it was suggested that GEF-H1 promotes tubulin-acetylation following microtubule binding and stabilization, while phosphorylation of GEF-H1 by Par1b releases GEF-H1 from microtubules and induces microtubule depolymerization. Our findings suggest that microtubule acetylation could also be affected in Trio morphant NC cells. However, the results are inconclusive, since only one experiment of acetylated tubulin staining was conducted and not all Trio morphant cells exhibited defects in tubulin acetylation. To examine the impact of Trio on microtubule acetylation, fluorescence intensity measurements of acetylated tubulin could be performed in Trio morphant cells. In addition, the ratio of tubulin to acetylated tubulin in single cells could be measured by fluorescence intensity or using western blotting. Furthermore, Trio could affect additional posttranslational modifications of microtubules. Interesting targets for testing are microtubule tyrosination and detyrosination. Dynamic microtubules are mainly tyrosinated, while detyrosination can inhibit microtubule disassembly (Palazzo et al., 2004). Here, again, immunostainings could be performed to analyze the levels of microtubule tyrosination and detyrosination in Trio morphant NC cells. The enzyme tubulin tyrosine ligase (TTL) catalyzes C-terminal α-tubulin tyrosination on αβ-tubulin heterodimers and restores tyrosinated-tubulin. The lab of Ralf Jacob established stable TTL-overexpressing Madin-Darby Canine Kidney ($MDCK_{TTL\text{-}GFP}$) and TTL deficient $MDCK_{\Delta TTL}$ cell lines (Müller et al., 2021), which could be used to study the effect of Trio on microtubule tyrosination and detyrosination. Initial experiments were started to cultivate these cell lines in our lab and various TRIO constructs were successfully expressed in MDCK wild type cells (supplemental figure 8.1). To elucidate the regulation of microtubule dynamics, upcoming experiments could investigate the effects of Trio or specific Trio domains on microtubule tyrosination and detyrosination.

Another binding partner of Trio, that is known to affect microtubule stability is Dishevelled. In

neurons, Dishevelled induces inhibition of GSK3β, which phosphorylates and inactivates microtubule-associated proteins (Ciani et al., 2004; Krylova et al., 2000). Here, we show that Trio loss-of-function impairs Dishevelled signalosome trafficking via microtubules. The initial findings indicate a reduced presence of Dishevelled signalosomes in Trio morphant cells, with those, that are present, exhibiting a shorter trafficking length. These experiments should be repeated to establish statistical evidence. Furthermore, co-localization and life-cell imaging analysis for Trio in combination with Dishevelled could be performed in NC cells, since our previous results, showing that Trio is recruited to Dishevelled positive signalosomes, were obtained using immunostaining in HEK293 cells (Kratzer et al., 2020). A remaining question is whether Dishevelled trafficking is indeed impaired in Trio morphant NC cells, despite our findings that Dishevelled rescues Trio loss-of-function induced NC migration defects (Kratzer et al., 2020). One hypothesis could be that Trio and Dishevelled operate at the same signaling level, capable of activating Rac1 and RhoA, while the absence of one component may still result in incomplete Trio or Dishevelled signaling functionality. Rescue experiments using Trio overexpression in Disheveled-deficient NC cells could be performed to test this hypothesis. The fact that Dishevelled can interact with the GEF Tiam1 to activate Rac1 (Cajanek et al., 2013; Habas et al., 2003), but is also known as a regulator of RhoA activity (Gao and Chen, 2010) supports this hypothesis. We have shown that Dishevelled interacts with the GEF2 domain of Trio and restores Trio morphant NC cell defects and Rac1 activity (Kratzer et al., 2020). Thus, there may be additional links in how the GEF2 domain is involved in the regulation of microtubule dynamics, potentially through specific interaction partners. At present, the molecular mechanisms, that regulate microtubule dynamics in various subcellular locations by Trio remain unclear. Nevertheless, our data suggests that the GEF2 domain plays a crucial role for Trio's functionality, in addition to the already well-defined function of the GEF1 domain.

6.3 Trio is required for focal adhesion dynamics in NC cells

In addition to its effects on microtubule dynamics, Trio appears to play a role in focal adhesion turnover during NC cell migration. This is not unexpected, as Trio localizes to paxillin-positive focal adhesion sites in non-NC cells (Muller et al., 2020) and has been shown to interact with and enhance the activity of FAK in COS-7 cells (Medley et al., 2003). Additionally, Trio was shown to be transported via acentrosomal microtubules toward focal adhesions (Cheng et al., 2019). Furthermore, Trio interacts with Cadherin-11 in NC cells (Backer et al., 2007; Kashef et al., 2009), which also localizes to focal adhesions and promotes adhesion to fibronectin (Langhe et al., 2016). Microtubules can specifically grow towards focal adhesions and promote focal adhesion turnover rate at the cell periphery, which facilitates cell retraction necessary for motility (Etienne-Manneville, 2004). Furthermore, migration depends on cell adhesion to the extracellular matrix (ECM), which occurs via focal adhesions, that connect the ECM to the cell cytoskeleton. To regulate focal adhesion turnover, there is a bidirectional crosstalk between stress fibers located at focal adhesions and microtubules. This crosstalk is guided by Rho-

GTPase signaling. Microtubule-mediated transport of RhoA regulators may be critical for the establishment of Rho GTPase activity zones, which have been shown to be necessary at focal adhesion sites and at the leading edge (Müller et al., 2020; Stehbens and Wittmann, 2012). Thus, via microtubule plus-end mediated transport, Trio could be directly transported to focal adhesions. Here, the GEF2 domain may play an essential role, since it was shown that RhoA activity is regulating both microtubule stability via the effector mDia, resulting in focal adhesion disassembly, as well as the development of stress fibers, which induces focal adhesion formation (Etienne-Manneville, 2004).

In this study, we show that loss of Trio leads to disturbed focal adhesion localization. Furthermore, by using live-cell imaging, we observed an increased focal adhesion size in Trio morphant cells. Additionally, focal adhesions seem to be less dynamic over time in Trio morphant cells compared to controls, the focal adhesion lifetime, however, was not significantly affected. The GEF STEF (Sif and Tiam1-like exchange factor) was shown to be required for multiple targeting of focal adhesions by microtubules, leading to Rac1 activation. STEF knockdown cells displayed a reduced focal adhesion disassembly rate leading to impaired cell migration (Rooney et al., 2010). Furthermore, MAPRE2 was shown to play a role in the crosstalk between microtubules and focal adhesions, since MAPRE2 knockdown caused enlarged focal adhesions leading to increased cell adhesion and impaired cell migration (Thues et al., 2021). To evaluate the impact of Trio loss-of-function on cell-matrix adhesion, a flipping assay could be performed alongside Atomic force microcopy-based single-cell force spectroscopy (SCFS), to determine if ECM adhesion is increased in Trio morphant NC cells as well.

Furthermore, it would be intriguing to visualize, how RhoA and Rac1 activity is impaired in Trio morphant NC cells. Since data from embryo lysates cannot provide insight into the intracellular localization of RhoA and Rac1, we attempted to measure Rac1 and RhoA activity in single cells using Rac1-GTP and RhoA-GTP antibodies, but the results were inconclusive. The measurement of Rac1-GTP fluorescence intensity exhibited no significant difference compared to control NC cells (supplemental figure 8.2). However, a comparison of Rac1-GTP levels at the leading edge and the cell-cell contact may provide more convincing results. Analysing Rac1 and RhoA activity using live-cell imaging would be even more promising. Therefore, FRET imaging using Rac1 and RhoA biosensors could be performed (Matthews et al., 2008). Additionally, live-cell imaging sensors have been developed to track active Rac1 and RhoA, which were found to be effective in *Xenopus* NC cells (Benink and Bement, 2005). Utilizing these, it would be very interesting to visualize if specific zones of RhoA and Rac1 signaling in distinct regions at the leading edge and at cell-cell contacts are affected by Trio loss-of-function, leading to impaired focal adhesion turnover and, thereby, to cell migration defects.

6.4 Additional Trio domains may play an essential role in Trio localization and function

In the literature, the frequency of *TRIO GEF2* mutations in patients is low (Gazdagh et al., 2023), raising the question of whether the GEF2 domain is less significant for TRIO's function in developmental processes or if loss-of-function mutations in the *GEF2* domain would be lethal due to its essential role. Interestingly, depletion of RhoA signaling in leukocytes leads to a loss of migratory polarity similar to the blebbing phenotype observed in Trio morphants (Heasman et al., 2010), indicating the potential relevance of Trio's GEF2 domain, which activates RhoA. This aligns with our previous findings that only the GEF2, but not GEF1 domain, can rescue Trio-loss-of-function induced NC cell migration defects (Kratzer et al., 2020). In contrast, we have shown here that both catalytically-dead-GEF1- and catalytically-dead-GEF2-full-length-TRIO are able to rescue Trio knockdown induced NC cell migration defects. On one hand, this could mean that it is irrelevant which GEF domain is functional, or that one GEF domain can take over the functionality of the other. The second possibility is suggested by our previous results, showing that the interaction between the GEF2 domain and Dishevelled could potentially lead to the activation of Rac1 (Kratzer et al., 2020). Additionally, it is possible that not only the GEF domains of Trio play a crucial role for its function, but also the additional domains that can potentially regulate Trio's localization and binding to specific effectors. This further supports that microtubule trafficking of Trio facilitates the spatiotemporally regulated activity of the Trio GEF domains.

It is likely that the other Trio domains, such as the Sec14 domain, the spectrin repeats or the SH3 domains, are also able to influence the subcellular localization of Trio, possibly by interacting with specific up- or downstream effectors recruiting it to functional sites. We tried to examine the specific functions of the N-terminal Trio GEF1 region, the microtubule binding motif and the Trio kinase domain by using splice blocking morpholinos. However, we were unable to demonstrate that these morpholinos resulted in the intended splicing event and/or caused specific downregulation effects in *Xenopus* embryos (data not shown). To analyze the relevance of the additional Trio domains for its subcellular localization, additional deletion mutants of Trio can be employed for localization studies. To analyze their biological relevance, rescue experiments using deletion constructs could be performed. In addition, CRISPR/Cas-based gene editing can be utilized to create targeted deletions or point mutations. In this case, *Xenopus tropicalis* is preferred over *Xenopus laevis* due to its diploid nature, which simplifies the editing process compared to the tetraploid *Xenopus laevis*.

6.5 Mapre2 and Tubb are required for NC cell migration and craniofacial development

Mapre2 is a member of the evolutionary conserved family of microtubule end binding proteins (Su and Qi, 2001) and was shown to be required for proper NC cell migration *in vitro* and the development of craniofacial structures *in vivo* (Thues et al., 2021). Furthermore, it is suggested that MAPRE2 plays a role in the crosstalk between microtubules and focal adhesions. Similar to the observed impairment of focal adhesions in Trio loss-of-function NC cells demonstrated here, Thues et al. showed that knockdown of MAPRE2 results in enlarged focal adhesion size, which enhances cell adhesion and impairs migration. To investigate the disease-related association between Trio and Mapre2 and understand their molecular function in NC cell migration, we performed initial experiments to determine if deficiencies of Mapre2 and Tubb in *Xenopus* embryos lead to similar phenotypes as observed in patients with mutations in the *MAPRE2* or *TUBB* genes. Individuals with *MAPRE2* mutations exhibit intellectual disability, microcephaly and facial dysmorphism, similar to those with *TRIO* gene mutations (Isrie et al., 2015). Mutations in the *TUBB* gene, which encodes for a beta-tubulin and is highly expressed during central nervous system development (Sferra et al., 2020), result in similar phenotypes (Isrie et al., 2015).

Our findings show that the injection of Mapre2 and Tubb morpholinos results in severe defects in *Xenopus* embryos comparable to those observed in patients with *MAPRE2* or *TUBB* mutations. Especially the development of craniofacial structures is significantly impaired. Furthermore, we showed that the knockdown of Mapre2 and Tubb has an impact on both early and late *in vivo* migration of NC cells. In a subsequent undergraduate project, it was demonstrated, that the loss of Mapre2 and Tubb also impacts the induction of NC cells (Hosenseidl, L., Bachelor thesis, 2023). Furthermore, the injection of Mapre2 and Tubb MOs impacts brain development in *Xenopus* embryos. It is currently unclear whether Trio and Mapre2 function together or interact with the same effectors to regulate the crosstalk between microtubules and focal adhesions. First, it would be interesting to study whether the loss of Mapre2 results in the same blebbing phenotype observed in Trio morphant NC cells. Furthermore, it could be tested if the impact of Mapre2 downregulation on microtubule dynamics and the potential effects on focal adhesion turnover are similar in *Xenopus* NC cells to what has been observed in human iPSC-derived NC cells (Thues et al., 2021). By utilizing immunoprecipitation or the yeast two-hybrid system, it could be analyzed whether Trio and Mapre2 act as direct binding partners. Conclusively, additional research is necessary to elucidate the interaction partners and signaling pathways affected by Trio and Mapre2 and to reveal their developmental functions.

7. Conclusion

The Rho GEF Trio is a known regulator of cell migration and is essential for filopodia and lamellipodia formation in NC cells (Kratzer et al., 2020). Furthermore, the small GTPases Rac1 and RhoA function downstream of Trio in the regulation of NC cell migration. Several pathogenic missense or nonsense variants in *TRIO* have been described in patients, leading to various clinical manifestations, such as developmental delay, microcephaly, macrocephaly, skeletal issues and facial dysmorphisms (Gazdagh et al., 2023). Understanding the molecular functions of Trio in cell migration processes is of great interest for comprehending human diseases linked to *TRIO* mutations. While previous studies have primarily examined the role of the GEF1 domain in activating Rac1, limited information exists on the functionality, regulation and interaction partners of the GEF2 domain, which activates RhoA. This study demonstrates that Trio is transported intracellularly via microtubule plus-ends and regulates microtubule dynamics. Additionally, Trio regulates focal adhesion dynamics in migrating NC cells. Since RhoA activity is required for both focal adhesion assembly and disassembly (Etienne-Manneville, 2004), the involvement of Trio in focal adhesion formation supports a crucial role for the GEF2 domain in this process. In addition, Rac1 activity is likely also involved in focal adhesion turnover (Rooney et al., 2010). We have shown here, that both full-length Trio with catalytically dead-GEF1 or catalytically dead-GEF2 rescued the Trio loss-of-function induced NC migration defects, although the GEF1 domain alone did not (Kratzer et al., 2020). This suggests that not only the two GEF domains are required for Trio's role in NC cell migration, but the additional domains may also be crucial in controlling Trio's localization and effector binding. Furthermore, it is possible that the Trio GEF domains mediate the function of both Rho GTPases through specific binding partners. For example, binding of the Trio GEF2 domain to Dishevelled could facilitate Rac1 activation induced by Dishevelled (Kratzer et al., 2020). Another potential binding partner of Trio could be Mapre2, as it is a microtubule end-binding protein that contributes to focal adhesion formation. Additionally, mutations in *MAPRE2* in patients have resulted in phenotypes similar to those observed in patients with *TRIO* mutations. Our findings show that the effects of Mapre2 loss-of-function can be analyzed using the model organism *Xenopus*. Future experiments will reveal whether Trio and Mapre2 act in the same signaling pathway and how both of these proteins affect cellular processes, such as cytoskeletal rearrangement, cell-matrix adhesion and protrusive activity.

Furthermore, we were able to replicate the Tubb loss-of-function malformations reported in patients with *TUBB* mutations in *Xenopus* embryos. Since Trio, Mapre2 and Tubb are involved in tubulin organization, this provides a connection to tubulopathies, which are a class of disorders in which genes encoding for tubulin are affected (Hoff et al., 2022). These disorders can as well result in neurodevelopmental malfunction. Furthermore, the tubulin biology required for NC cell migration links tubulin regulating factors to the functionality of chromatin

regulators, since these were often shown to regulate both histones and tubulin. Defects in chromatin regulators can also lead to neurodevelopmental disorders like observed for Trio, Mapre2 and Tubb (Lasser et al., 2023). In conclusion, it is of great interest to gain an understanding of the molecular interactions and signaling pathways, that govern microtubule and focal adhesion dynamics - crucial mechanisms underlying cell migration. Deciphering the roles of Trio, Mapre2 and Tubb in neural crest cell migration will provide further insight into the regulation of these processes. Ultimately, this will be an important step for the discovery of new treatments for neurodevelopmental disorders, that affect tubulin-regulating genes.

8. Supplement

8.1 Time lapse movies

Movie 1: xGEF2-positive spots co-localize at EMTB-tomato-positive microtubules in NC cells. Experiment was performed as described in Fig. 5.1 B. xGEF2-GFP (green) is dynamically localized, EMTB-tomato (red) marks microtubules, merge (green + red) shows that xGEF2-GFP co-localizes to EMTB-tomato marked microtubules and moves from the cell center to the cell membrane. Scale bar = 5 µm, recording time is indicated.

Movie 2: xGEF2-positive spots co-localize with the +TIP marker EB3-mCherry in NC cells. Experiment was performed as described in Fig. 5.3. xGEF2-GFP (green) dynamically co-localizes with EB3-mCherry (red) positive microtubule plus-ends, visible in the merge channel (green + red). Scale bar = 5 µm, recording time is indicated.

Movie 3: xGEF2-SRNN mutant abolishes co-localization to microtubule tips. Experiment was performed as described in Fig. 5.3. xGEF2-SRNN-GFP (green) does not co-localize with EB3-mCherry (red) positive microtubule plus-ends, visible in the merge channel (green + red). Scale bar = 5 µm, recording time is indicated.

Movie 4: xGEF2-SSNN mutant co-localization to microtubule tips. Experiment was performed as described in Fig. 5.3. xGEF2-SSNN-GFP (green) dynamically co-localizes with EB3-mCherry (red) positive microtubule plus-ends, visible in the merge channel (green + red). Scale bar = 5 µm, recording time is indicated.

Movie 5: Migrating control NC cell showing microtubule plus-end dynamics. Experiment was performed as described in Fig. 5.6. EB3-mCherry positive microtubule tips are shown in red and the cell membrane is marked in green by membrane-GFP. Scale bar = 5 µm, recording time is indicated.

Movie 6: Migrating Trio morphant NC cell showing microtubule plus-end dynamics. Experiment was performed as described in Fig. 5.6. EB3-mCherry positive microtubule tips are shown in red and the cell membrane is marked in green by membrane-GFP. Scale bar = 5 µm, recording time is indicated.

Movie 7: Trio morphant and control NC cell during cell-cell contact showing microtubule plus-end dynamics. Experiment was performed as described in Fig. 5.6. Control cell shows EB3-mCherry positive microtubule tips and Trio morphant cell shows EB3-GFP positive microtubule tips. Scale bar = 5 µm, recording time is indicated.

Movie 8: Trio loss-of-function impairs focal adhesion formation. Experiment was performed as described in Fig. 5.9. Control cell shows dynamic focal adhesion marked by Paxillin-mCherry. Trio morphant cell shows impaired focal adhesion dynamics marked by Paxillin-mCherry. Scale bar = 5 µm, recording time is indicated.

Movie 9: Dishevelled trafficking is impaired in Trio morphant NC cells. Experiment was performed as described in Fig. 5.10. Control cells (left channel) show dynamic Dishevelled-GFP signalosomes (green) and EB3-mCherry (red) signal. Trio morphant cells (right channel) show less Dishevelled-GFP signalosomes (green), that are less mobile compared to controls. EB3-mCherry signal is shown in red. Scale bar = 10 µm, recording time is indicated.

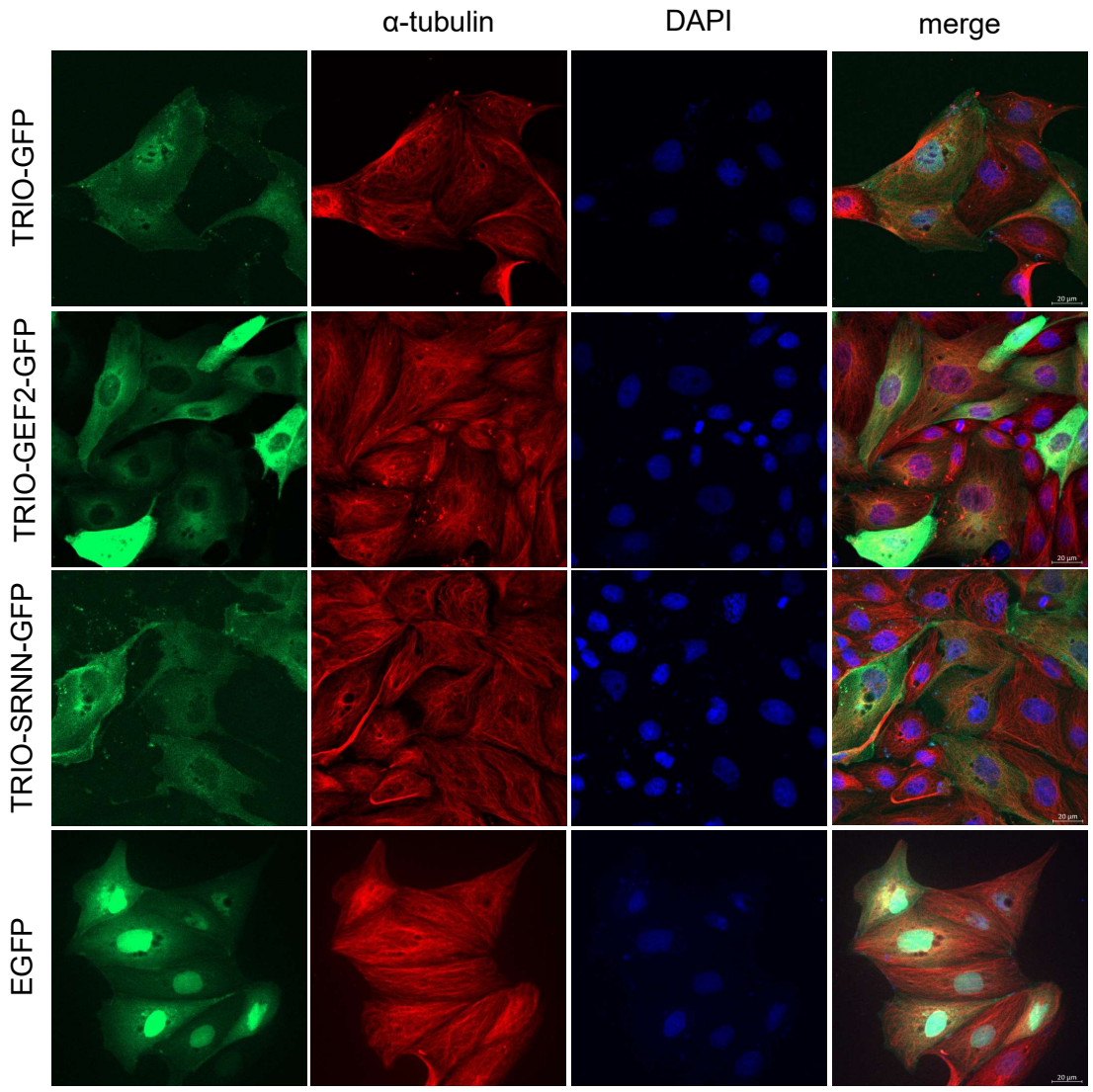

Supplemental Figure 8.1 Immunostaining of MDCK wild type cells transfected with different TRIO constructs. MDCK wild type cells were transfected with 800 ng DNA of TRIO-GFP, TRIO-GEF2-GFP, TRIO-SRNN-GFP or EGFP. Immunostaining was performed against α-tubulin and the nucleus was marked by DAPI staining. Scale bar = 20 µm

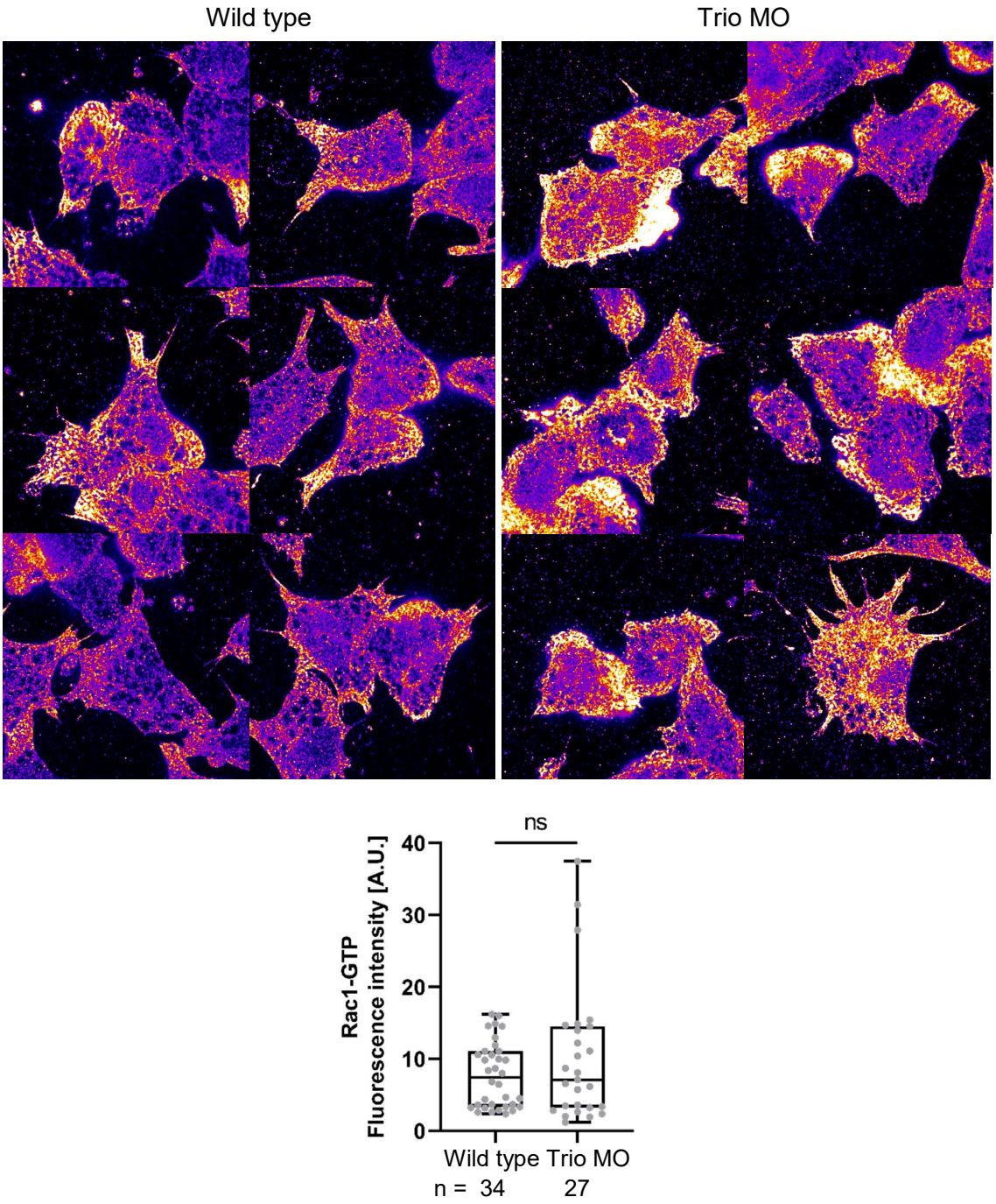

Supplemental Figure 8.2 Rac1-GTP level in Trio morphant NC cells compared to controls. *Xenopus* embryos were injected with 4 ng Trio MO together with *membrane-GFP* RNA as lineage tracer in the eight-cell stage. Wild type NC cells served as control. NC cells were explanted at stage 18 and, after fixation, immunostaining against Rac1-GTP was performed. Randomly picked example cells are shown. Signal intensity is visualized using a “fire” color scale, where blue indicates no signal and white indicates strong signal. Statistical analysis revealed no significant difference in Rac1 fluorescence intensity between Trio morphant cells and control cells. Box plots show median, 25th to 75th percentiles and Whiskers from min to max for three independent experiments. Single values for analyzed cells are shown in gray, numbers of cells are indicated, ns = not significant (Mann-Whitney test).

9. References

Abiatari, I., Gillen, S., DeOliveira, T., Klose, T., Bo, K., Giese, N. A., Friess, H. and Kleeff, J. (2009). The microtubule-associated protein MAPRE2 is involved in perineural invasion of pancreatic cancer cells. *International journal of oncology* **35**, 1111–1116. doi:10.3892/ijo_00000426.

Akhmanova, A. and Steinmetz, M. O. (2010). Microtubule +TIPs at a glance. *Journal of cell science* **123**, 3415–3419. doi:10.1242/jcs.062414.

András Szabó and Roberto Mayor. Mechanisms of Neural Crest Migration.

Ba, W., Yan, Y., Reijnders, M. R. F., Schuurs-Hoeijmakers, J. H. M., Feenstra, I., Bongers, E. M. H. F., Bosch, D. G. M., Leeuw, N. de, **Pfundt, R. and Gilissen, C. et al.** (2016). TRIO loss of function is associated with mild intellectual disability and affects dendritic branching and synapse function. *Human molecular genetics* **25**, 892–902. doi:10.1093/hmg/ddv618.

Backer, S., Lokmane, L., Landragin, C., Deck, M., Garel, S. and Bloch-Gallego, E. (2018). Trio GEF mediates RhoA activation downstream of Slit2 and coordinates telencephalic wiring. *Development (Cambridge, England)* **145**. doi:10.1242/dev.153692.

Bandekar, S. J., Arang, N., Tully, E. S., Tang, B. A., Barton, B. L., Li, S., Gutkind, J. S. and Tesmer, J. J. G. (2019). Structure of the C-terminal guanine nucleotide exchange factor module of Trio in an autoinhibited conformation reveals its oncogenic potential. *Science signaling* **12**. doi:10.1126/scisignal.aav2449.

Bandekar, S. J., Chen, C.-L., Ravala, S. K., Cash, J. N., Avramova, L. V., Zhalnina, M. V., Gutkind, J. S., Li, S. and Tesmer, J. J. G. (2022). Structural/functional studies of Trio provide insights into its configuration and show that conserved linker elements enhance its activity for Rac1. *The Journal of biological chemistry* **298**, 102209. doi:10.1016/j.jbc.2022.102209.

Barbosa, S., Greville-Heygate, S., Bonnet, M., Godwin, A., Fagotto-Kaufmann, C., Kajava, A. V., Laouteouet, D., Mawby, R., Wai, H. A. and Dingemans, A. J. M. et al. (2020). Opposite Modulation of RAC1 by Mutations in TRIO Is Associated with Distinct, Domain-Specific Neurodevelopmental Disorders. *American journal of human genetics* **106**, 338–355. doi:10.1016/j.ajhg.2020.01.018.

Barriga, E. H. and Mayor, R. (2015). Embryonic cell-cell adhesion: a key player in collective neural crest migration. *Current topics in developmental biology* **112**, 301–323. doi:10.1016/bs.ctdb.2014.11.023.

Becker, S. F. S., Mayor, R. and Kashef, J. (2013). Cadherin-11 mediates contact inhibition of locomotion during Xenopus neural crest cell migration. *PloS one* **8**, e85717. doi:10.1371/journal.pone.0085717.

Bellanger, J. M., Astier, C., Sardet, C., Ohta, Y., Stossel, T. P. and Debant, A. (2000). The Rac1- and RhoG-specific GEF domain of Trio targets filamin to remodel cytoskeletal actin. *Nature cell biology* **2**, 888–892. doi:10.1038/35046533.

Bellanger, J.-M., Estrach, S., Schmidt, S., Briançon-Marjollet, A., Zugasti, O., Fromont, S. and Debant, A. (2003). Different regulation of the Trio Dbl-Homology domains by their associated PH domains. *Biology of the cell* **95**, 625–634. doi:10.1016/j.biolcel.2003.10.002.

Benink, H. A. and Bement, W. M. (2005). Concentric zones of active RhoA and Cdc42 around single cell wounds. *The Journal of cell biology* **168**, 429–439. doi:10.1083/jcb.200411109.

Berginski, M. E. and Gomez, S. M. (2013). The Focal Adhesion Analysis Server: a web tool for analyzing focal adhesion dynamics. *F1000Res*. doi:10.3410/f1000research.2-68.v1.

Bircher, J. E., Corcoran, E. E., Lam, T. T., Trnka, M. J. and Koleske, A. J. (2022). Autoinhibition of the GEF activity of cytoskeletal regulatory protein Trio is disrupted in neurodevelopmental disorder-related genetic variants. *The Journal of biological chemistry* **298**, 102361. doi:10.1016/j.jbc.2022.102361.

Bircher, J. E. and Koleske, A. J. (2023). Correction: Trio family proteins as regulators of cell migration and morphogenesis in development and disease - mechanisms and cellular contexts. *Journal of cell science* **136**. doi:10.1242/jcs.260984.

Blangy, A., Vignal, E., Schmidt, S., Debant, A., Gauthier-Rouvière, C. and Fort, P. (2000). TrioGEF1 controls Rac- and Cdc42-dependent cell structures through the direct activation of rhoG. *Journal of cell science* **113 (Pt 4)**, 729–739. doi:10.1242/jcs.113.4.729.

Bonnet, M., Roche, F., Fagotto-Kaufmann, C., Gazdagh, G., Truong, I., Comunale, F., Barbosa, S., Bonhomme, M., Nafati, N. and Hunt, D. et al. (2023). Pathogenic TRIO variants associated with neurodevelopmental disorders perturb the molecular regulation of TRIO and axon pathfinding in vivo. *Molecular psychiatry* **28**, 1527–1544. doi:10.1038/s41380-023-01963-x.

Bulinski, J. C., Odde, D. J., Howell, B. J., Salmon, T. D. and Waterman-Storer, C. M. (2001). Rapid dynamics of the microtubule binding of ensconsin in vivo. *Journal of cell science* **114**, 3885–3897. doi:10.1242/jcs.114.21.3885.

Čajánek, L., Ganji, R. S., Henriques-Oliveira, C., Theofilopoulos, S., Koník, P., Bryja, V. and Arenas, E. (2013). Tiam1 regulates the Wnt/Dvl/Rac1 signaling pathway and the differentiation of midbrain dopaminergic neurons. *Molecular and cellular biology* **33**, 59–70. doi:10.1128/MCB.00745-12.

Campellone, K. G. and Welch, M. D. (2010). A nucleator arms race: cellular control of actin assembly. *Nature reviews. Molecular cell biology* **11**, 237–251. doi:10.1038/nrm2867.

Cannet, A., Schmidt, S., Delaval, B. and Debant, A. (2014). Identification of a mitotic Rac-GEF, Trio, that counteracts MgcRacGAP function during cytokinesis. *Molecular biology of the cell* **25**, 4063–4071. doi:10.1091/mbc.E14-06-1153.

Carmona-Fontaine, C., Matthews, H. K., Kuriyama, S., Moreno, M., Dunn, G. A., Parsons, M., Stern, C. D. and Mayor, R. (2008). Contact inhibition of locomotion in vivo controls neural crest directional migration. *Nature* **456**, 957–961. doi:10.1038/nature07441.

Chang, Y.-C., Nalbant, P., Birkenfeld, J., Chang, Z.-F. and Bokoch, G. M. (2008). GEF-H1 couples nocodazole-induced microtubule disassembly to cell contractility via RhoA. *Molecular biology of the cell* **19**, 2147–2153. doi:10.1091/mbc.e07-12-1269.

Charrasse, S., Comunale, F., Fortier, M., Portales-Casamar, E., Debant, A. and Gauthier-Rouvière, C. (2007). M-cadherin activates Rac1 GTPase through the Rho-GEF trio during myoblast fusion. *Molecular biology of the cell* **18**, 1734–1743. doi:10.1091/mbc.e06-08-0766.

Cheng, H.-W., Hsiao, C.-T., Chen, Y.-Q., Huang, C.-M., Chan, S.-I., Chiou, A. and Kuo, J.-C. (2019). Centrosome guides spatial activation of Rac to control cell polarization and directed cell migration. *Life science alliance* **2**. doi:10.26508/lsa.201800135.

Ciani, L., Krylova, O., Smalley, M. J., Dale, T. C. and Salinas, P. C. (2004). A divergent canonical WNT-signaling pathway regulates microtubule dynamics: dishevelled signals locally to stabilize microtubules. *The Journal of cell biology* **164**, 243–253. doi:10.1083/jcb.200309096.

Debant, A., Serra-Pagès, C., Seipel, K., O'Brien, S., Tang, M., Park, S. H. and Streuli, M. (1996). The multidomain protein Trio binds the LAR transmembrane tyrosine phosphatase, contains a protein kinase domain, and has separate rac-specific and rho-specific guanine nucleotide exchange factor domains. *Proceedings of the National Academy of Sciences of the United States of America* **93**, 5466–5471. doi:10.1073/pnas.93.11.5466.

DeGeer, J., Kaplan, A., Mattar, P., Morabito, M., Stochaj, U., Kennedy, T. E., Debant, A., Cayouette, M., Fournier, A. E. and Lamarche-Vane, N. (2015). Hsc70 chaperone activity underlies Trio GEF function in axon growth and guidance induced by netrin-1. *The Journal of cell biology* **210**, 817–832. doi:10.1083/jcb.201505084.

Djinovic-Carugo, K., Gautel, M., Ylänne, J. and Young, P. (2002). The spectrin repeat: a structural platform for cytoskeletal protein assemblies. *FEBS letters* **513**, 119–123. doi:10.1016/s0014-5793(01)03304-x.

Efimov, A., Schiefermeier, N., Grigoriev, I., Ohi, R., Brown, M. C., Turner, C. E., Small, J. V. and Kaverina, I. (2008). Paxillin-dependent stimulation of microtubule catastrophes at focal adhesion sites. *Journal of cell science* **121**, 196–204. doi:10.1242/jcs.012666.

Eshun-Wilson, L., Zhang, R., Portran, D., Nachury, M. V., Toso, D. B., Löhr, T., Vendruscolo, M., Bonomi, M., Fraser, J. S. and Nogales, E. (2019). Effects of α-tubulin acetylation on microtubule

structure and stability. *Proceedings of the National Academy of Sciences of the United States of America* **116**, 10366–10371. doi:10.1073/pnas.1900441116.

Etienne-Manneville, S. (2004). Actin and microtubules in cell motility: which one is in control? *Traffic (Copenhagen, Denmark)* **5**, 470–477. doi:10.1111/j.1600-0854.2004.00196.x.

Etienne-Manneville, S. (2013). Microtubules in cell migration. *Annual review of cell and developmental biology* **29**, 471–499. doi:10.1146/annurev-cellbio-101011-155711.

Etienne-Manneville, S. and Hall, A. (2002). Rho GTPases in cell biology. *Nature* **420**, 629–635. doi:10.1038/nature01148.

Fisher, M., James-Zorn, C., Ponferrada, V., Bell, A. J., Sundararaj, N., Segerdell, E., Chaturvedi, P., Bayyari, N., Chu, S. and Pells, T. et al. (2023). Xenbase: key features and resources of the Xenopus model organism knowledgebase. *Genetics* **224**. doi:10.1093/genetics/iyad018.

Forsthoefel, D. J., Liebl, E. C., Kolodziej, P. A. and Seeger, M. A. (2005). The Abelson tyrosine kinase, the Trio GEF and Enabled interact with the Netrin receptor Frazzled in Drosophila. *Development (Cambridge, England)* **132**, 1983–1994. doi:10.1242/dev.01736.

Fritz, R. D., Letzelter, M., Reimann, A., Martin, K., Fusco, L., Ritsma, L., Ponsioen, B., Fluri, E., Schulte-Merker, S. and van Rheenen, J. et al. (2013). A versatile toolkit to produce sensitive FRET biosensors to visualize signaling in time and space. *Science signaling* **6**, rs12. doi:10.1126/scisignal.2004135.

Galjart, N. (2010). Plus-end-tracking proteins and their interactions at microtubule ends. *Current biology : CB* **20**, R528-37. doi:10.1016/j.cub.2010.05.022.

Gao, C. and Chen, Y.-G. (2010). Dishevelled: The hub of Wnt signaling. *Cellular signalling* **22**, 717–727. doi:10.1016/j.cellsig.2009.11.021.

Gazdagh, G., Hunt, D., Gonzalez, A. M. C., Rodriguez, M. P., Chaudhry, A., Madruga, M., Vansenne, F., Shears, D., Curie, A. and Stattin, E.-L. et al. (2023). Extending the phenotypes associated with TRIO gene variants in a cohort of 25 patients and review of the literature. *American journal of medical genetics. Part A* **191**, 1722–1740. doi:10.1002/ajmg.a.63194.

Goldspink, D. A., Gadsby, J. R., Bellett, G., Keynton, J., Tyrrell, B. J., Lund, E. K., Powell, P. P., Thomas, P. and Mogensen, M. M. (2013). The microtubule end-binding protein EB2 is a central regulator of microtubule reorganisation in apico-basal epithelial differentiation. *Journal of cell science* **126**, 4000–4014. doi:10.1242/jcs.129759.

Grubisha, M. J., DeGiosio, R. A., Wills, Z. P. and Sweet, R. A. (2022). Trio and Kalirin as unique enactors of Rho/Rac spatiotemporal precision. *Cellular signalling* **98**, 110416. doi:10.1016/j.cellsig.2022.110416.

Guo, S., Meng, L., Liu, H., Yuan, L., Zhao, N., Ni, J., Zhang, Y., Ben, J., Li, Y.-P. and Ma, J. (2021). Trio cooperates with Myh9 to regulate neural crest-derived craniofacial development. *Theranostics* **11**, 4316–4334. doi:10.7150/thno.51745.

Habas, R., Dawid, I. B. and He, X. (2003). Coactivation of Rac and Rho by Wnt/Frizzled signaling is required for vertebrate gastrulation. *Genes & development* **17**, 295–309. doi:10.1101/gad.1022203.

Harland, R. M. (1991). In situ hybridization: an improved wholemount method for Xenopus embryos. *Methods Cell Biol*, 685–695.

Heasman, S. J., Carlin, L. M., Cox, S., Ng, T. and Ridley, A. J. (2010). Coordinated RhoA signaling at the leading edge and uropod is required for T cell transendothelial migration. *The Journal of cell biology* **190**, 553–563. doi:10.1083/jcb.201002067.

Henty-Ridilla, J. L., Rankova, A., Eskin, J. A., Kenny, K. and Goode, B. L. (2016). Accelerated actin filament polymerization from microtubule plus ends. *Science (New York, N.Y.)* **352**, 1004–1009. doi:10.1126/science.aaf1709.

Hodge, R. G. and Ridley, A. J. (2016). Regulating Rho GTPases and their regulators. *Nature reviews. Molecular cell biology* **17**, 496–510. doi:10.1038/nrm.2016.67.

Hoff, K. J., Neumann, A. J. and Moore, J. K. (2022). The molecular biology of tubulinopathies: Understanding the impact of variants on tubulin structure and microtubule regulation. *Frontiers in*

cellular neuroscience **16**, 1023267. doi:10.3389/fncel.2022.1023267.

Honnappa, S., Gouveia, S. M., Weisbrich, A., Damberger, F. F., Bhavesh, N. S., Jawhari, H., Grigoriev, I., van Rijssel, F. J. A., Buey, R. M. and Lawera, A. et al. (2009). An EB1-binding motif acts as a microtubule tip localization signal. *Cell* **138**, 366–376. doi:10.1016/j.cell.2009.04.065.

Hopwood, N. D., Pluck, A. and Gurdon, J. B. (1989). A Xenopus mRNA related to Drosophila twist is expressed in response to induction in the mesoderm and the neural crest. *Cell* **59**, 893–903. doi:10.1016/0092-8674(89)90612-0.

Hosenseidl, L., Bachelor thesis (2023). The function of the end-binding protein Mapre2 during neural crest cell migration in Xenopus laevis.

Iimori, M., Watanabe, S., Kiyonari, S., Matsuoka, K., Sakasai, R., Saeki, H., Oki, E., Kitao, H. and Maehara, Y. (2016). Phosphorylation of EB2 by Aurora B and CDK1 ensures mitotic progression and genome stability. *Nature communications* **7**, 11117. doi:10.1038/ncomms11117.

Isrie, M., Breuss, M., Tian, G., Hansen, A. H., Cristofoli, F., Morandell, J., Kupchinsky, Z. A., Sifrim, A., Rodriguez-Rodriguez, C. M. and Dapena, E. P. et al. (2015). Mutations in Either TUBB or MAPRE2 Cause Circumferential Skin Creases Kunze Type. *American journal of human genetics* **97**, 790–800. doi:10.1016/j.ajhg.2015.10.014.

Kamato, D., Mitra, P., Davis, F., Osman, N., Chaplin, R., Cabot, P. J., Afroz, R., Thomas, W., Zheng, W. and Kaur, H. et al. (2017). Gaq proteins: molecular pharmacology and therapeutic potential. *Cellular and molecular life sciences : CMLS* **74**, 1379–1390. doi:10.1007/s00018-016-2405-9.

Kashef, J., Köhler, A., Kuriyama, S., Alfandari, D., Mayor, R. and Wedlich, D. (2009). Cadherin-11 regulates protrusive activity in Xenopus cranial neural crest cells upstream of Trio and the small GTPases. *Genes & development* **23**, 1393–1398. doi:10.1101/gad.519409.

Katrancha, S. M., Wu, Y., Zhu, M., Eipper, B. A., Koleske, A. J. and Mains, R. E. (2017). Neurodevelopmental disease-associated de novo mutations and rare sequence variants affect TRIO GDP/GTP exchange factor activity. *Human molecular genetics* **26**, 4728–4740. doi:10.1093/hmg/ddx355.

Kaverina, I., Rottner, K. and Small, J. V. (1998). Targeting, capture, and stabilization of microtubules at early focal adhesions. *The Journal of cell biology* **142**, 181–190. doi:10.1083/jcb.142.1.181.

Kempers, L., Driessen, A. J. M., van Rijssel, J., Nolte, M. A. and van Buul, J. D. (2021). The RhoGEF Trio: A Protein with a Wide Range of Functions in the Vascular Endothelium. *International journal of molecular sciences* **22**. doi:10.3390/ijms221810168.

Kloth, K., Graul-Neumann, L., Hermann, K., Johannsen, J., Bierhals, T. and Kortüm, F. (2021). More evidence on TRIO missense mutations in the spectrin repeat domain causing severe developmental delay and recognizable facial dysmorphism with macrocephaly. *Neurogenetics* **22**, 221–224. doi:10.1007/s10048-021-00648-3.

Kolbjer, S., Martin, D. A., Pettersson, M., Dahlin, M. and Anderlid, B.-M. (2021). Lissencephaly in an epilepsy cohort: Molecular, radiological and clinical aspects. *European journal of paediatric neurology : EJPN : official journal of the European Paediatric Neurology Society* **30**, 71–81. doi:10.1016/j.ejpn.2020.12.011.

Komarova, Y., Groot, C. O. de, **Grigoriev, I., Gouveia, S. M., Munteanu, E. L., Schober, J. M., Honnappa, S., Buey, R. M., Hoogenraad, C. C. and Dogterom, M. et al.** (2009). Mammalian end binding proteins control persistent microtubule growth. *The Journal of cell biology* **184**, 691–706. doi:10.1083/jcb.200807179.

Kratzer, M.-C., Becker, S. F. S., Grund, A., Merks, A., Harnoš, J., Bryja, V., Giehl, K., Kashef, J. and Borchers, A. (2020). The Rho guanine nucleotide exchange factor Trio is required for neural crest cell migration and interacts with Dishevelled. *Development (Cambridge, England)* **147**. doi:10.1242/dev.186338.

Kratzer, M.-C., England, L., Apel, D., Hassel, M. and Borchers, A. (2019). Evolution of the Rho guanine nucleotide exchange factors Kalirin and Trio and their gene expression in Xenopus development. *Gene expression patterns : GEP* **32**, 18–27. doi:10.1016/j.gep.2019.02.004.

Kruse, K., Lee, Q. S., Sun, Y., Klomp, J., Yang, X., Huang, F., Sun, M. Y., Zhao, S., Hong, Z. and

Vogel, S. M. et al. (2019). N-cadherin signaling via Trio assembles adherens junctions to restrict endothelial permeability. *The Journal of cell biology* **218**, 299–316. doi:10.1083/jcb.201802076.

Krylova, O., Messenger, M. J. and Salinas, P. C. (2000). Dishevelled-1 regulates microtubule stability: a new function mediated by glycogen synthase kinase-3beta. *The Journal of cell biology* **151**, 83–94. doi:10.1083/jcb.151.1.83.

Kurochkina, N. and Guha, U. (2013). SH3 domains: modules of protein-protein interactions. *Biophysical reviews* **5**, 29–39. doi:10.1007/s12551-012-0081-z.

Lane, J., Martin, T. A., Mansel, R. E. and Jiang, W. G. (2008). The expression and prognostic value of the guanine nucleotide exchange factors (GEFs) Trio, Vav1 and TIAM-1 in human breast cancer. *International seminars in surgical oncology : ISSO* **5**, 23. doi:10.1186/1477-7800-5-23.

Langhe, R. P., Gudzenko, T., Bachmann, M., Becker, S. F., Gonnermann, C., Winter, C., Abbruzzese, G., Alfandari, D., Kratzer, M.-C. and Franz, C. M. et al. (2016). Cadherin-11 localizes to focal adhesions and promotes cell-substrate adhesion. *Nature communications* **7**, 10909. doi:10.1038/ncomms10909.

Lasser, M., Sun, N., Xu, Y., Wang, S., Drake, S., Law, K., Gonzalez, S., Wang, B., Drury, V. and Castillo, O. et al. (2023). Pleiotropy of autism-associated chromatin regulators. *Development (Cambridge, England)* **150**. doi:10.1242/dev.201515.

Lemmon, M. A. and Ferguson, K. M. (2000). Signal-dependent membrane targeting by pleckstrin homology (PH) domains. *Biochemical Journal* **350**, 1–18.

Li, Y., Guo, Z., Chen, H., Dong, Z., Pan, Z. K., Ding, H., Su, S.-B. and Huang, S. (2011). HOXC8-Dependent Cadherin 11 Expression Facilitates Breast Cancer Cell Migration through Trio and Rac. *Genes & cancer* **2**, 880–888. doi:10.1177/1947601911433129.

Li, Y., Pustovalova, Y., Doukov, T. I., Hoch, J. C., Mains, R. E., Eipper, B. A. and Hao, B. (2023). Structure of the Sec14 domain of Kalirin reveals a distinct class of lipid-binding module in RhoGEFs. *Nature communications* **14**, 96. doi:10.1038/s41467-022-35678-4.

Liebl, E. C., Forsthoefel, D. J., Franco, L. S., Sample, S. H., Hess, J. E., Cowger, J. A., Chandler, M. P., Shupert, A. M. and Seeger, M. A. (2000). Dosage-sensitive, reciprocal genetic interactions between the Abl tyrosine kinase and the putative GEF trio reveal trio's role in axon pathfinding. *Neuron* **26**, 107–118. doi:10.1016/S0896-6273(00)81142-3.

Liu, H., Yue, J., Huang, H., Gou, X., Chen, S.-Y., Zhao, Y. and Wu, X. (2015). Regulation of Focal Adhesion Dynamics and Cell Motility by the EB2 and Hax1 Protein Complex. *The Journal of biological chemistry* **290**, 30771–30782. doi:10.1074/jbc.M115.671743.

Liu, H. and Naismith, J. H. (2008). An efficient one-step site-directed deletion, insertion, single and multiple-site plasmid mutagenesis protocol. *BMC biotechnology* **8**, 91. doi:10.1186/1472-6750-8-91.

Liu, Y., Liang, Z., Cai, W., Shao, Q. and Pan, Q. (2022). Case report: Phenotype expansion and analysis of TRIO and CNKSR2 variations. *Frontiers in neurology* **13**, 948877. doi:10.3389/fneur.2022.948877.

Lutz, S., Shankaranarayanan, A., Coco, C., Ridilla, M., Nance, M. R., Vettel, C., Baltus, D., Evelyn, C. R., Neubig, R. R. and Wieland, T. et al. (2007). Structure of Galphaq-p63RhoGEF-RhoA complex reveals a pathway for the activation of RhoA by GPCRs. *Science (New York, N.Y.)* **318**, 1923–1927. doi:10.1126/science.1147554.

Machacek, M., Hodgson, L., Welch, C., Elliott, H., Pertz, O., Nalbant, P., Abell, A., Johnson, G. L., Hahn, K. M. and Danuser, G. (2009). Coordination of Rho GTPase activities during cell protrusion. *Nature* **461**, 99–103. doi:10.1038/nature08242.

Matthews, H. K., Marchant, L., Carmona-Fontaine, C., Kuriyama, S., Larraín, J., Holt, M. R., Parsons, M. and Mayor, R. (2008). Directional migration of neural crest cells in vivo is regulated by Syndecan-4/Rac1 and non-canonical Wnt signaling/RhoA. *Development (Cambridge, England)* **135**, 1771–1780. doi:10.1242/dev.017350.

Mayor, R. and Etienne-Manneville, S. (2016). The front and rear of collective cell migration. *Nature reviews. Molecular cell biology* **17**, 97–109. doi:10.1038/nrm.2015.14.

Mayor, R. and Theveneau, E. (2013). The neural crest. *Development (Cambridge, England)* **140**, 2247–2251. doi:10.1242/dev.091751.

Medley, Q. G., Serra-Pagès, C., Iannotti, E., Seipel, K., Tang, M., O'Brien, S. P. and Streuli, M. (2000). The trio guanine nucleotide exchange factor is a RhoA target. Binding of RhoA to the trio immunoglobulin-like domain. *The Journal of biological chemistry* **275**, 36116–36123. doi:10.1074/jbc.M003775200.

Medley, Q. G., Buchbinder, E. G., Tachibana, K., Ngo, H., Serra-Pagès, C. and Streuli, M. (2003). Signaling between focal adhesion kinase and trio. *The Journal of biological chemistry* **278**, 13265–13270. doi:10.1074/jbc.M300277200.

Megason, S. G. and Fraser, S. E. (2003). Digitizing life at the level of the cell: high-performance laser-scanning microscopy and image analysis for in toto imaging of development. *Mechanisms of development* **120**, 1407–1420. doi:10.1016/j.mod.2003.07.005.

Mertens, A. E. E., Rygiel, T. P., Olivo, C., van der Kammen, R. and Collard, J. G. (2005). The Rac activator Tiam1 controls tight junction biogenesis in keratinocytes through binding to and activation of the Par polarity complex. *The Journal of cell biology* **170**, 1029–1037. doi:10.1083/jcb.200502129.

Miller, J. R., Rowning, B. A., Larabell, C. A., Yang-Snyder, J. A., Bates, R. L. and Moon, R. T. (1999). Establishment of the dorsal-ventral axis in Xenopus embryos coincides with the dorsal enrichment of dishevelled that is dependent on cortical rotation. *The Journal of cell biology* **146**, 427–437. doi:10.1083/jcb.146.2.427.

Moore, R., Theveneau, E., Pozzi, S., Alexandre, P., Richardson, J., Merks, A., Parsons, M., Kashef, J., Linker, C. and Mayor, R. (2013). Par3 controls neural crest migration by promoting microtubule catastrophe during contact inhibition of locomotion. *Development (Cambridge, England)* **140**, 4763–4775. doi:10.1242/dev.098509.

Moriyoshi, K., Richards, L. J., Akazawa, C., O'Leary, D. D. and Nakanishi, S. (1996). Labeling neural cells using adenoviral gene transfer of membrane-targeted GFP. *Neuron* **16**, 255–260. doi:10.1016/S0896-6273(00)80044-6.

Müller, M., Ringer, K., Hub, F., Kamm, N., Worzfeld, T. and Jacob, R. (2021). TTL-Expression Modulates Epithelial Morphogenesis. *Frontiers in cell and developmental biology* **9**, 635723. doi:10.3389/fcell.2021.635723.

Müller, P. M., Rademacher, J., Bagshaw, R. D., Wortmann, C., Barth, C., van Unen, J., Alp, K. M., Giudice, G., Eccles, R. L. and Heinrich, L. E. et al. (2020). Systems analysis of RhoGEF and RhoGAP regulatory proteins reveals spatially organized RAC1 signalling from integrin adhesions. *Nature cell biology* **22**, 498–511. doi:10.1038/s41556-020-0488-x.

Nekooki-Machida, Y. and Hagiwara, H. (2020). Role of tubulin acetylation in cellular functions and diseases. *Medical molecular morphology* **53**, 191–197. doi:10.1007/s00795-020-00260-8.

Nieuwkoop, P. D. and Faber, J. (1994). Normal Table of Xenopus laevis (Daudin). *New York: Garland Publishing Inc.*

Otey, C. A., Dixon, R., Stack, C. and Goicoechea, S. M. (2009). Cytoplasmic Ig-domain proteins: cytoskeletal regulators with a role in human disease. *Cell motility and the cytoskeleton* **66**, 618–634. doi:10.1002/cm.20385.

Palazzo, A. F., Cook, T. A., Alberts, A. S. and Gundersen, G. G. (2001). mDia mediates Rho-regulated formation and orientation of stable microtubules. *Nature cell biology* **3**, 723–729. doi:10.1038/35087035.

Palazzo, A. F., Eng, C. H., Schlaepfer, D. D., Marcantonio, E. E. and Gundersen, G. G. (2004). Localized stabilization of microtubules by integrin- and FAK-facilitated Rho signaling. *Science (New York, N.Y.)* **303**, 836–839. doi:10.1126/science.1091325.

Palazzo, A. F. and Gundersen, G. G. (2002). Microtubule-actin cross-talk at focal adhesions. *Science's STKE : signal transduction knowledge environment* **2002**, pe31. doi:10.1126/stke.2002.139.pe31.

Paul, N. R., Allen, J. L., Chapman, A., Morlan-Mairal, M., Zindy, E., Jacquemet, G., Del Fernandez Ama, L., Ferizovic, N., Green, D. M. and Howe, J. D. et al. (2015). α5β1 integrin recycling promotes Arp2/3-independent cancer cell invasion via the formin FHOD3. *The Journal of cell biology*

210, 1013–1031. doi:10.1083/jcb.201502040.

Pegtel, D. M., Ellenbroek, S. I. J., Mertens, A. E. E., van der Kammen, R. A., Rooij, J. de and **Collard, J. G.** (2007). The Par-Tiam1 complex controls persistent migration by stabilizing microtubule-dependent front-rear polarity. *Current biology : CB* **17**, 1623–1634. doi:10.1016/j.cub.2007.08.035.

Pertz, O., Hodgson, L., Klemke, R. L. and Hahn, K. M. (2006). Spatiotemporal dynamics of RhoA activity in migrating cells. *Nature* **440**, 1069–1072. doi:10.1038/nature04665.

Pilon, N. (2016). Pigmentation-based insertional mutagenesis is a simple and potent screening approach for identifying neurocristopathy-associated genes in mice. *Rare diseases (Austin, Tex.)* **4**, e1156287. doi:10.1080/21675511.2016.1156287.

Pilon, N. (2021). Treatment and Prevention of Neurocristopathies. *Trends in molecular medicine* **27**, 451–468. doi:10.1016/j.molmed.2021.01.009.

Plageman, T. F., Chauhan, B. K., Yang, C., Jaudon, F., Shang, X., Zheng, Y., Lou, M., Debant, A., Hildebrand, J. D. and Lang, R. A. (2011). A Trio-RhoA-Shroom3 pathway is required for apical constriction and epithelial invagination. *Development (Cambridge, England)* **138**, 5177–5188. doi:10.1242/dev.067868.

Rabiner, C. A., Mains, R. E. and Eipper, B. A. (2005). Kalirin: a dual Rho guanine nucleotide exchange factor that is so much more than the sum of its many parts. *The Neuroscientist : a review journal bringing neurobiology, neurology and psychiatry* **11**, 148–160. doi:10.1177/1073858404271250.

Rajnicek, A. M., Foubister, L. E. and McCaig, C. D. (2006). Temporally and spatially coordinated roles for Rho, Rac, Cdc42 and their effectors in growth cone guidance by a physiological electric field. *Journal of cell science* **119**, 1723–1735. doi:10.1242/jcs.02896.

Revenu, C., Streichan, S., Donà, E., Lecaudey, V., Hufnagel, L. and Gilmour, D. (2014). Quantitative cell polarity imaging defines leader-to-follower transitions during collective migration and the key role of microtubule-dependent adherens junction formation. *Development (Cambridge, England)* **141**, 1282–1291. doi:10.1242/dev.101675.

Rojas, R. J., Yohe, M. E., Gershburg, S., Kawano, T., Kozasa, T. and Sondek, J. (2007). Galphaq directly activates p63RhoGEF and Trio via a conserved extension of the Dbl homology-associated pleckstrin homology domain. *The Journal of biological chemistry* **282**, 29201–29210. doi:10.1074/jbc.M703458200.

Rooney, C., White, G., Nazgiewicz, A., Woodcock, S. A., Anderson, K. I., Ballestrem, C. and Malliri, A. (2010). The Rac activator STEF (Tiam2) regulates cell migration by microtubule-mediated focal adhesion disassembly. *EMBO reports* **11**, 292–298. doi:10.1038/embor.2010.10.

Sadybekov, A., Tian, C., Arnesano, C., Katritch, V. and Herring, B. E. (2017). An autism spectrum disorder-related de novo mutation hotspot discovered in the GEF1 domain of Trio. *Nature communications* **8**, 601. doi:10.1038/s41467-017-00472-0.

Saito, K., Tautz, L. and Mustelin, T. (2007). The lipid-binding SEC14 domain. *Biochimica et biophysica acta* **1771**, 719–726. doi:10.1016/j.bbalip.2007.02.010.

Salhia, B., Tran, N. L., Chan, A., Wolf, A., Nakada, M., Rutka, F., Ennis, M., McDonough, W. S., Berens, M. E. and Symons, M. et al. (2008). The guanine nucleotide exchange factors trio, Ect2, and Vav3 mediate the invasive behavior of glioblastoma. *The American journal of pathology* **173**, 1828–1838. doi:10.2353/ajpath.2008.080043.

Schmidt, S. and Debant, A. (2014). Function and regulation of the Rho guanine nucleotide exchange factor Trio. *Small GTPases* **5**, e29769. doi:10.4161/sgtp.29769.

Schober, M., Raghavan, S., Nikolova, M., Polak, L., Pasolli, H. A., Beggs, H. E., Reichardt, L. F. and Fuchs, E. (2007). Focal adhesion kinase modulates tension signaling to control actin and focal adhesion dynamics. *The Journal of cell biology* **176**, 667–680. doi:10.1083/jcb.200608010.

Schultz-Rogers, L., Muthusamy, K., Pinto E Vairo, F., Klee, E. W. and Lanpher, B. (2020). Novel loss-of-function variants in TRIO are associated with neurodevelopmental disorder: case report. *BMC medical genetics* **21**, 219. doi:10.1186/s12881-020-01159-y.

Seetharaman, S. and Etienne-Manneville, S. (2019). Microtubules at focal adhesions - a double-

edged sword. *Journal of cell science* **132**. doi:10.1242/jcs.232843.

Seipel, K., O'Brien, S. P., Iannotti, E., Medley, Q. G. and Streuli, M. (2001). Tara, a novel F-actin binding protein, associates with the Trio guanine nucleotide exchange factor and regulates actin cytoskeletal organization. *Journal of cell science* **114**, 389–399. doi:10.1242/jcs.114.2.389.

Session, A. M., Uno, Y., Kwon, T., Chapman, J. A., Toyoda, A., Takahashi, S., Fukui, A., Hikosaka, A., Suzuki, A. and Kondo, M. et al. (2016). Genome evolution in the allotetraploid frog Xenopus laevis. *Nature* **538**, 336–343. doi:10.1038/nature19840.

Sferra, A., Petrini, S., Bellacchio, E., Nicita, F., Scibelli, F., Dentici, M. L., Alfieri, P., Cestra, G., Bertini, E. S. and Zanni, G. (2020). TUBB Variants Underlying Different Phenotypes Result in Altered Vesicle Trafficking and Microtubule Dynamics. *International journal of molecular sciences* **21**. doi:10.3390/ijms21041385.

Singh, T., Poterba, T., Curtis, D., Akil, H., Al Eissa, M., Barchas, J. D., Bass, N., Bigdeli, T. B., Breen, G. and Bromet, E. J. et al. (2022). Rare coding variants in ten genes confer substantial risk for schizophrenia. *Nature* **604**, 509–516. doi:10.1038/s41586-022-04556-w.

Smith, W. C. and Harland, R. M. (1991). Injected Xwnt-8 RNA acts early in Xenopus embryos to promote formation of a vegetal dorsalizing center. *Cell* **67**, 753–765. doi:10.1016/0092-8674(91)90070-F.

Son, K., Smith, T. C. and Luna, E. J. (2015). Supervillin binds the Rac/Rho-GEF Trio and increases Trio-mediated Rac1 activation. *Cytoskeleton (Hoboken, N.J.)* **72**, 47–64. doi:10.1002/cm.21210.

Sonoshita, M., Itatani, Y., Kakizaki, F., Sakimura, K., Terashima, T., Katsuyama, Y., Sakai, Y. and Taketo, M. M. (2015). Promotion of colorectal cancer invasion and metastasis through activation of NOTCH-DAB1-ABL-RHOGEF protein TRIO. *Cancer discovery* **5**, 198–211. doi:10.1158/2159-8290.CD-14-0595.

Spiering, D. and Hodgson, L. (2011). Dynamics of the Rho-family small GTPases in actin regulation and motility. *Cell adhesion & migration* **5**, 170–180. doi:10.4161/cam.5.2.14403.

Stanganello, E., Hagemann, A. I. H., Mattes, B., Sinner, C., Meyen, D., Weber, S., Schug, A., Raz, E. and Scholpp, S. (2015). Filopodia-based Wnt transport during vertebrate tissue patterning. *Nature communications* **6**, 5846. doi:10.1038/ncomms6846.

Stehbens, S. and Wittmann, T. (2012). Targeting and transport: how microtubules control focal adhesion dynamics. *The Journal of cell biology* **198**, 481–489. doi:10.1083/jcb.201206050.

Stepanova, T., Slemmer, J., Hoogenraad, C. C., Lansbergen, G., Dortland, B., Zeeuw, C. I. de, **Grosveld, F., van Cappellen, G., Akhmanova, A. and Galjart, N.** (2003). Visualization of microtubule growth in cultured neurons via the use of EB3-GFP (end-binding protein 3-green fluorescent protein). *The Journal of neuroscience : the official journal of the Society for Neuroscience* **23**, 2655–2664. doi:10.1523/JNEUROSCI.23-07-02655.2003.

Su, L. K. and Qi, Y. (2001). Characterization of human MAPRE genes and their proteins. *Genomics* **71**, 142–149. doi:10.1006/geno.2000.6428.

Szabó, A. and Mayor, R. (2018). Mechanisms of Neural Crest Migration. *Annual review of genetics* **52**, 43–63. doi:10.1146/annurev-genet-120417-031559.

Tao, T., Sun, J., Peng, Y., Li, Y., Wang, P., Chen, X., Zhao, W., Zheng, Y.-Y., Wei, L. and Wang, W. et al. (2019a). Golgi-resident TRIO regulates membrane trafficking during neurite outgrowth. *The Journal of biological chemistry* **294**, 10954–10968. doi:10.1074/jbc.RA118.007318.

Tao, T., Sun, J., Peng, Y., Wang, P., Chen, X., Zhao, W., Li, Y., Wei, L., Wang, W. and Zheng, Y. et al. (2019b). Distinct functions of Trio GEF domains in axon outgrowth of cerebellar granule neurons. *Journal of genetics and genomics = Yi chuan xue bao* **46**, 87–96. doi:10.1016/j.jgg.2019.02.003.

Theveneau, E., Marchant, L., Kuriyama, S., Gull, M., Moepps, B., Parsons, M. and Mayor, R. (2010). Collective chemotaxis requires contact-dependent cell polarity. *Developmental cell* **19**, 39–53. doi:10.1016/j.devcel.2010.06.012.

Theveneau, E. and Mayor, R. (2012). Neural crest migration: interplay between chemorepellents, chemoattractants, contact inhibition, epithelial-mesenchymal transition, and collective cell migration.

Wiley interdisciplinary reviews. Developmental biology **1**, 435–445. doi:10.1002/wdev.28.

Thues, C., Valadas, J. S., Deaulmerie, L., Geens, A., Chouhan, A. K., Duran-Romaña, R., Schymkowitz, J., Rousseau, F., Bartusel, M. and Rehimi, R. et al. (2021). MAPRE2 mutations result in altered human cranial neural crest migration, underlying craniofacial malformations in CSC-KT syndrome. *Scientific reports* **11**, 4976. doi:10.1038/s41598-021-83771-3.

Timmerman, I., Heemskerk, N., Kroon, J., Schaefer, A., van Rijssel, J., Hoogenboezem, M., van Unen, J., Goedhart, J., Gadella, T. W. J. and Yin, T. et al. (2015). A local VE-cadherin and Trio-based signaling complex stabilizes endothelial junctions through Rac1. *Journal of cell science* **128**, 3041–3054. doi:10.1242/jcs.168674.

van Haren, J., Boudeau, J., Schmidt, S., Basu, S., Liu, Z., Lammers, D., Demmers, J., Benhari, J., Grosveld, F. and Debant, A. et al. (2014). Dynamic microtubules catalyze formation of navigator-TRIO complexes to regulate neurite extension. *Current biology : CB* **24**, 1778–1785. doi:10.1016/j.cub.2014.06.037.

van Rijssel, J., Kroon, J., Hoogenboezem, M., van Alphen, F. P. J., Jong, R. J. de, **Kostadinova, E., Geerts, D., Hordijk, P. L. and van Buul, J. D.** (2012). The Rho-guanine nucleotide exchange factor Trio controls leukocyte transendothelial migration by promoting docking structure formation. *Molecular biology of the cell* **23**, 2831–2844. doi:10.1091/mbc.e11-11-0907.

Vanderzalm, P. J., Pandey, A., Hurwitz, M. E., Bloom, L., Horvitz, H. R. and Garriga, G. (2009). C. elegans CARMIL negatively regulates UNC-73/Trio function during neuronal development. *Development (Cambridge, England)* **136**, 1201–1210. doi:10.1242/dev.026666.

Villaseca, S., Leal, J. I., Guajardo, J., Morales-Navarrete, H., Mayor, R. and Torrejón, M. (2023). *Gαi2-Mediated Regulation of Microtubules Dynamics and Rac1 Activity Orchestrates Cranial Neural Crest Cell Migration in Xenopus*.

Wang, B., Fang, J., Qu, L., Cao, Z., Zhou, J. and Deng, B. (2015). Upregulated TRIO expression correlates with a malignant phenotype in human hepatocellular carcinoma. *Tumour biology : the journal of the International Society for Oncodevelopmental Biology and Medicine* **36**, 6901–6908. doi:10.1007/s13277-015-3377-3.

Wang, J., Yuan, L., Xu, X., Zhang, Z., Ma, Y., Hong, L. and Ma, J. (2021). Rho-GEF Trio regulates osteosarcoma progression and osteogenic differentiation through Rac1 and RhoA. *Cell death & disease* **12**, 1148. doi:10.1038/s41419-021-04448-3.

Wang, T., Rao, D., Yu, C., Sheng, J., Luo, Y., Xia, L. and Huang, W. (2022). RHO GTPase family in hepatocellular carcinoma. *Experimental hematology & oncology* **11**, 91. doi:10.1186/s40164-022-00344-4.

Wang, Y., Liu, S., Zhang, Y. and Yang, J. (2019). Myosin Heavy Chain 9: Oncogene or Tumor Suppressor Gene? *Medical science monitor : international medical journal of experimental and clinical research* **25**, 888–892. doi:10.12659/MSM.912320.

Warner, H., Wilson, B. J. and Caswell, P. T. (2019). Control of adhesion and protrusion in cell migration by Rho GTPases. *Current opinion in cell biology* **56**, 64–70. doi:10.1016/j.ceb.2018.09.003.

Waterman-Storer, C. M., Worthylake, R. A., Liu, B. P., Burridge, K. and Salmon, E. D. (1999). Microtubule growth activates Rac1 to promote lamellipodial protrusion in fibroblasts. *Nature cell biology* **1**, 45–50. doi:10.1038/9018.

Wehner, P., Shnitsar, I., Urlaub, H. and Borchers, A. (2011). RACK1 is a novel interaction partner of PTK7 that is required for neural tube closure. *Development (Cambridge, England)* **138**, 1321–1327. doi:10.1242/dev.056291.

Wei, C., Sun, M., Sun, X., Meng, H., Li, Q., Gao, K., Yue, W., Wang, L., Zhang, D. and Li, J. (2022). RhoGEF Trio Regulates Radial Migration of Projection Neurons via Its Distinct Domains. *Neuroscience bulletin* **38**, 249–262. doi:10.1007/s12264-021-00804-7.

Williams, S. L., Lutz, S., Charlie, N. K., Vettel, C., Ailion, M., Coco, C., Tesmer, J. J. G., Jorgensen, E. M., Wieland, T. and Miller, K. G. (2007). Trio's Rho-specific GEF domain is the missing Galpha q effector in C. elegans. *Genes & development* **21**, 2731–2746. doi:10.1101/gad.1592007.

Winning, R. S., Shea, L. J., Marcus, S. J. and Sargent, T. D. (1991). Developmental regulation of

transcription factor AP-2 during Xenopus laevis embryogenesis. *Nucleic acids research* **19**, 3709–3714. doi:10.1093/nar/19.13.3709.

Wittmann, T. and Waterman-Storer, C. M. (2001). Cell motility: can Rho GTPases and microtubules point the way? *Journal of cell science* **114**, 3795–3803. doi:10.1242/jcs.114.21.3795.

Woo, S. and Gomez, T. M. (2006). Rac1 and RhoA promote neurite outgrowth through formation and stabilization of growth cone point contacts. *The Journal of neuroscience : the official journal of the Society for Neuroscience* **26**, 1418–1428. doi:10.1523/JNEUROSCI.4209-05.2006.

Wouters, L., Rodriguez Rodriguez, C. M., Dapena, E. P., Poorten, V. V., Devriendt, K. and van Esch, H. (2011). Circumferential skin creases, cleft palate, typical face, intellectual disability and growth delay: "circumferential skin creases Kunze type". *European journal of medical genetics* **54**, 236–240. doi:10.1016/j.ejmg.2011.01.003.

Yan, Y., Eipper, B. A. and Mains, R. E. (2015). Kalirin-9 and Kalirin-12 Play Essential Roles in Dendritic Outgrowth and Branching. *Cerebral cortex (New York, N.Y. : 1991)* **25**, 3487–3501. doi:10.1093/cercor/bhu182.

Yang-Snyder, J., Miller, J. R., Brown, J. D., Lai, C. J. and Moon, R. T. (1996). A frizzled homolog functions in a vertebrate Wnt signaling pathway. *Current biology : CB* **6**, 1302–1306. doi:10.1016/S0960-9822(02)70716-1.

Yano, T., Yamazaki, Y., Adachi, M., Okawa, K., Fort, P., Uji, M., Tsukita, S. and Tsukita, S. (2011). Tara up-regulates E-cadherin transcription by binding to the Trio RhoGEF and inhibiting Rac signaling. *The Journal of cell biology* **193**, 319–332. doi:10.1083/jcb.201009100.

Yohe, M. E., Rossman, K. and Sondek, J. (2008). Role of the C-terminal SH3 domain and N-terminal tyrosine phosphorylation in regulation of Tim and related Dbl-family proteins. *Biochemistry* **47**, 6827–6839. doi:10.1021/bi702543p.

Yoshimura, Y. and Miki, H. (2011). Dynamic regulation of GEF-H1 localization at microtubules by Par1b/MARK2. *Biochemical and biophysical research communications* **408**, 322–328. doi:10.1016/j.bbrc.2011.04.032.

Yoshizuka, N., Moriuchi, R., Mori, T., Yamada, K., Hasegawa, S., Maeda, T., Shimada, T., Yamada, Y., Kamihira, S. and Tomonaga, M. et al. (2004). An alternative transcript derived from the trio locus encodes a guanosine nucleotide exchange factor with mouse cell-transforming potential. *The Journal of biological chemistry* **279**, 43998–44004. doi:10.1074/jbc.M406082200.

Yue, J., Xie, M., Gou, X., Lee, P., Schneider, M. D. and Wu, X. (2014). Microtubules regulate focal adhesion dynamics through MAP4K4. *Developmental cell* **31**, 572–585. doi:10.1016/j.devcel.2014.10.025.

Danksagung

An erster Stelle möchte ich mich besonders bei meiner Betreuerin Prof. Dr. Annette Borchers sowohl für die Möglichkeit bedanken, meine Promotion in ihrer Arbeitsgruppe durchzuführen, als auch für die spannenden Projekte, an denen ich arbeiten durfte. Vielen Dank für die Betreuung und Beratung während dieser Zeit.

Ebenfalls möchte ich mich bei Prof. Dr. Christian Helker für die Übernahme meines Zweitgutachtens und bei der gesamten AG Helker für die tolle Zusammenarbeit bedanken. Weiterhin bedanke ich mich vielmals bei Prof. Dr. Ralf Jacob für die Bereitstellung von Antikörpern und der MDCK Zell-Linien, sowie für die sehr hilfreichen Diskussionen zu meinem Projekt. Ebenso bedanke ich mich bei Prof. Dr. Anne Debant für die Zusendung mehrerer Plasmide und die Diskussion meines Projektes. Ein großes Dankeschön gilt auch Prof. Dr. Sandra Hake: Vielen Dank für die tolle Zusammenarbeit und das spannende Kooperationsprojekt, durch das ich nochmal viel aus einem anderen Bereich lernen konnte. Hier gilt auch ein großer Dank an Tim und Andreas, die bei Fragen jederzeit zur Seite standen.

Weiterhin möchte ich mich bei allen aktuellen und ehemaligen Mitgliedern der AG Borchers für das tolle Arbeitsklima und die Unterstützung bedanken. Ein großes Dankeschön gilt hierbei Ingrid: Danke, dass du jederzeit bei allen möglichen Angelegenheiten geholfen hast. Vielen Dank auch an Hanna, Sarah, Irene und vor allem Katharina, für die spannenden Diskussionen, die vielen Ratschläge und den Zusammenhalt! Es war und ist ein großer Spaß mit so einem tollen Team zusammenzuarbeiten!

Ebenfalls möchte ich mich bei meiner Familie und insbesondere bei meinen Eltern und meiner lieben CHAOS-Crew bedanken. Danke, dass ihr immer für mich da seid und mich bei allem, was ich mir vornehme, unterstützt!
Zuletzt möchte ich mich ganz herzlich bei meinem Partner und zukünftigen Ehemann Tim bedanken. Danke, dass du mir jederzeit mit Rat und Tat zur Seite stehst und mich nicht nur unterstützt, aufbaust und ermutigst meinen Weg zu gehen, sondern egal was kommt, einfach immer für mich da bist.

Erklärung

Ich versichere, dass ich meine Dissertation mit dem Titel „The Rho GEF Trio is transported by microtubule plus-ends and involved in focal adhesion formation in migrating neural crest cells“ selbstständig ohne unerlaubte Hilfe angefertigt und mich dabei keiner anderen als der von mir ausdrücklich bezeichneten Quellen und Hilfsmittel bedient habe.

Diese Dissertation wurde in der jetzigen oder einer ähnlichen Form noch bei keiner anderen Hochschule eingereicht und hat noch keinen sonstigen Prüfungszwecken gedient.

Marburg, 27.11.2023	
Ort, Datum	Unterschrift (Vor- und Nachname)